Cosmic-Ray Positrons from Astrophysical Sources: GRBs, Pulsars and SNRs

Kunihito Ioka (KEK)

KI, arXiv:0812.4851
Kawanaka, KI & Nojiri, arXiv:0903.3782
Fujita, Kohri, Yamazaki & KI, arXiv:0903.5298

PAMELA

Positron excess above the predicted secondary

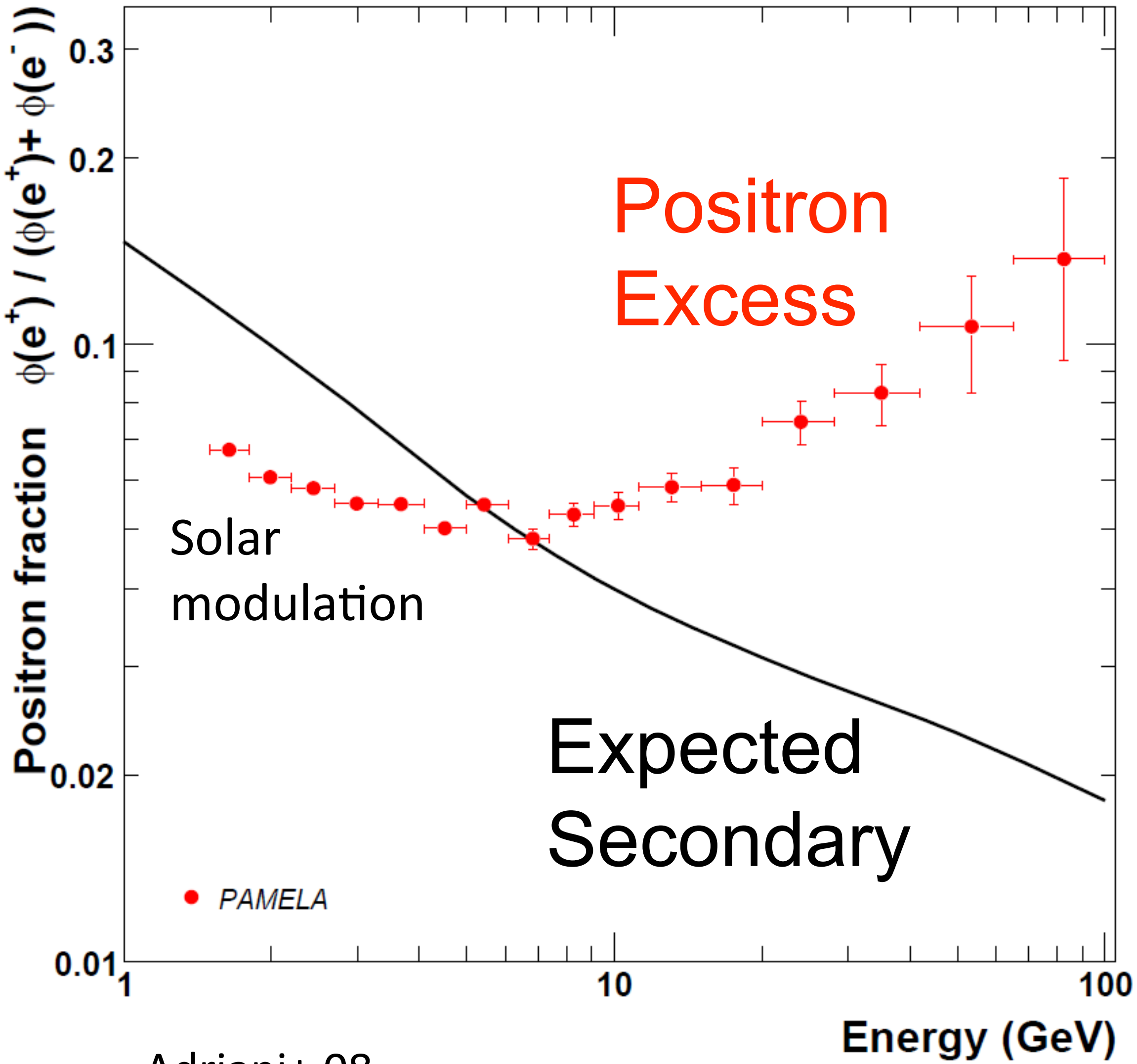

Adriani+ 08

⇒ Primary sources
- Dark matter?
- Astrophysical?

⇒ Many papers >100

Jul 06 - Feb 08
151672 e-, 9430 e+

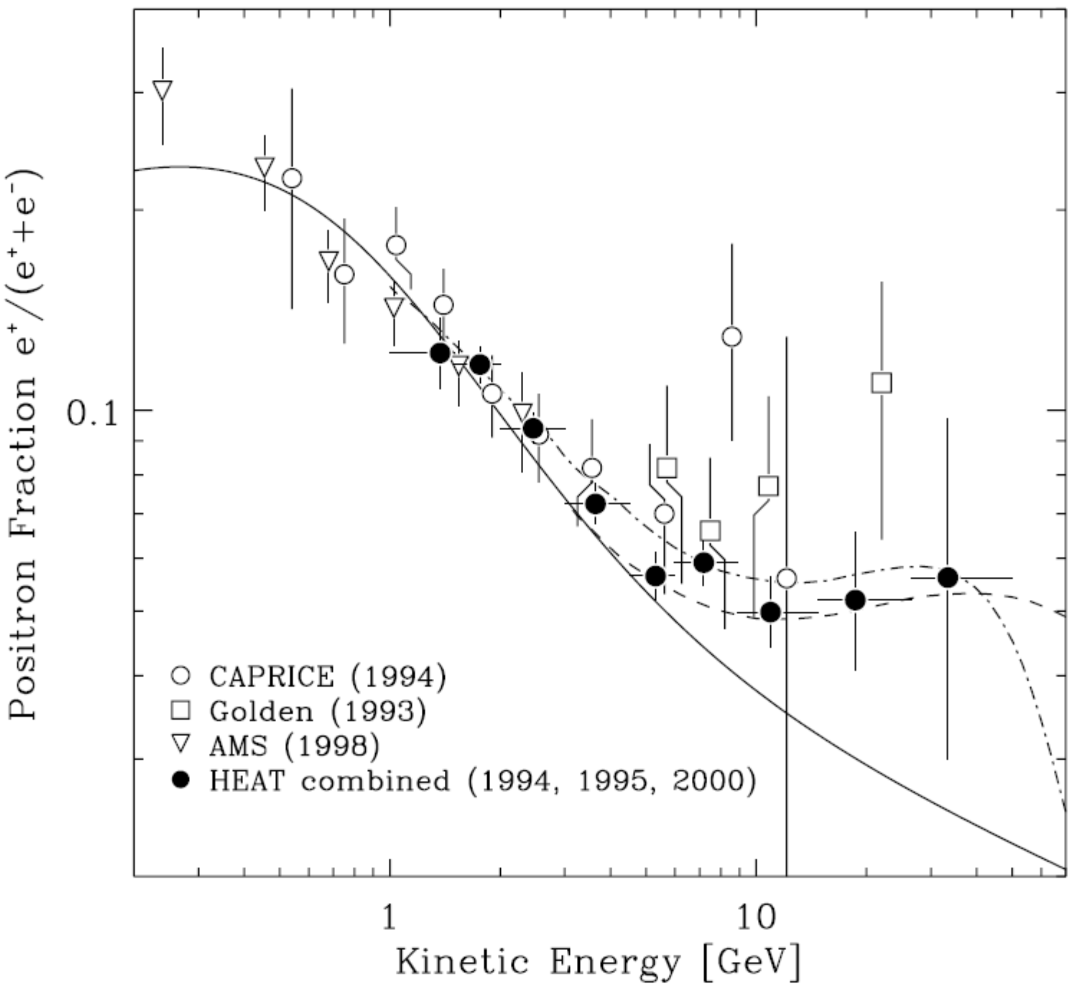

FIG. 4. The positron fraction as a function of energy for the combined HEAT-$e^{\pm}$ and HEAT-pbar data, compared to model predictions and other recent measurements (CAPRICE [3], Golden [29], AMS [4]). Dates in parentheses give the year of the measurement and not the publication. The solid curve is the positron fraction based on a purely secondary production of positrons given by [23]. The dashed and dot-dashed curves are the ratios including contributions from Higgsino LSP decay [15] and gamma-ray pulsars [6], respectively.

A hint was provided previously by AMS, HEAT etc., though not conclusive

Beatty+ 04

Principle of detection

Magnet ⇒ Rididity (pc/Ze), charge sign, value (dE/dx)

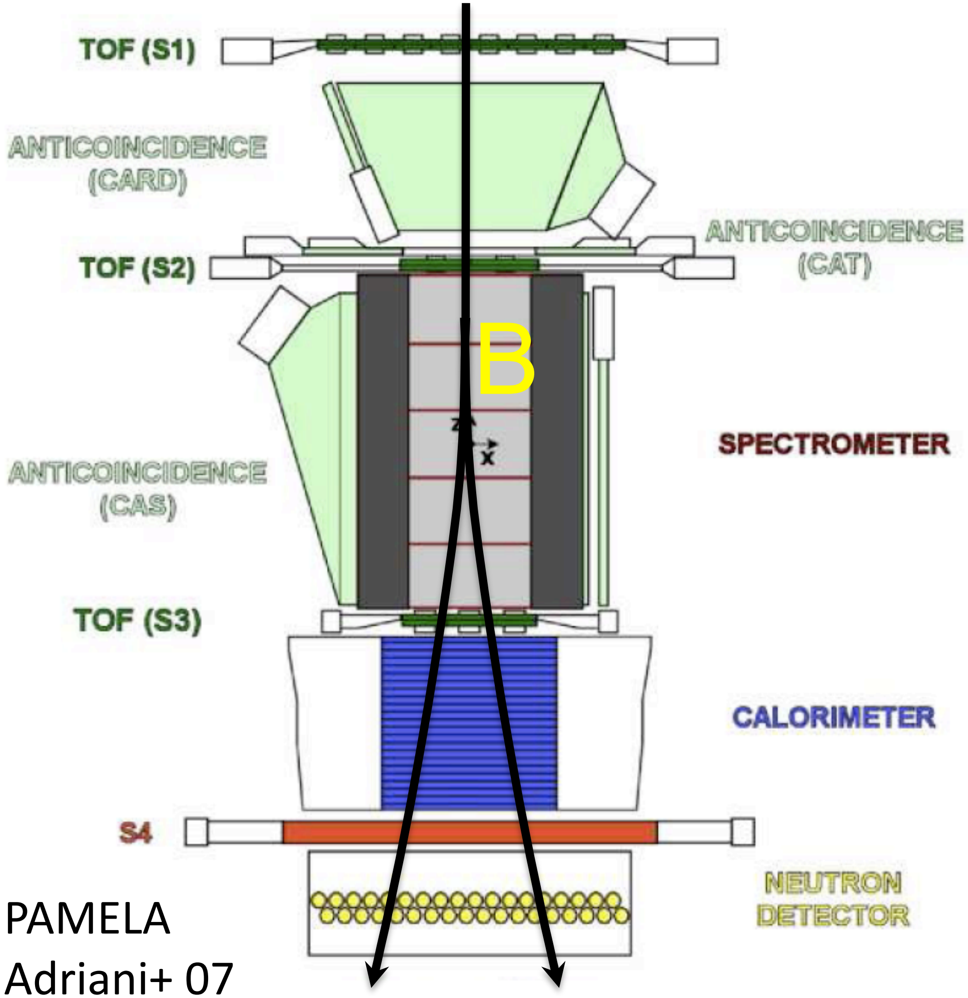

PAMELA
Adriani+ 07

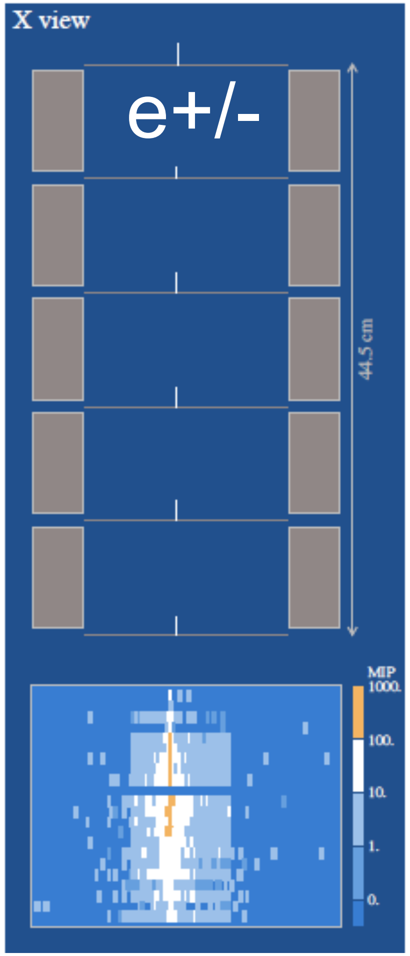

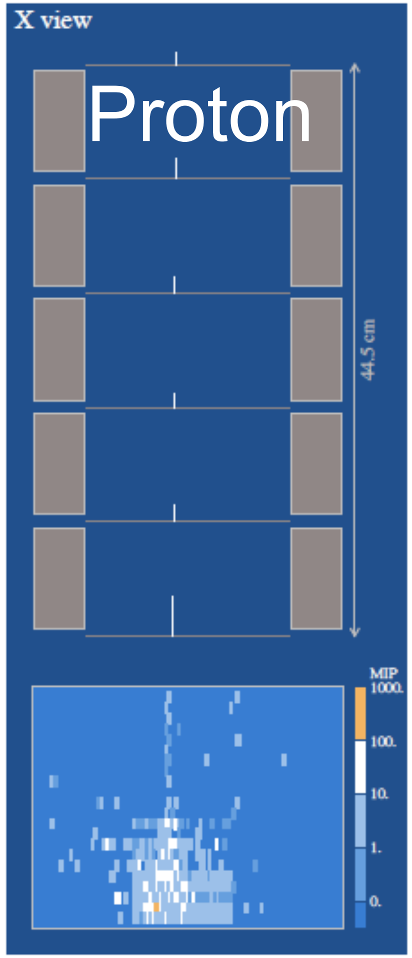

electron/hadron separation

- Shower starting point
- Longitudinal profile

Secondary positrons

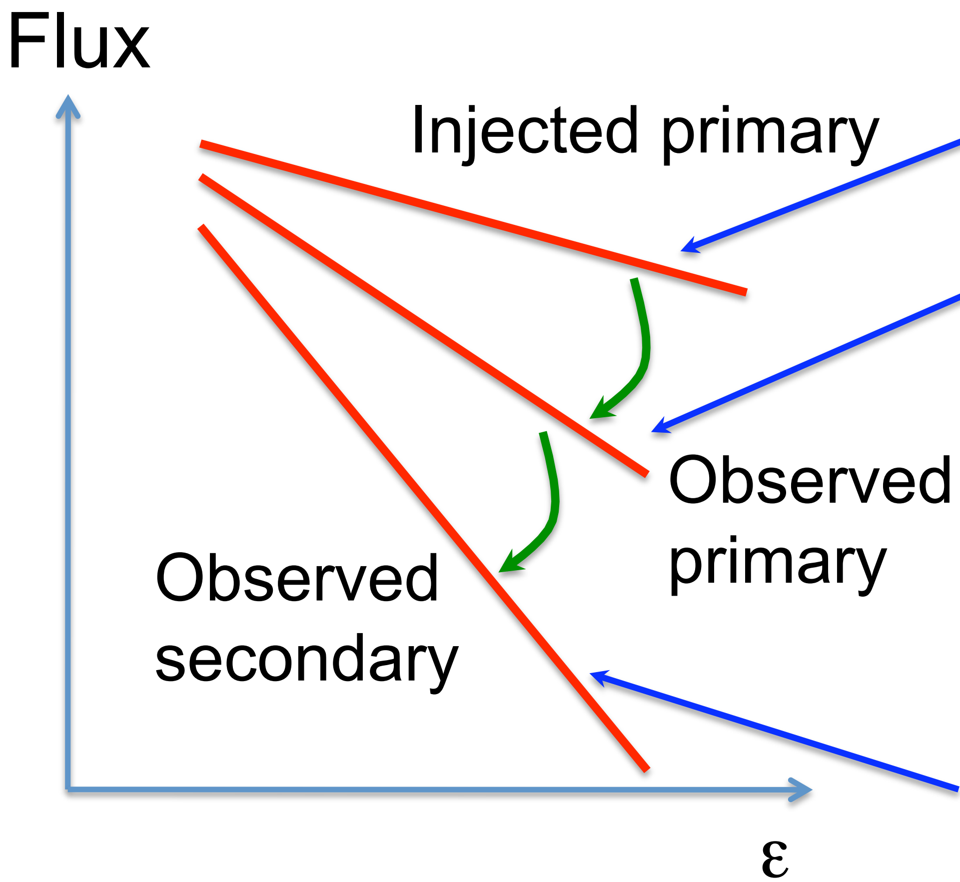

$$\Phi_1 \sim \frac{c}{4\pi} \bullet \tau_{\mathrm{esc}}(\varepsilon) \bullet Q_1(\varepsilon)$$

$$\propto \varepsilon^{-\delta} \bullet \varepsilon^{-\gamma}$$

$$Q_2(\varepsilon) \propto \sigma \bullet \Phi_1(\varepsilon)$$

$$\Phi_2 \sim \tau_{\mathrm{esc}}(\varepsilon) \bullet Q_2(\varepsilon)$$

$$\propto \varepsilon^{-\delta} \bullet \varepsilon^{-\delta} \varepsilon^{-\gamma}$$

This is robust if cooling/escape is faster for higher energy.

ATIC/PPB-BETS

An Excess also in ($e^+ + e^-$) Spectrum

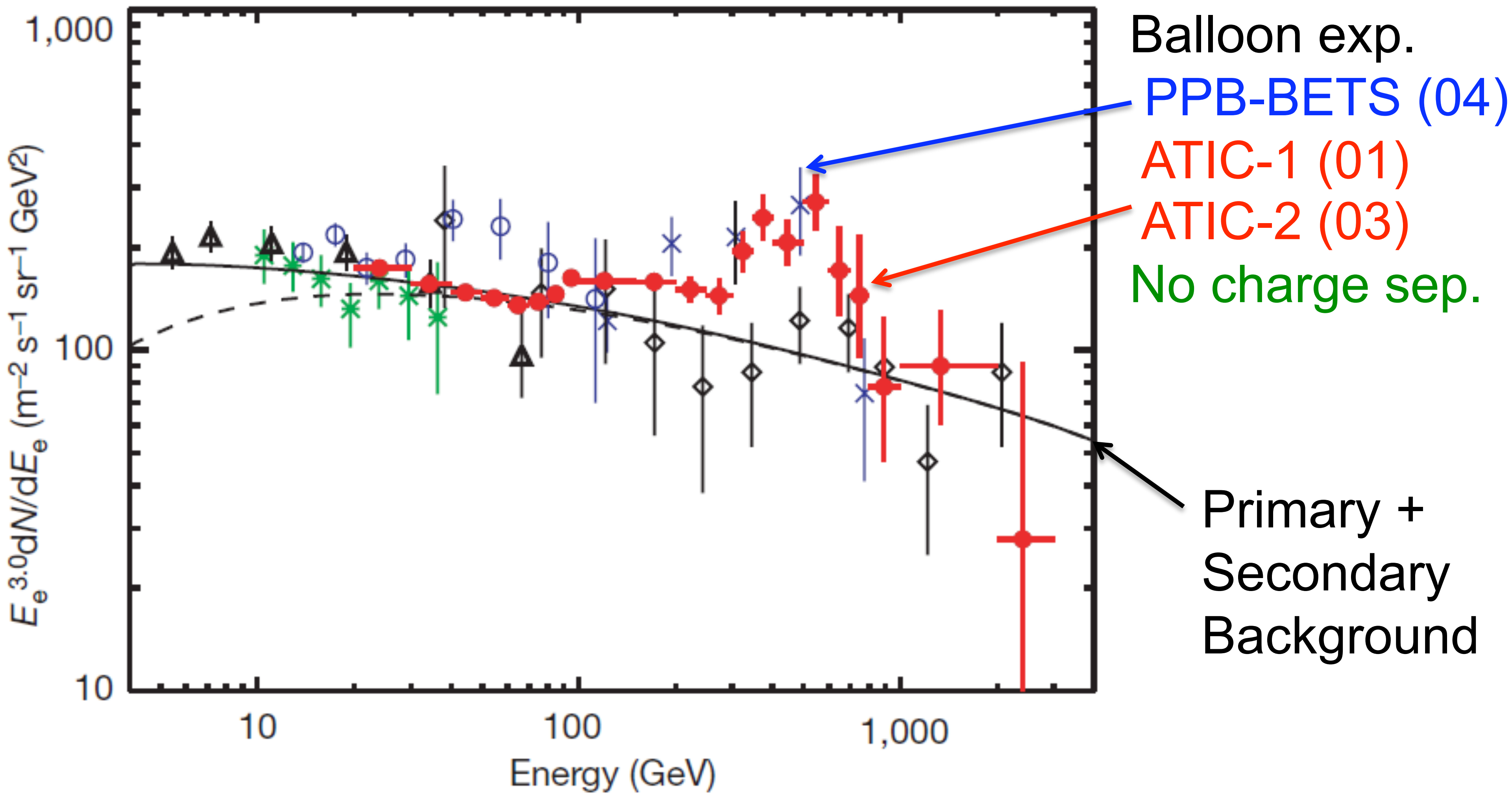

Chang+ 08, Torii+ 08

ATIC/PPB-BETS

Dark Matter (DM) Signal?

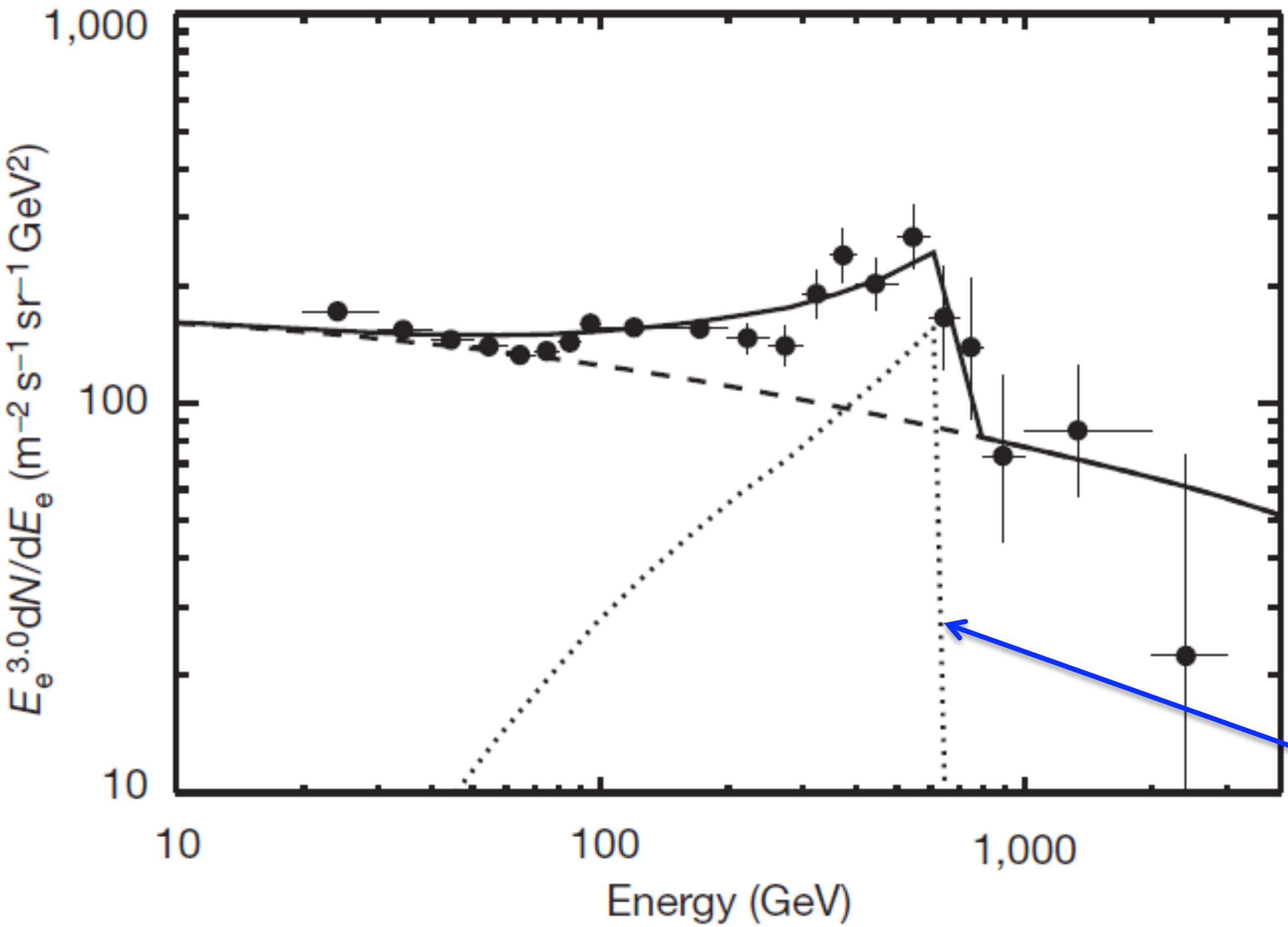

Peak + Cutoff?

Sharp cutoff is difficult to explain by astrophysical sources??

~600GeV DM?

Chang+ 08, Torii+ 08

Fermi

An Excess (but Not Peak) in (e^++e^-) Spectrum

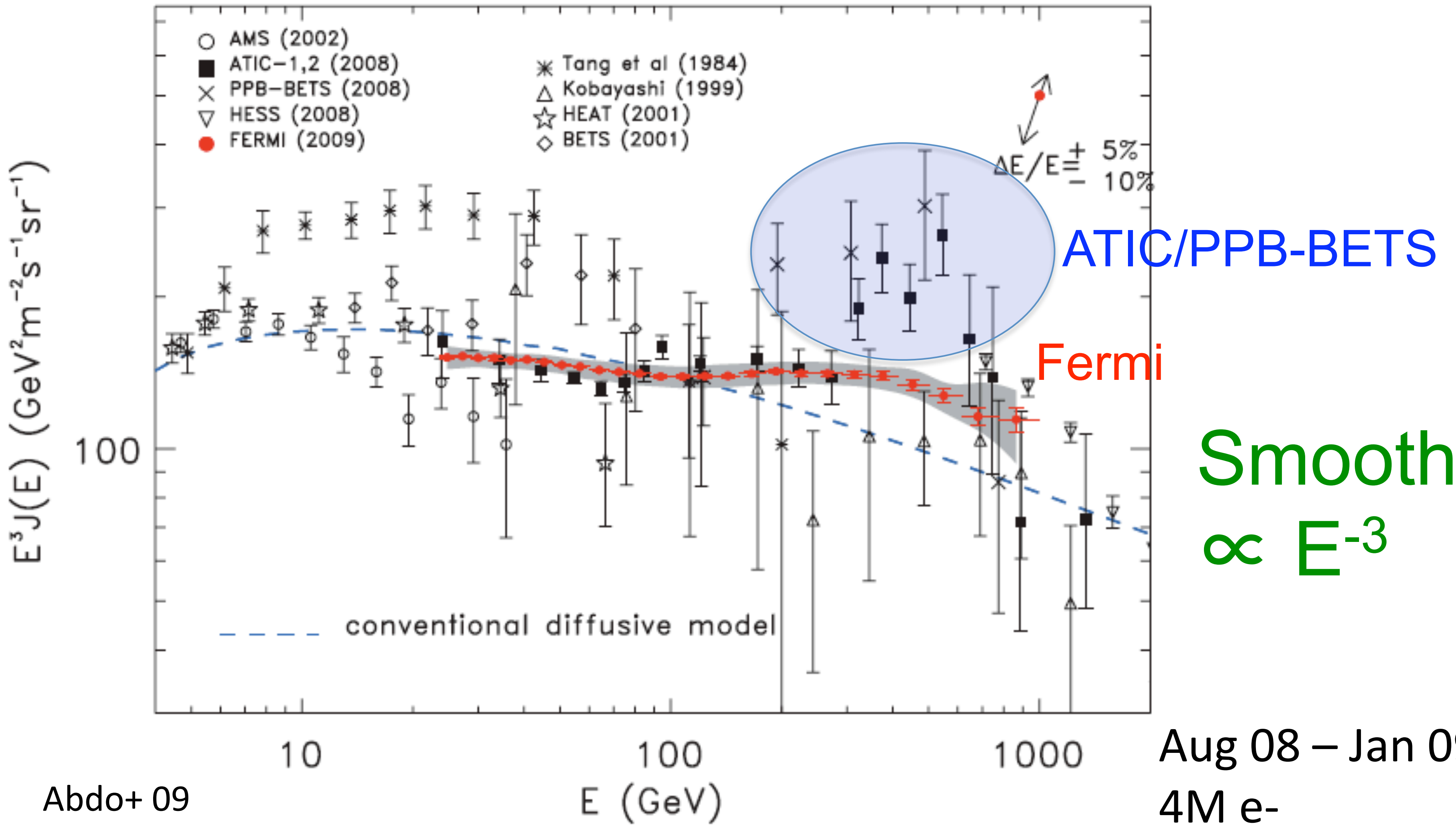

Abdo+ 09

Smooth

$\propto E^{-3}$

Aug 08 – Jan 09

4M e-

PAMELA electron (e-) flux

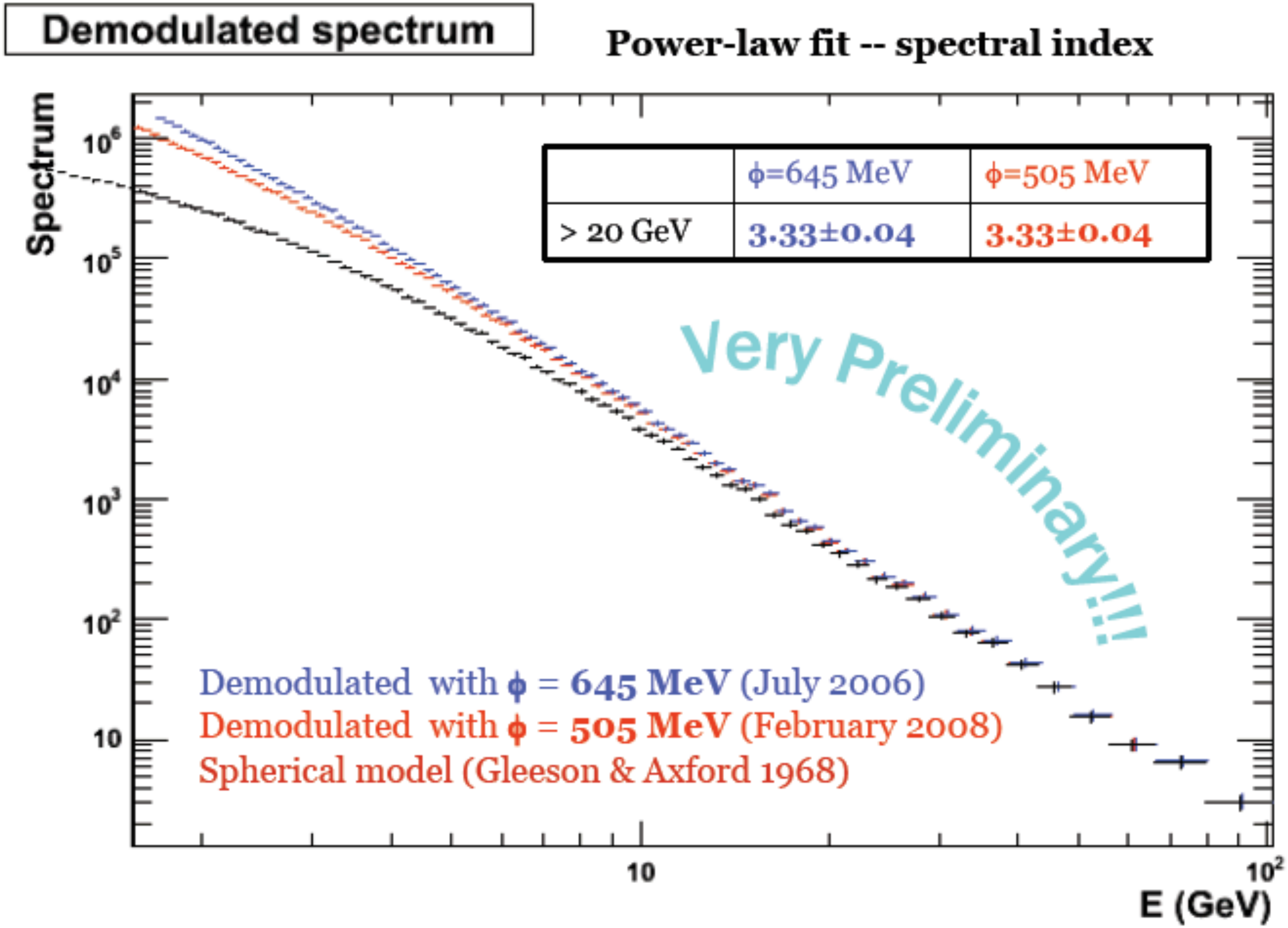

	ϕ=645 MeV	ϕ=505 MeV
> 20 GeV	3.33±0.04	3.33±0.04

Mocchiutti PAMELA RICAP09

HESS

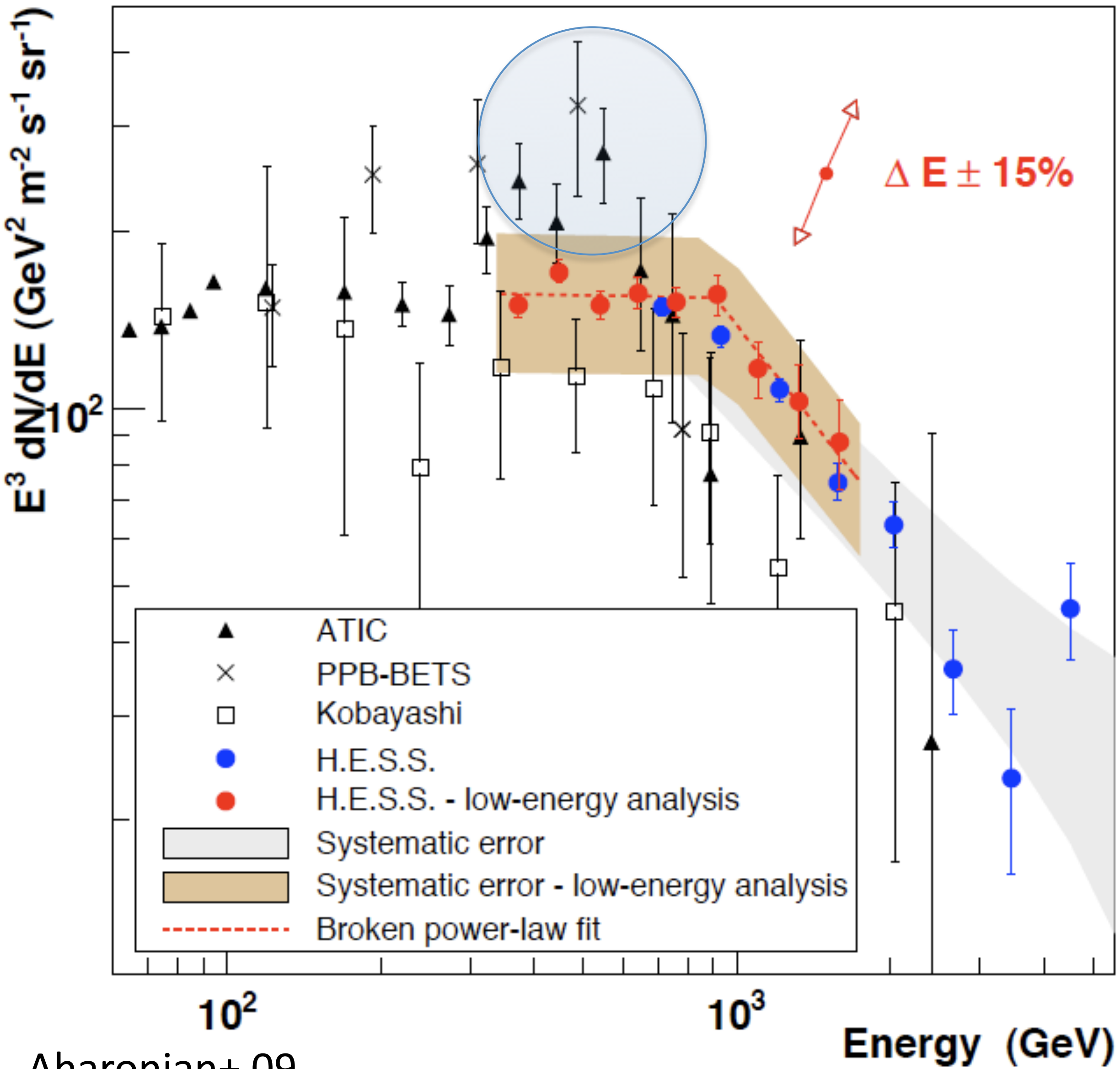

Aharonian+ 09

Consistent with Fermi

No ATIC peak (but not rule out)

Steep at >1TeV

Differences between ATIC/PPB-BETS & Fermi/HESS are controversial

Primary sources

$e^{\pm}$ cooling

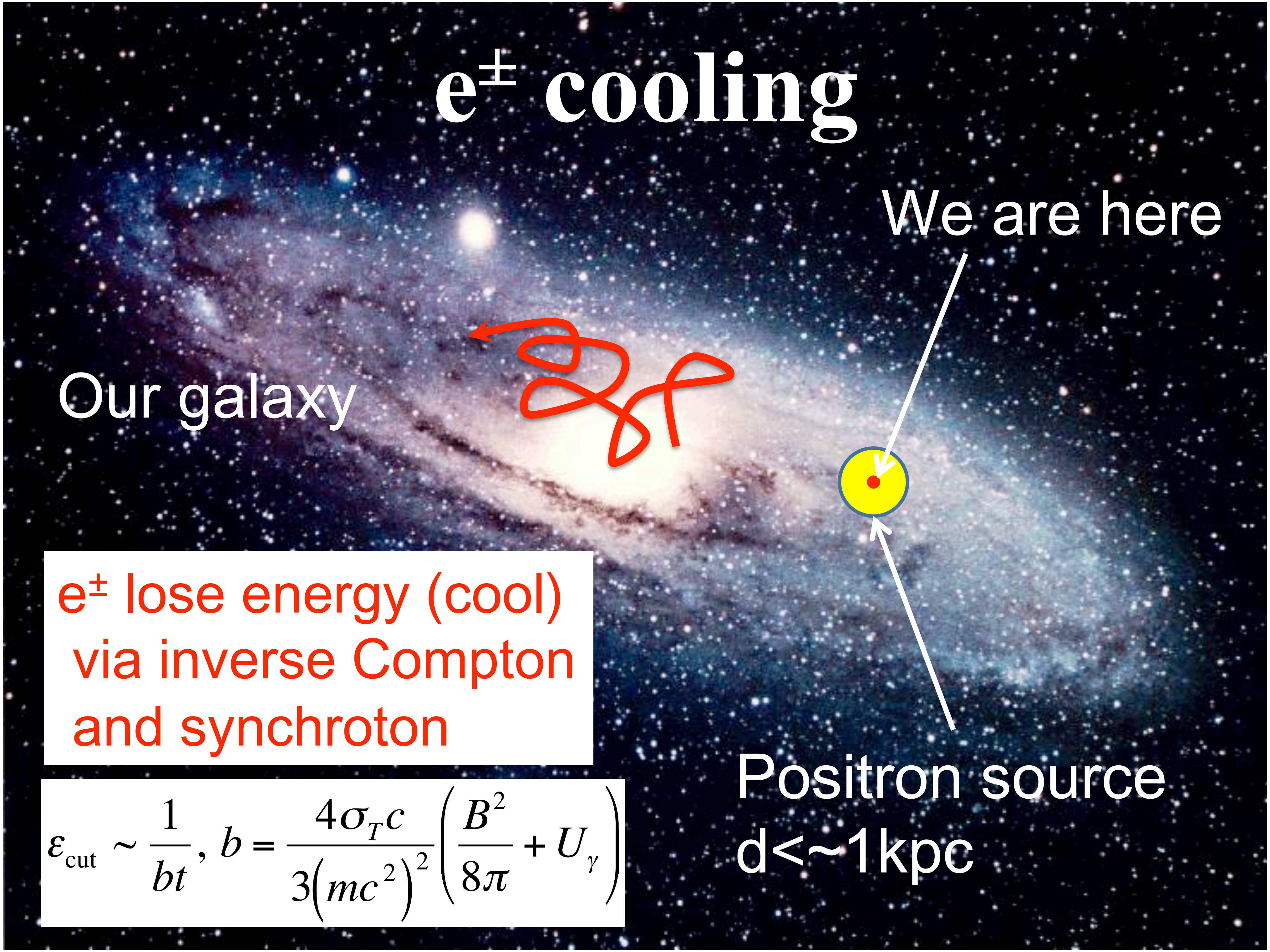

e± lose energy (cool) via inverse Compton and synchroton

$$\varepsilon_{\rm cut} \sim \frac{1}{bt},\ b = \frac{4\sigma_T c}{3(mc^2)^2}\left(\frac{B^2}{8\pi} + U_\gamma\right)$$

Energetics

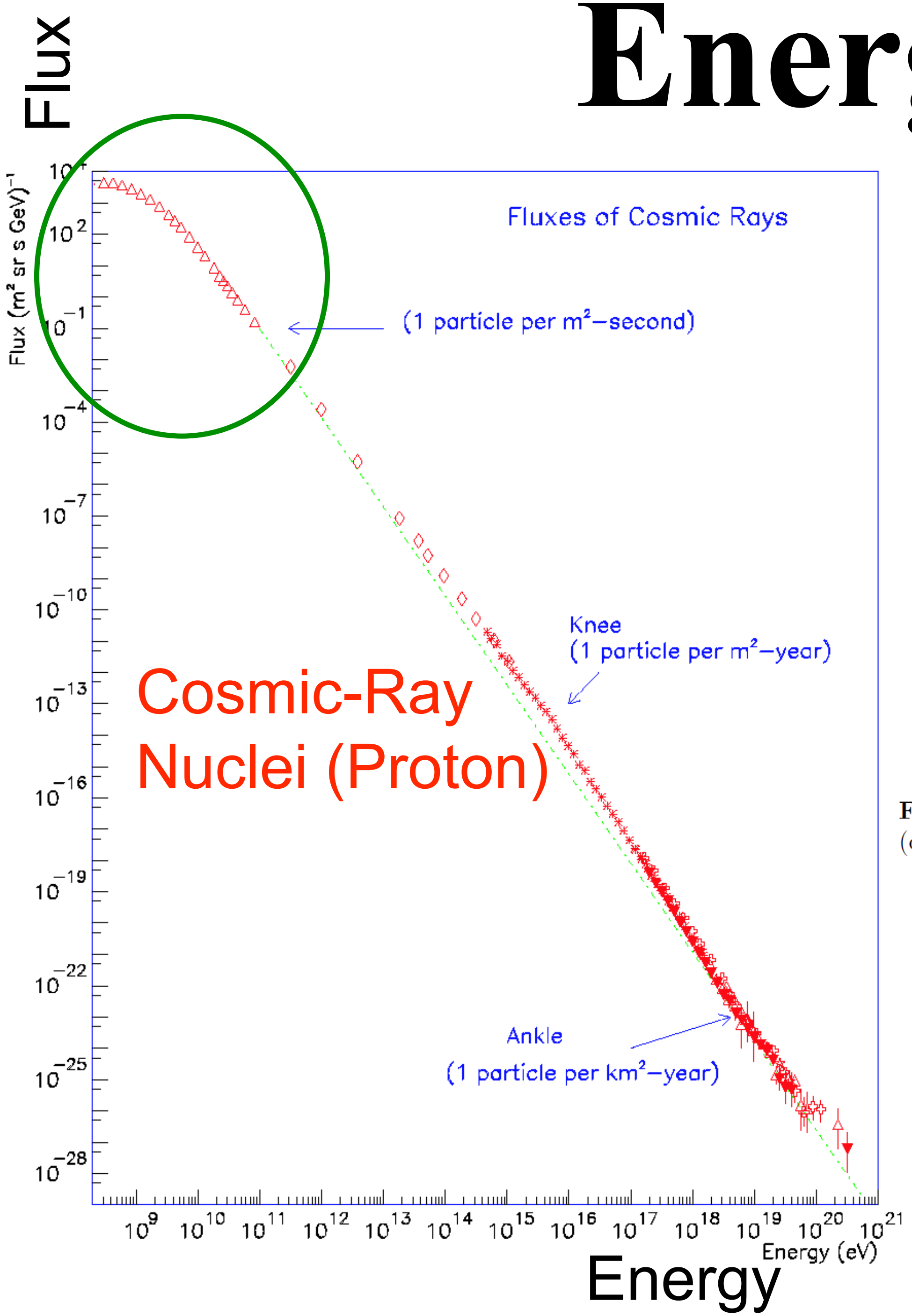

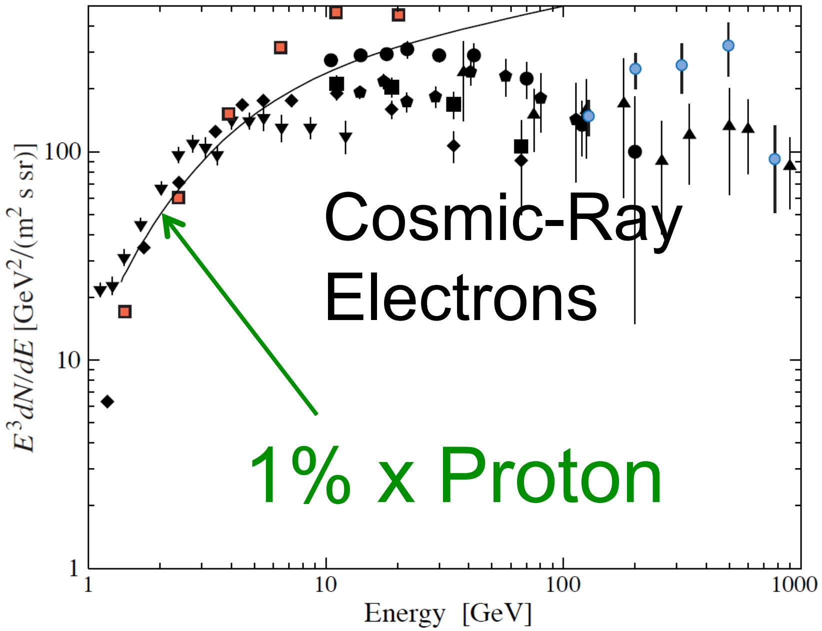

Figure 24.2: Differential spectrum of electrons plus positrons multiplied by E^3 (data from [15–22]) . The line shows the proton spectrum multiplied by 0.01.

ρ(proton)~1eV/cm^3

ρ(electron)~10^{-2}eV/cm^3

ρ(positron)~10^{-3}eV/cm^3

~ 0.1% of p

Dark Matter?

Annihilation

$Q \sim n^2$

$E_{cut} \sim m_{DM}$

$\langle\sigma v\rangle \sim 3\times10^{-24}\,\mathrm{cm^3/s}$

$>3\times10^{-26}\,\mathrm{cm^3/s}$

boost factor ~100

Decay

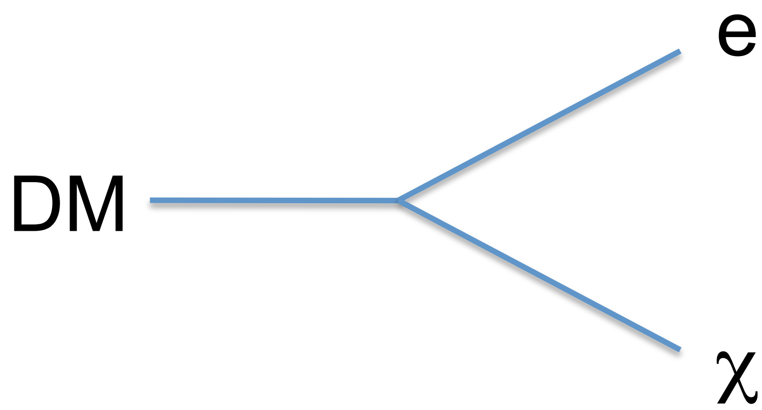

$Q \sim n$

$E_{cut} \sim m_{DM}/2$

$\tau_{decay} \sim 10^{26}\,\mathrm{sec}\ (>H^{-1})$

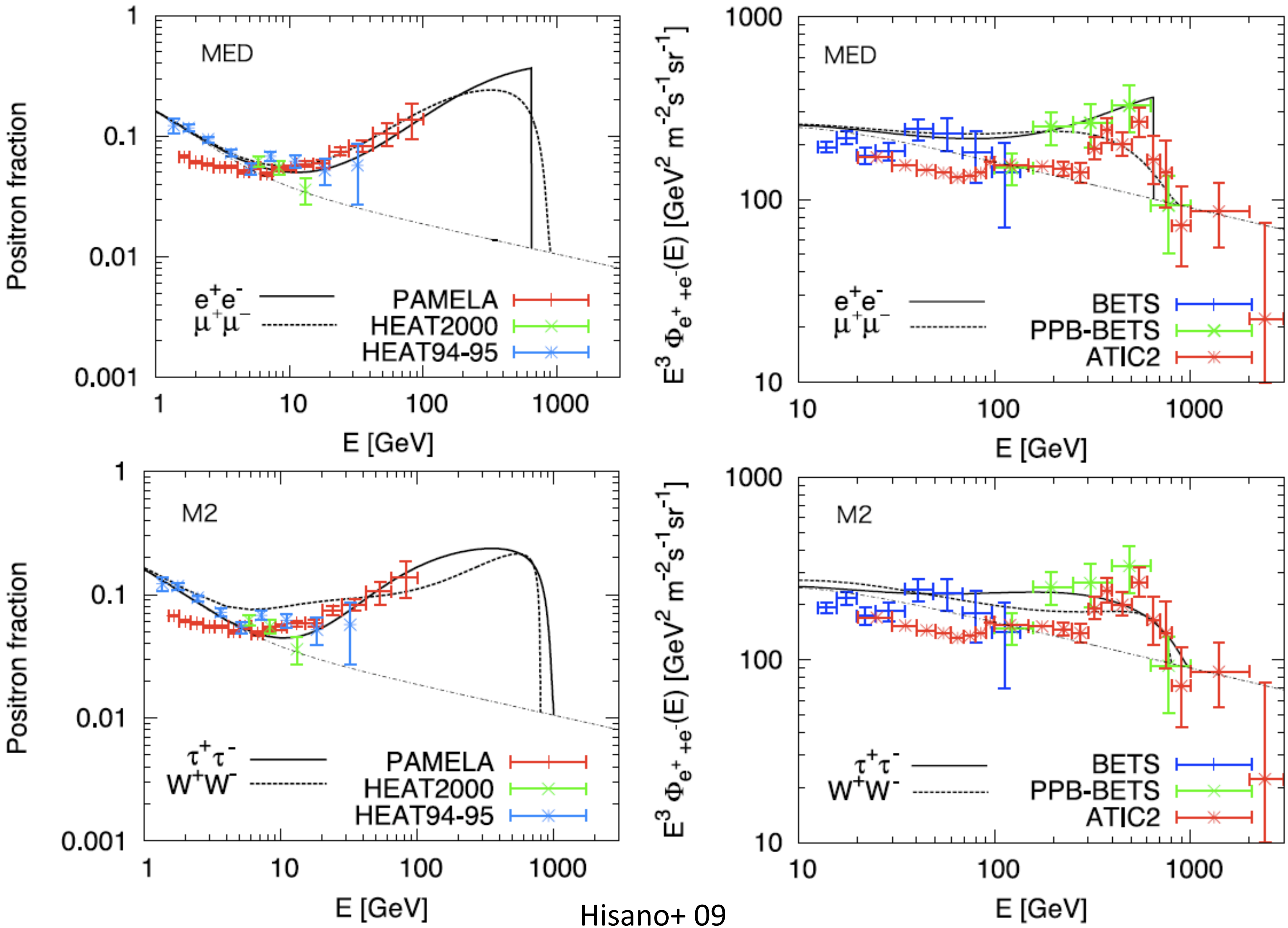

MED
Positron fraction
E [GeV]
e+e-
μ+μ-
PAMELA
HEAT2000
HEAT94-95
MED
E3 Φe+ +e-(E) [GeV2 m-2s-1sr-1]
E [GeV]
e+e-
μ+μ-
BETS
PPB-BETS
ATIC2
M2
Positron fraction
E [GeV]
τ+τ-
W+W-
PAMELA
HEAT2000
HEAT94-95
M2
E3 Φe+ +e-(E) [GeV2 m-2s-1sr-1]
E [GeV]
τ+τ-
W+W-
BETS
PPB-BETS
ATIC2

Hisano+ 09

Positron Fraction

Chen, Nojiri, Takahashi, Yanagida (2008)

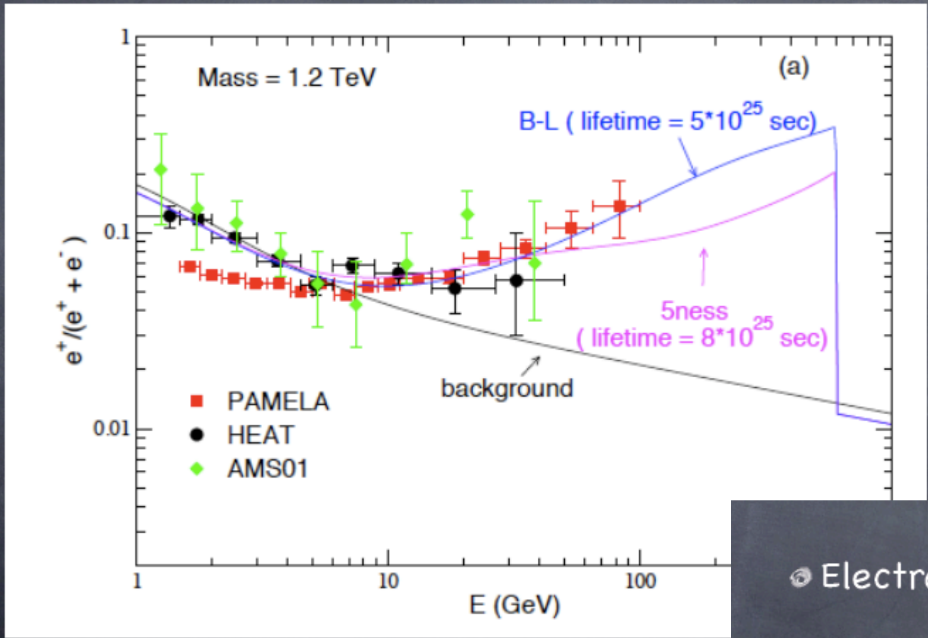

Electron + positron spectrum:

Chen, Nojiri, Takahashi, Yanagida (2008)

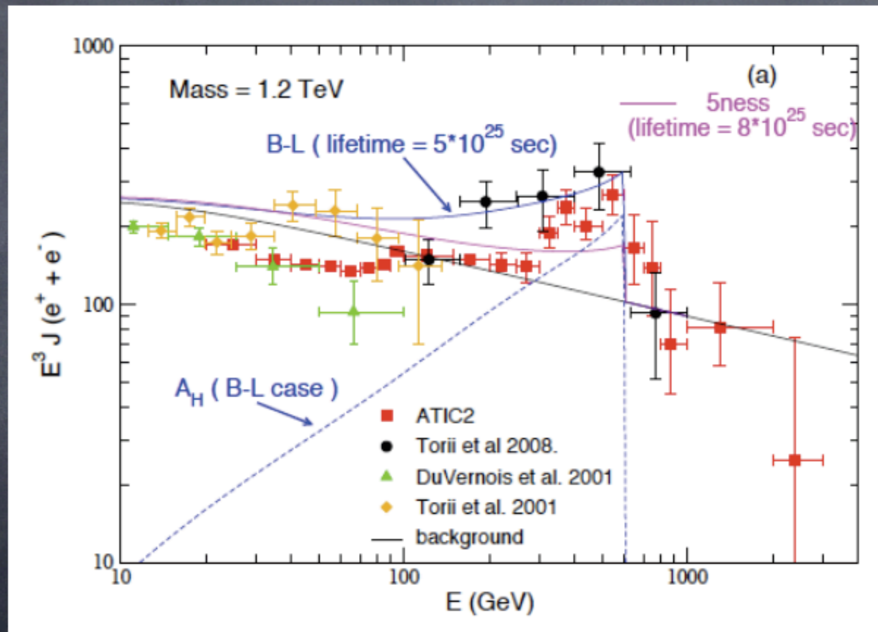

Astrophysical Origin?

Shen 70; Aharonian+ 95; Atoyan et al. 95; Chi+ 96; Zhang & Cheng 01; Grimani 07; Yuksel+ 08; Buesching+ 08; Hooper+ 08; Profumo 08; Malyshev+ 09; Grasso+ 09 Kawanaka, KI & Nojiri 09;

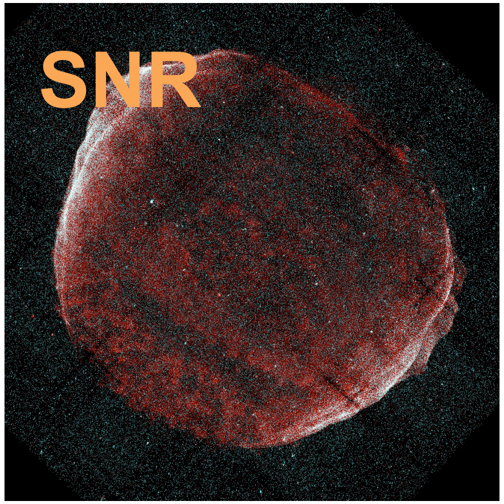

Shen & Berkey 68; Pohl & Esposito 98; Kobayashi+ 04; Shaviv+ 09; Hu+ 09; Fujita+KI 09; Blasi 09; Blasi & Serpico 09; Mertsch & Sarkar 09; Biermann+ 09

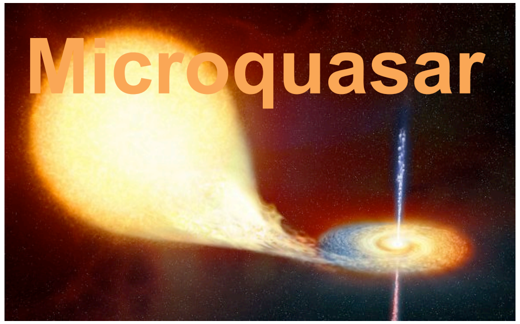

Heinz & Sunyaev 02

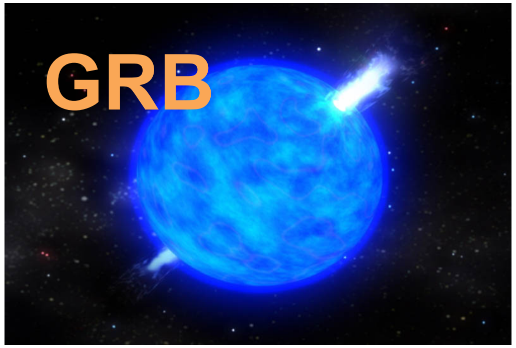

KI 08

Proton Comtami.

Fazely+ 09; Schubnell 09

Propagation

Delahaye+ 08; Cowsik & Burch 09

$$10^{-3} \times \overbrace{10^{50}\mathrm{erg/SN}}^{\text{Cosmic-ray Nuclei energy}}$$

$$\sim (1\mathrm{sec\ pulsar})/\mathrm{SN}$$

$$\sim 10^{50}\mathrm{erg}/10^{3}\mathrm{SN}$$

Simple model

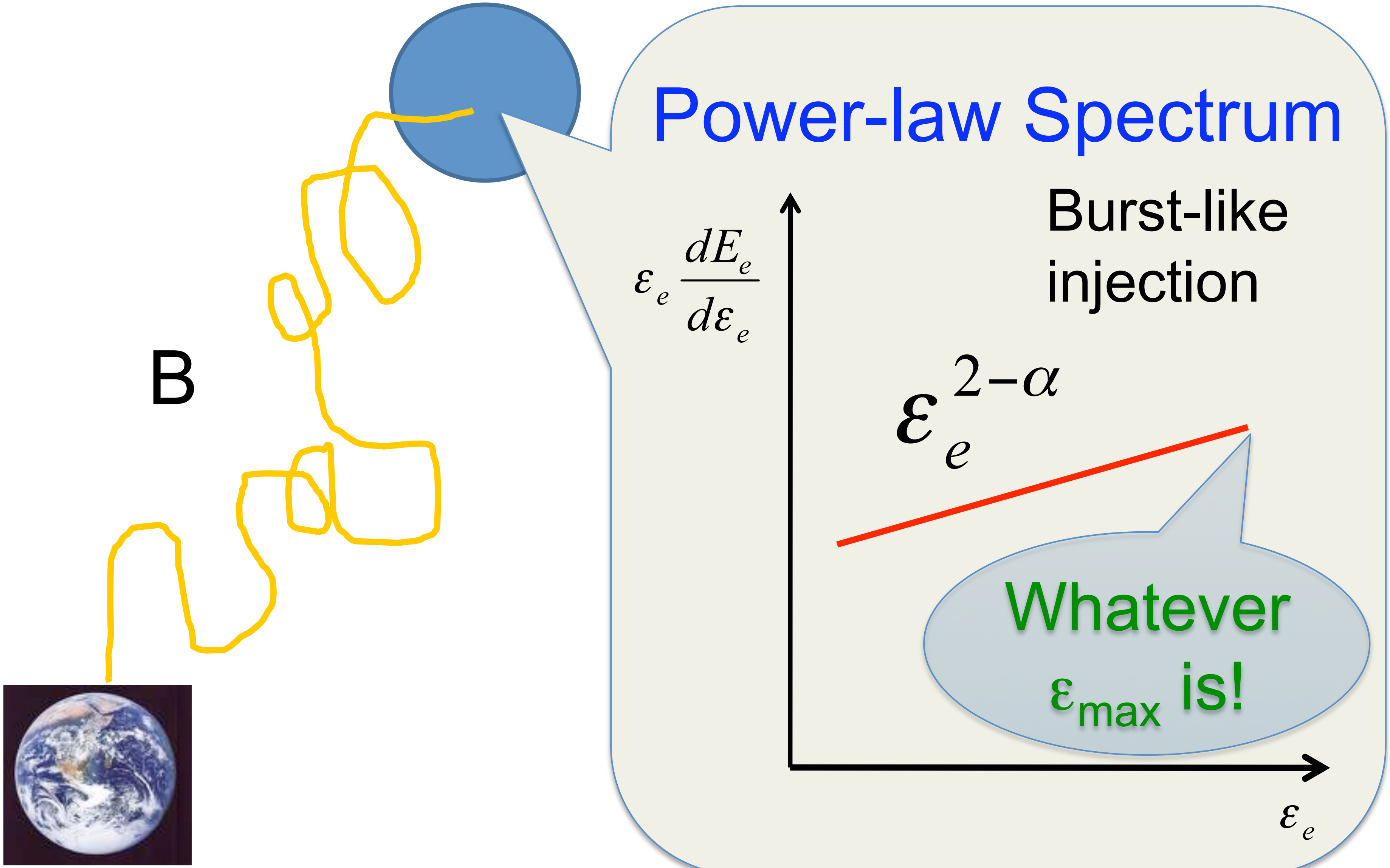

$e^{\pm}$ Propagation

$$\frac{\partial}{\partial t} f\left(t,\varepsilon_e,\vec{x}\right) = \boxed{K(\varepsilon_e)\nabla^2 f} + \boxed{\frac{\partial}{\partial \varepsilon_e}\left[b\varepsilon_e^2 f\right]} + \boxed{q\left(t,\varepsilon_e,\vec{x}\right)}$$

Diffusion

Energy loss by IC & synchro.

Injection

$$b \sim 10^{-16}\,\mathrm{GeV^{-1}s^{-1}}$$

$$K(\varepsilon_e) \sim 5.8\times 10^{28}\,\mathrm{cm^2s^{-1}}\left(1+\frac{\varepsilon_e}{4\mathrm{GeV}}\right)^{1/3}$$

← B/C ratio

For a single burst with $q \propto \varepsilon_e^{-\alpha}$ Power law spectrum

$$f = \frac{q_0\varepsilon_e^{-\alpha}}{\pi^{3/2}d_{diff}^3}\left(1-bt\varepsilon_e\right)^{\alpha-2} e^{-\left(d/d_{diff}\right)^2}$$

$$d_{diff}(t,\varepsilon_e) \sim 2\left[K(\varepsilon_e)t\right]^{1/2}$$

Atoyan+ 95, Shen 70

$$\boxed{\varepsilon_{\mathrm{cut}} \sim \frac{1}{bt}}$$

Positron

We can fit the PAMELA data well

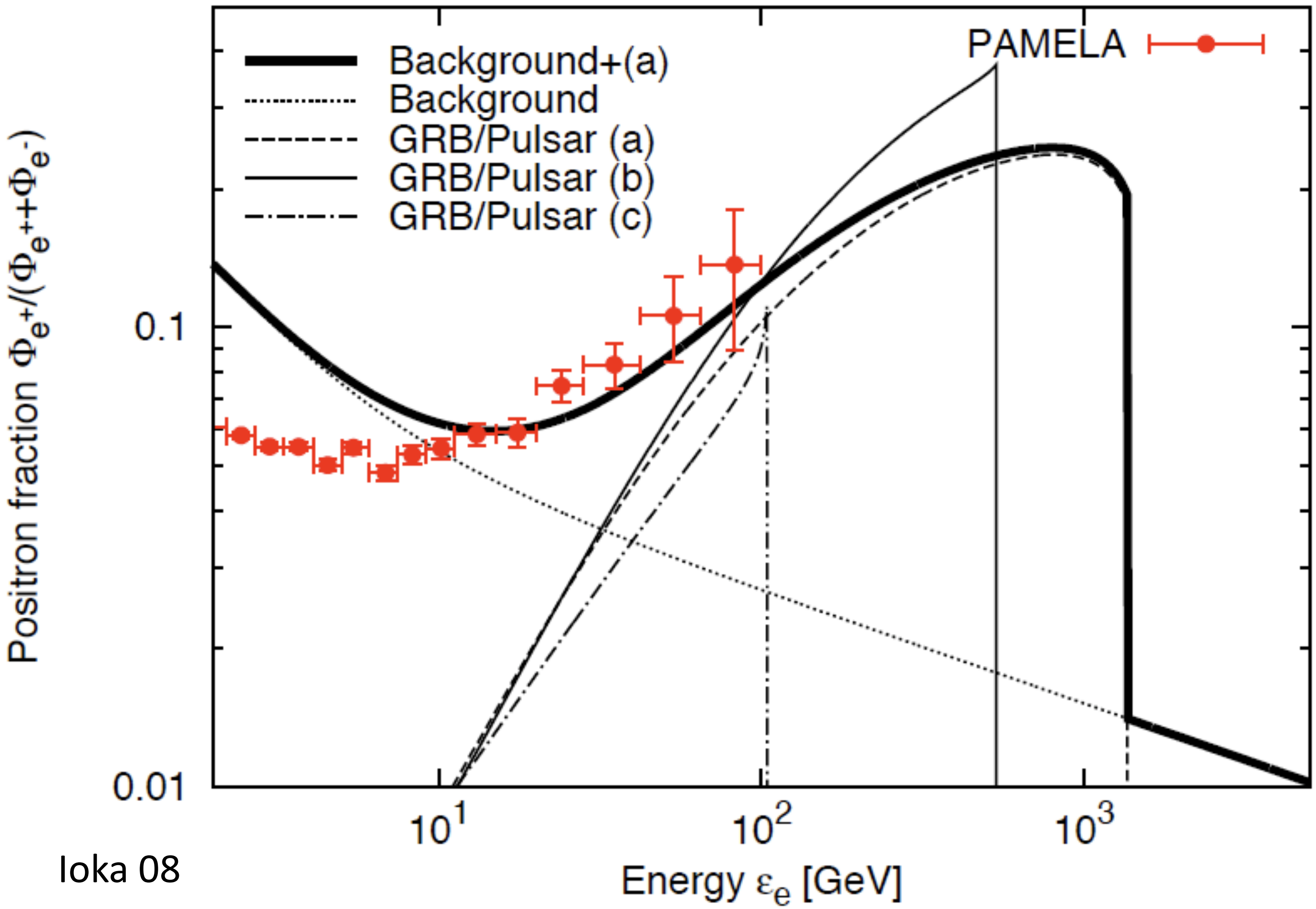

Ioka 08

d=1kpc

(a)
0.9d50 erg
2d5 yr
α=2.5

(b) Harder
0.8d50 erg
5.6d5 yr
α=1.8

(c) Older
3d50 erg
3d6 yr
α=1.8

Electron

ATIC/PPB-BETS & Fermi/HESS

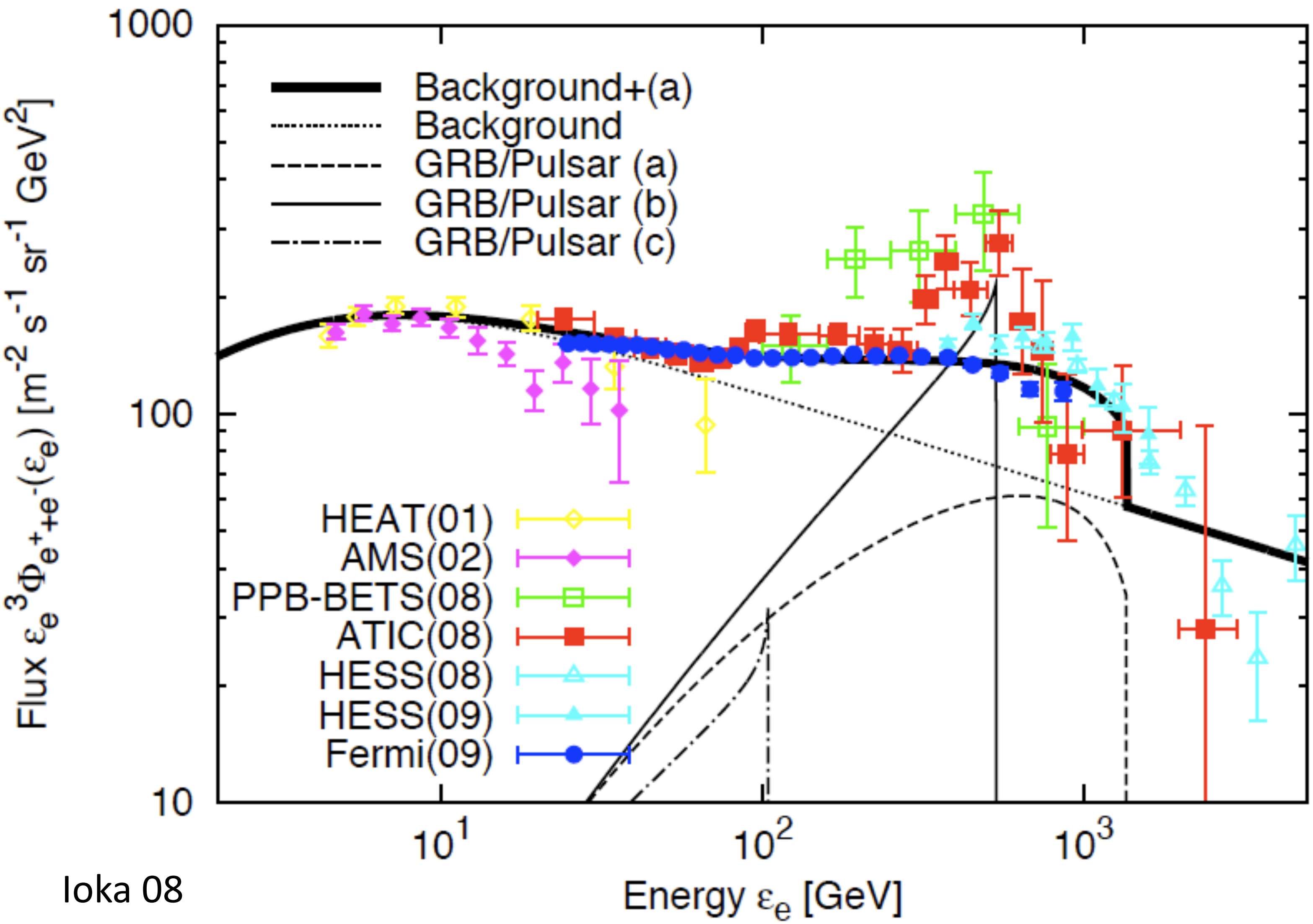

Ioka 08

d=1kpc

(a)
0.9d50 erg
2d5 yr
α=2.5

(b) Harder
0.8d50 erg
5.6d5 yr
α=1.8

(c) Older
3d50 erg
3d6 yr
α=1.8

DM-like Sharp Cutoff

Due to cooling

$$\varepsilon_{\rm cut} = \frac{1}{bt} \simeq 300 \left(\frac{10^6 {\rm yr}}{t_{\rm age}} \right) {\rm GeV}$$

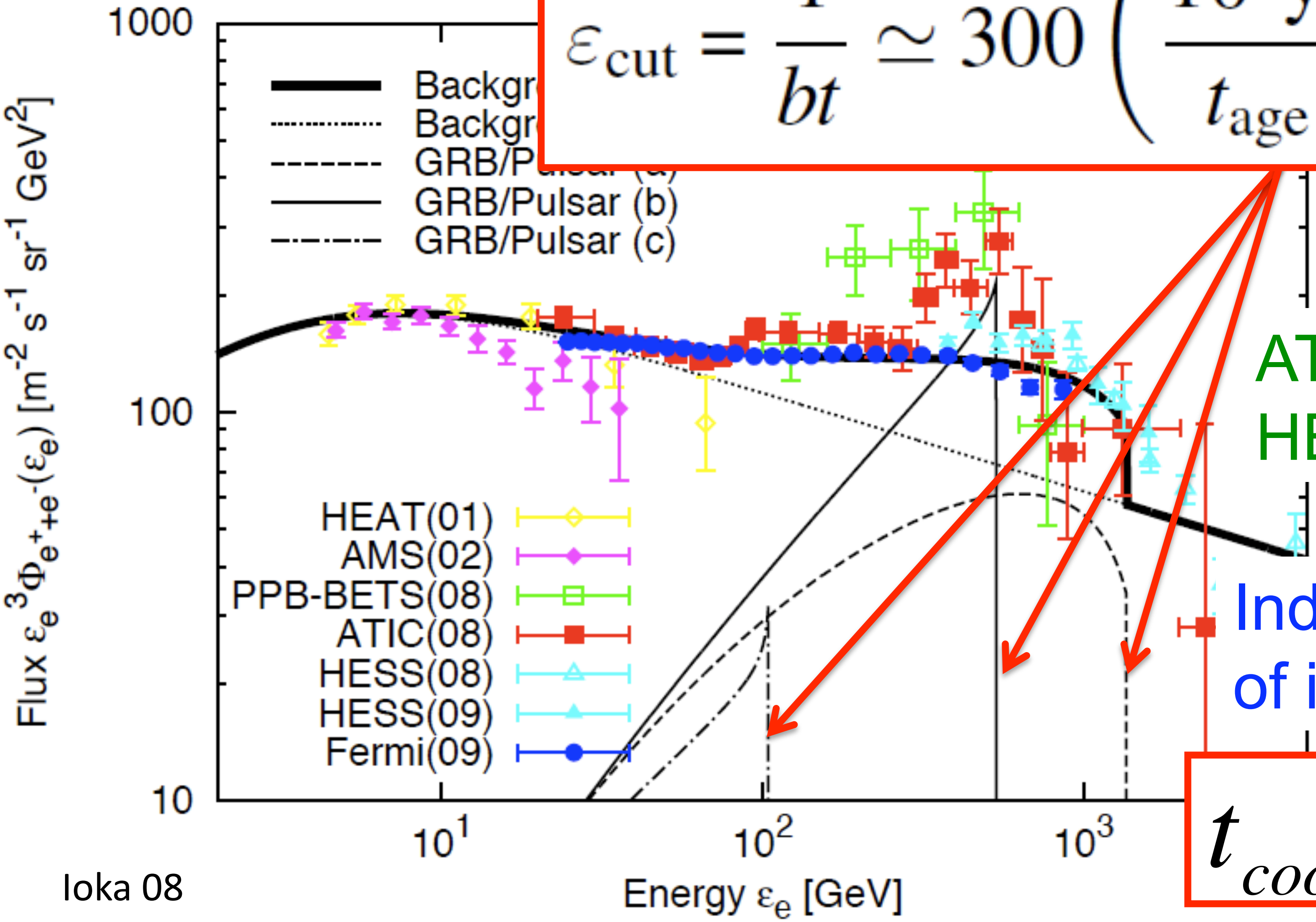

Ioka 08

ATIC peak
HESS cutoff

Independent of initial ε_{max}

$$t_{cool} \propto \varepsilon_e^{-1}$$

Continuous injection

$$F(t,\varepsilon_e) = \int_0^t dt' \frac{Q_0(t')\varepsilon_e^{-\alpha}}{\pi^{3/2} r_{diff}^3} \left(1 - bt'\varepsilon_e\right)^{\alpha-2} \exp\left(-\frac{r^2}{r_{diff}^2}\right)$$

Case 1: pulsar-type decay

$$Q_0(t) \propto L_{\text{spindown}} = \frac{E_{tot}}{\tau_0 \left(1 + t/\tau_0\right)^2}$$

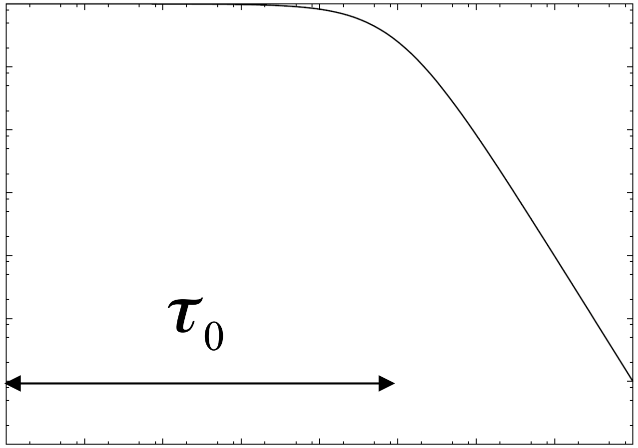

Case 2: exponential decay

$$Q_0(t) \propto \frac{E_{tot} \ln 4}{\tau_0} \exp\left(-\frac{t \ln 4}{\tau_0}\right)$$

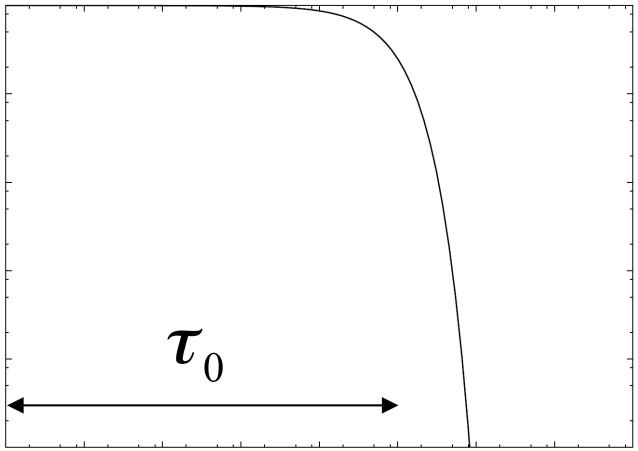

Continuous Injection

Cutoff width $\Delta\varepsilon_{cut}$

$$\left(\frac{\Delta\varepsilon_{\rm cut}}{\varepsilon_{\rm cut}}\right)_{\Delta t} \sim 10\% \left(\frac{\Delta t}{10^5 {\rm yr}}\right)\left(\frac{t_{\rm age}}{10^6 {\rm yr}}\right)^{-1}$$

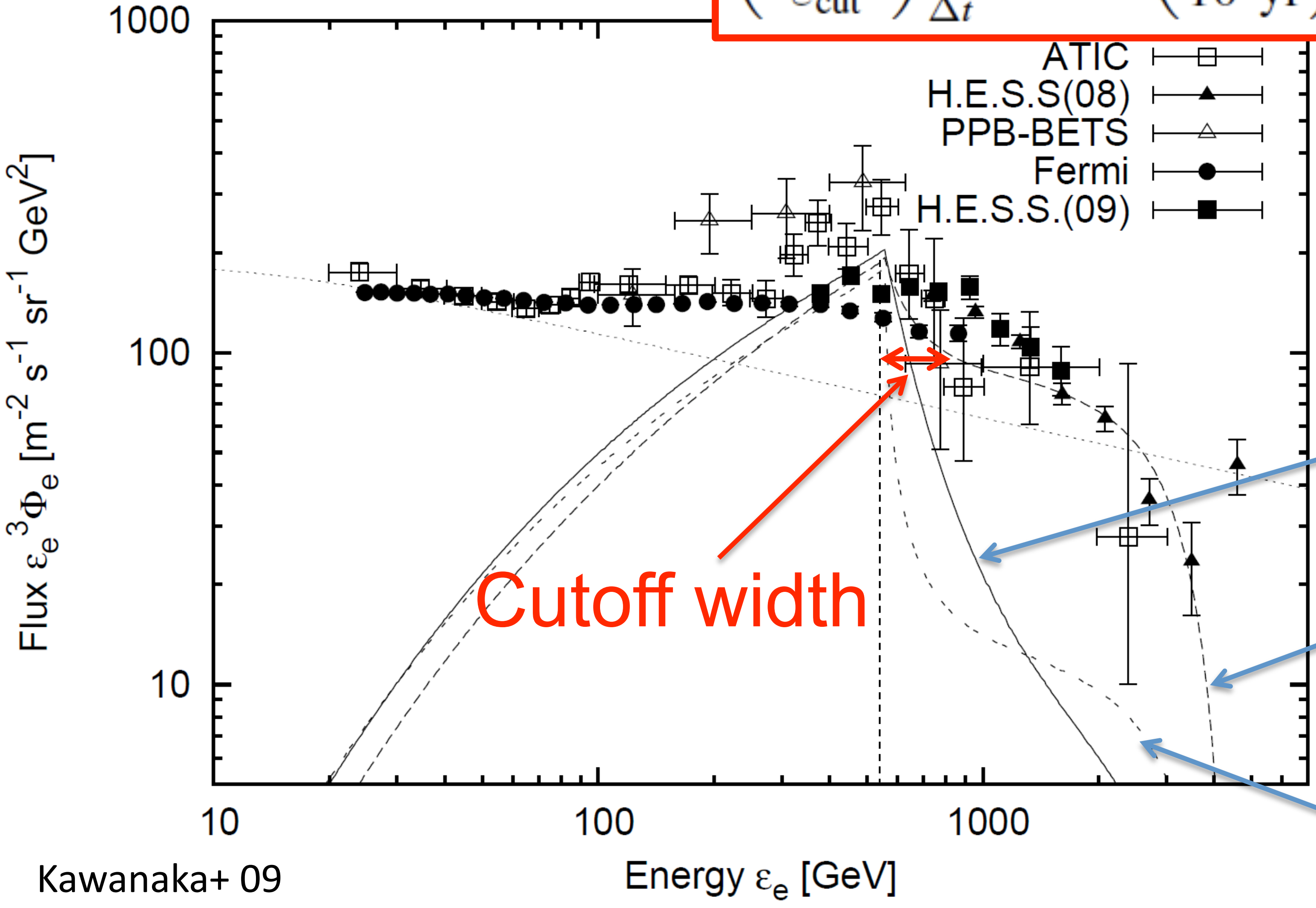

Kawanaka+ 09

⇒ Model selection (CALET)

Δt~10^5yr e^{-t} decay

Δt~10^5yr t^{-2} decay

Δt~10^4yr t^{-2} decay

Astrophysical Models

Shen 70; Aharonian+ 95; Atoyan et al. 95; Chi+ 96; Zhang & Cheng 01; Grimani 07; Yuksel+ 08; Buesching+ 08; Hooper+ 08; Profumo 08; Malyshev+ 09; Grasso+ 09 Kawanaka, KI & Nojiri 09;

Proton Comtami.

Fazely+ 09; Schubnell 09

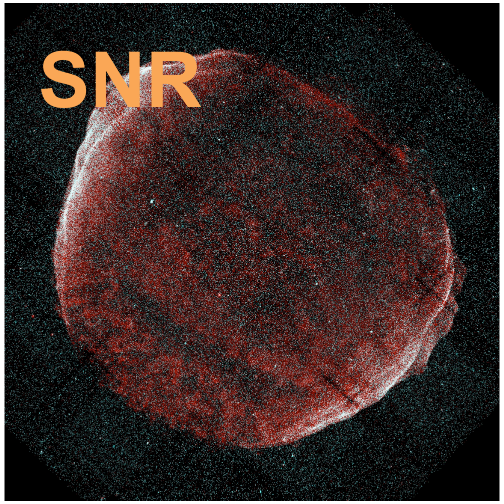

Shen & Berkey 68; Pohl & Esposito 98; Kobayashi+ 04; Shaviv+ 09; Hu+ 09; Fujita+KI 09; Blasi 09; Blasi & Serpico 09; Mertsch & Sarkar 09; Biermann+ 09

Propagation

Delahaye+ 08; Cowsik & Burch 09

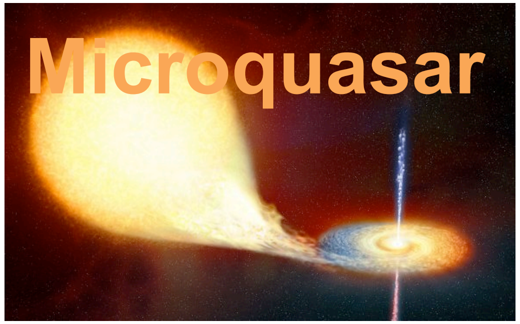

Heinz & Sunyaev 02

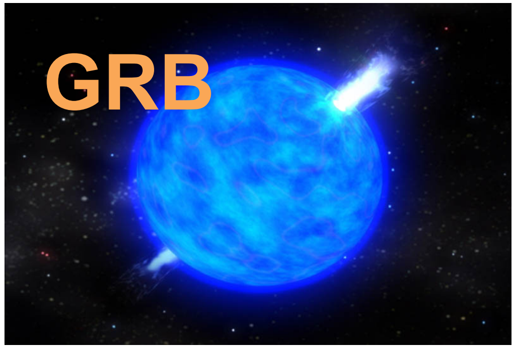

KI 08

$\sim 10^{50}$erg $e^{\pm}$

$\sim 10^{5\text{-}6}$yr ago

Pulsar

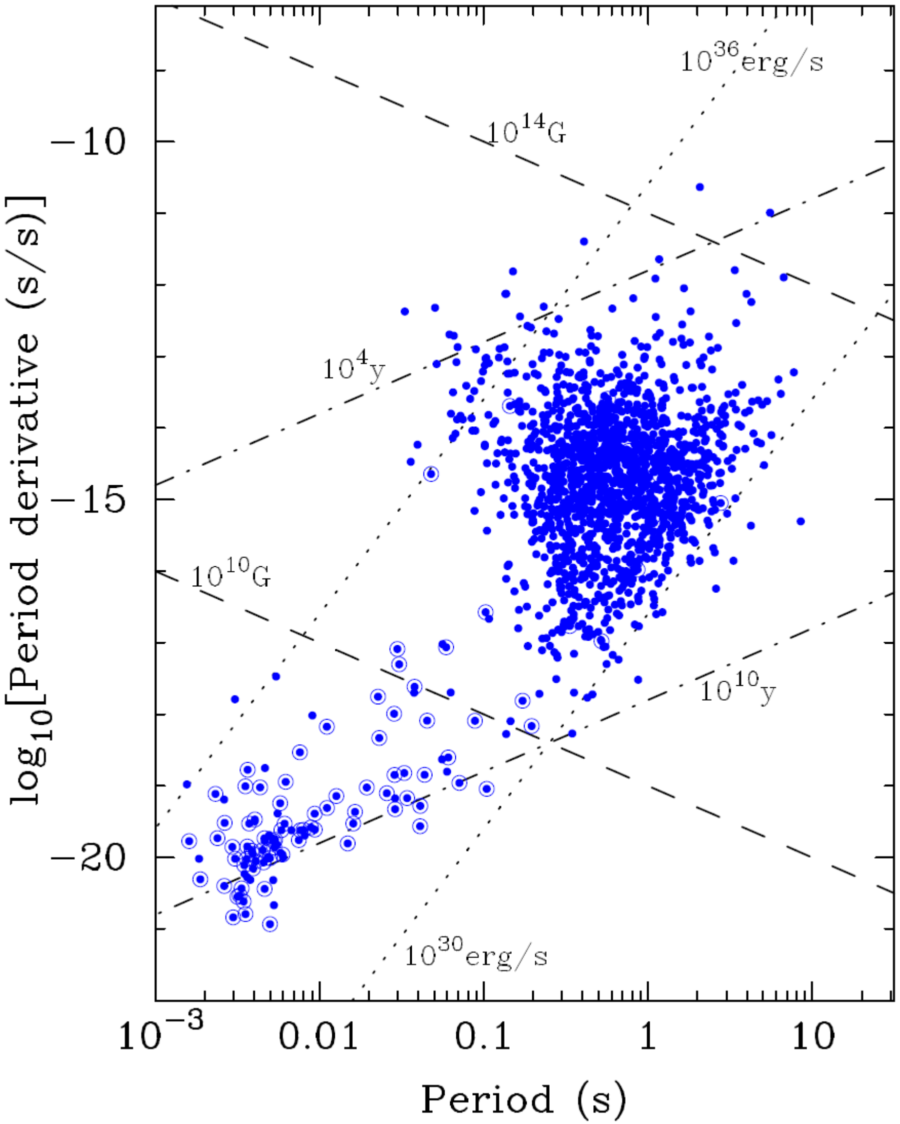

Lorimer 08

R. Romani's talk

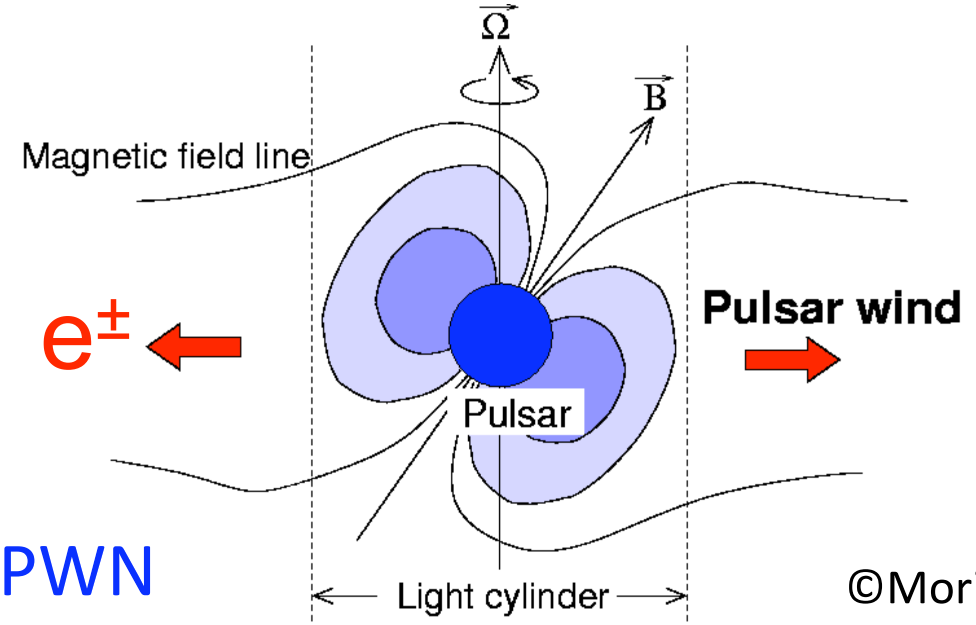

PWN

©Mori

$$\Delta V \approx \frac{\Omega^2 B_s R^3}{c^2}$$

$$= 10^{16} \left(\frac{\Omega}{10^2\ \mathrm{s}^{-1}}\right)^2 \left(\frac{B_s}{3 \times 10^{12}\ \mathrm{G}}\right)\left(\frac{R}{10^6\ \mathrm{cm}}\right)^3 \mathrm{V},$$

Goldreich&Julian 69

Multiple Injection (e^+)

⇒ Smooth Spectra & Reasonable Energy

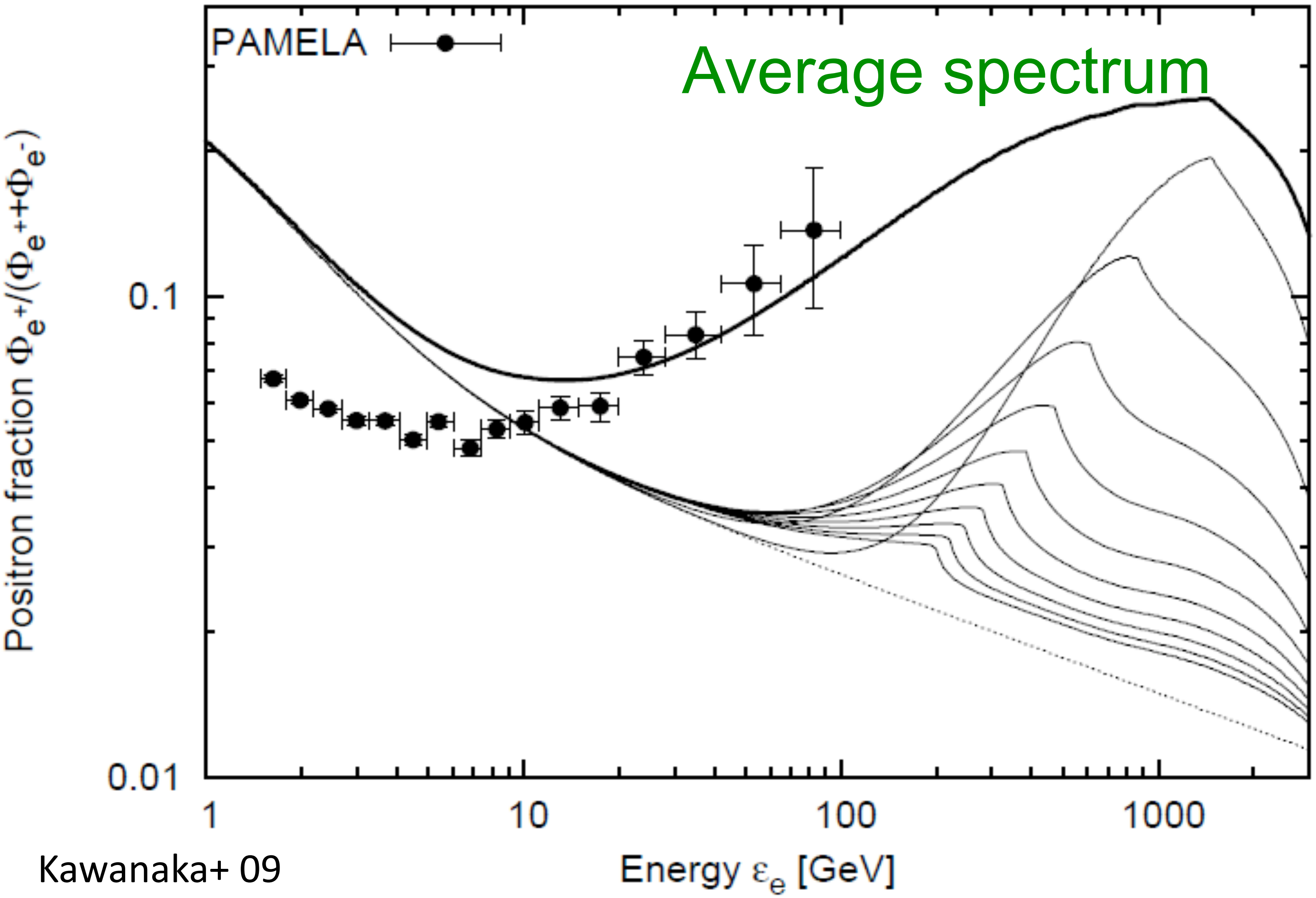

Kawanaka+ 09

Birth rate: one per 1.5×10^5 yr (including off-axis pulsars)

$E\sim10^{49}$erg

$\alpha\sim1.7$

Multiple Injection (e^-+e^+)

Average spectrum ~ Fermi but ≠ATIC

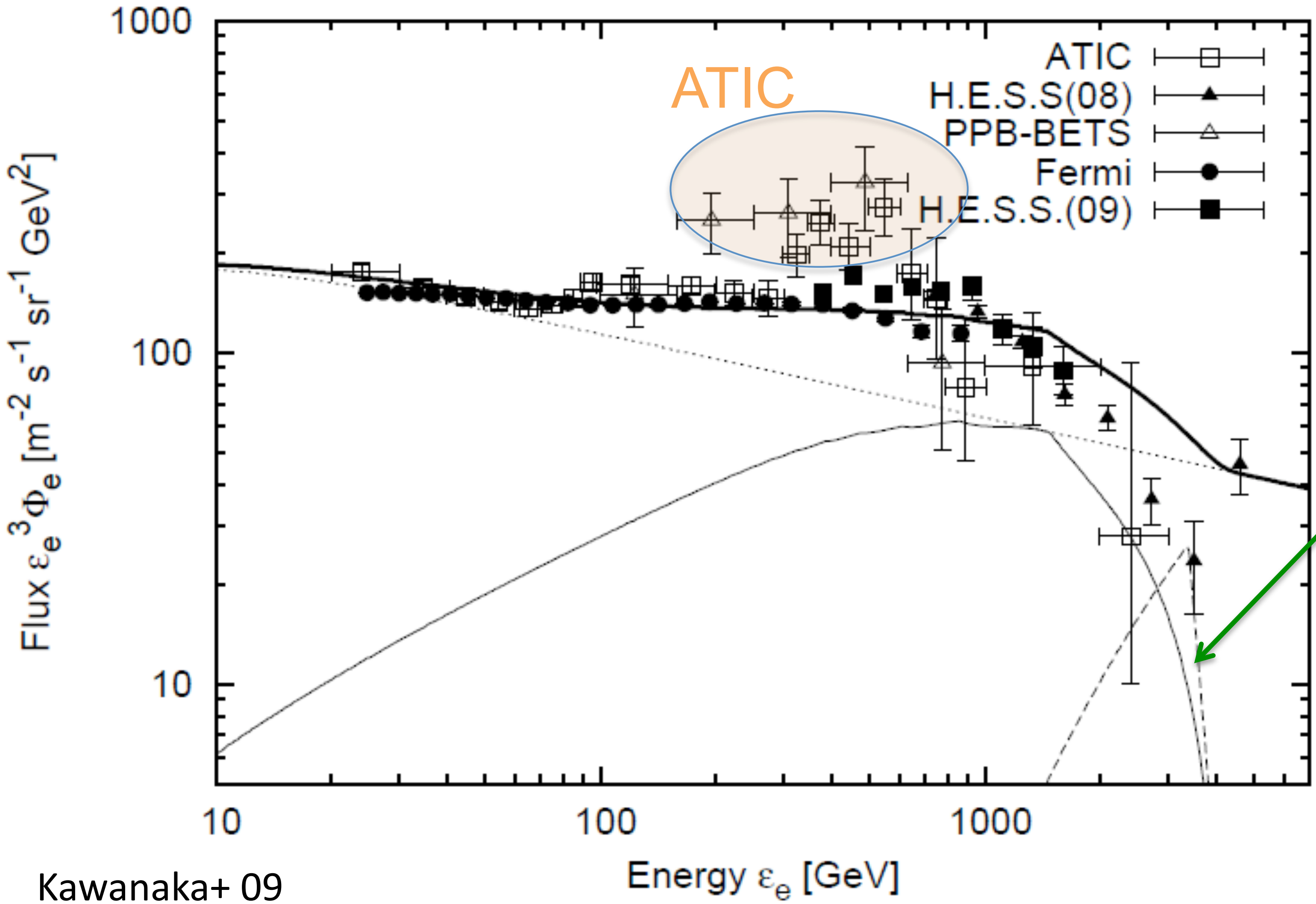

Kawanaka+ 09

ATIC peak requires energetic source

~3×10^4yr
~10^{48}erg
⇒ Young source is less energetic

Single v.s. Multiple

A single source ⇒ A relatively large anisotropy

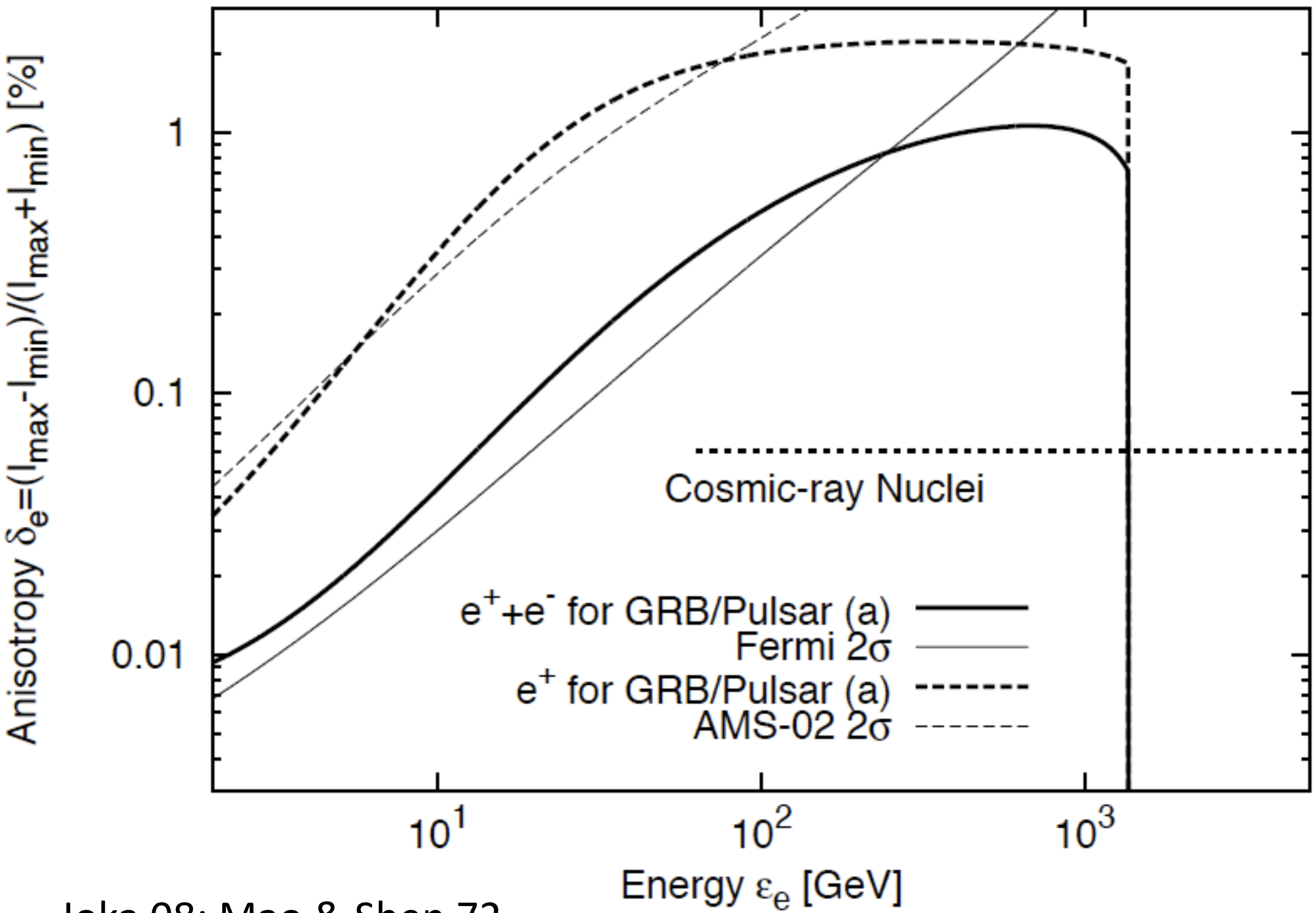

$$\delta = \frac{I_{\max} - I_{\min}}{I_{\max} + I_{\min}}$$

$$= \frac{3K|\nabla f|}{cf}$$

$$\sim \frac{3d}{2ct} @ \varepsilon_e \sim \varepsilon_{\max}$$

Challenging

DM clump

Ioka 08; Mao & Shen 72

Gamma-ray pulsars

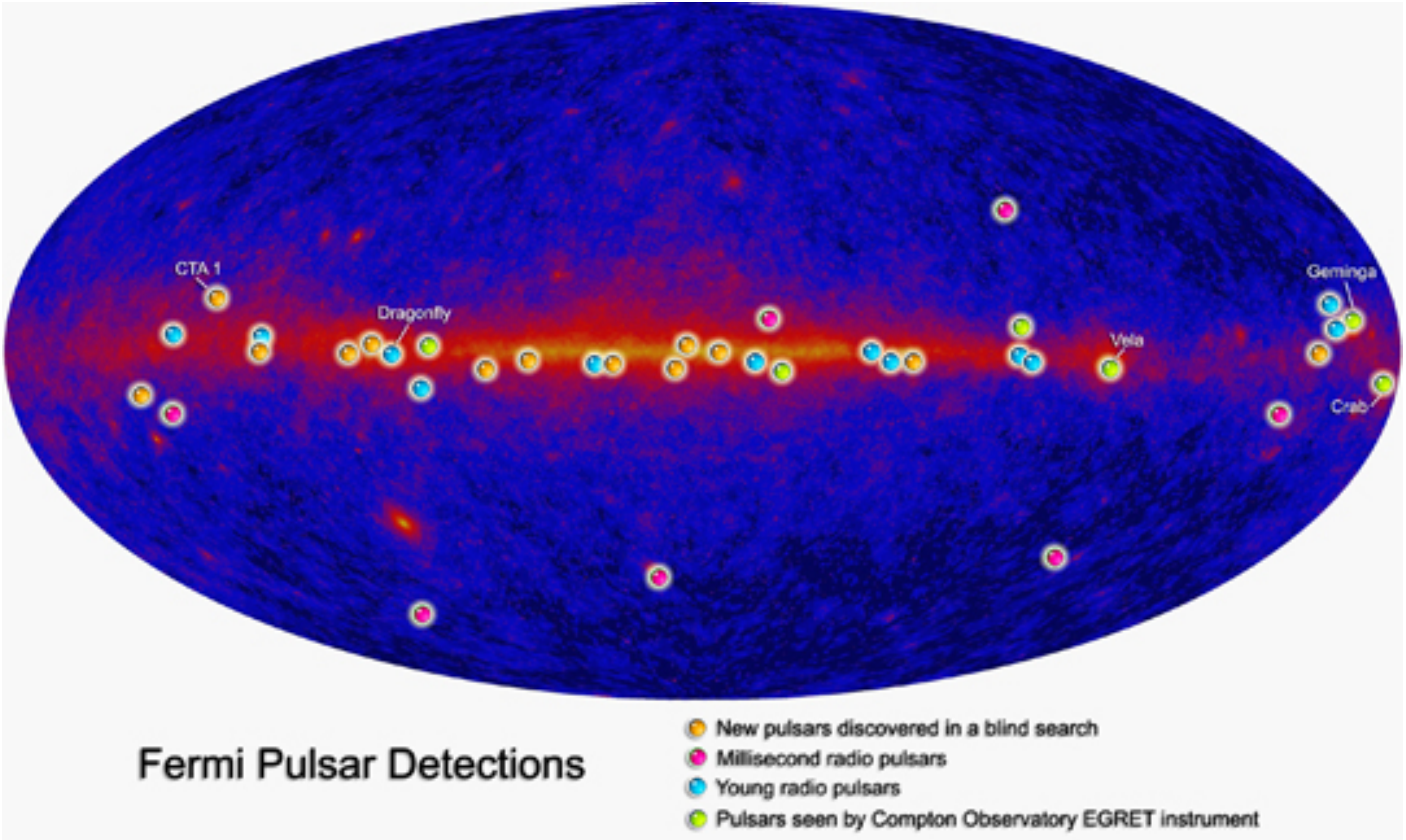

γ-ray only pulsar CTA1

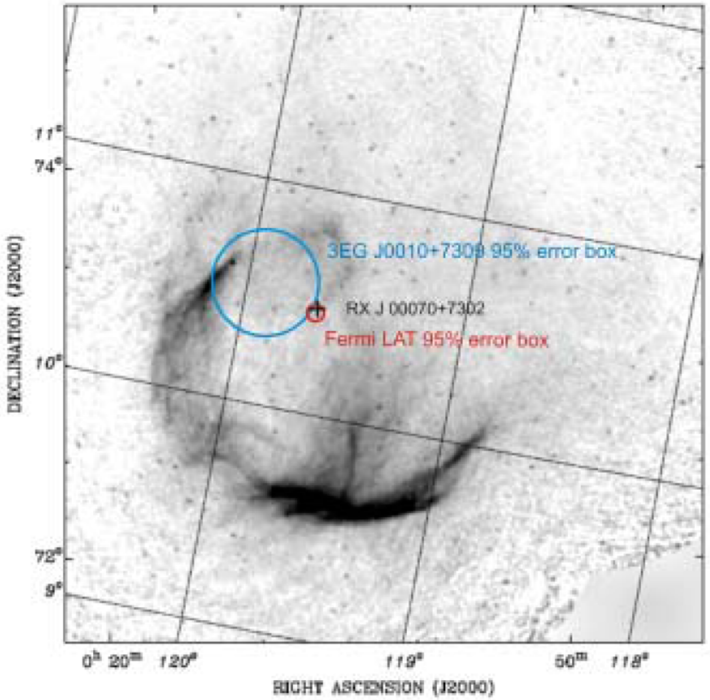

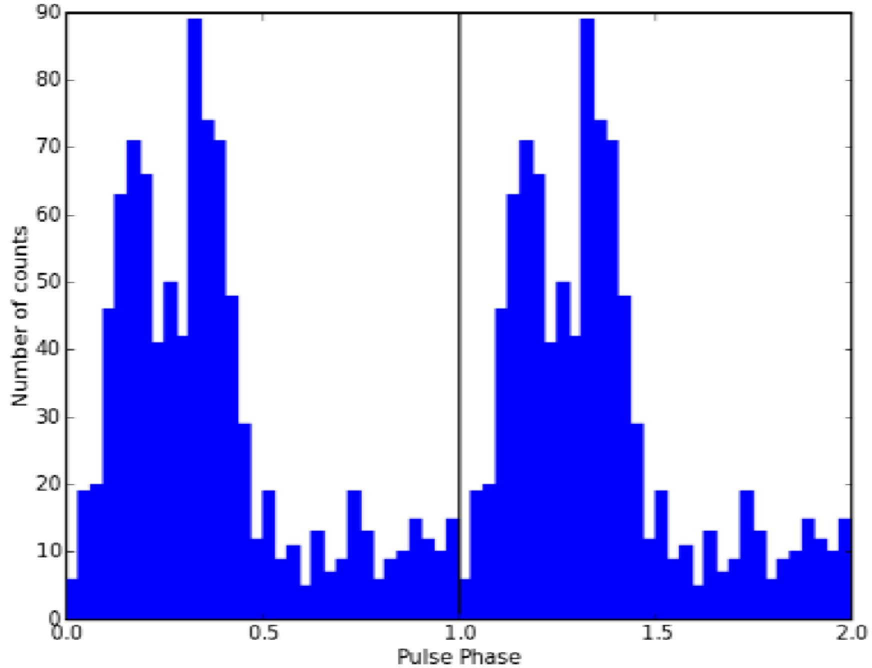

Abdo+ 08

Fig. 1: The *Fermi* LAT gamma-ray source, the central PWN X-ray source, and the corresponding *EGRET* source superimposed on a 1420 MHz map (*7*) of CTA 1. The LAT source and its 95% error region (small red circle) is displayed on the map together with the central PWN source RX J00070+7302 (cross) and the position and error of the corresponding *EGRET* source 3EG J0010+7309 (large blue circle). The coincidence of the pulsed gamma-ray source and the X-ray point source embedded in the off-center PWN is striking. The offset of the pulsar from the center of the radio SNR, which is thought to be the place of origin, is quite visible. The inferred transverse speed of the pulsar is ~450 km/s, which is a reasonable speed of a pulsar (*20*).

Fig. 3: Gamma-ray (>100 MeV) light-curve of the pulsar in CTA 1 shown over two periods of rotation with a resolution of 32 phase bins per period (corresponding to ~10 ms/bin). The two maxima in the broad emission feature each have a FWHM of ~0.12 and are separated by about 0.2 in phase. Overall, the LAT pulsar light-curve is similar to the gamma-ray light-curve of the *EGRET* pulsar PSR B1706-44 (*21*).

Pulsar and PWN

⇔ GeV-TeV unID sources

SNR

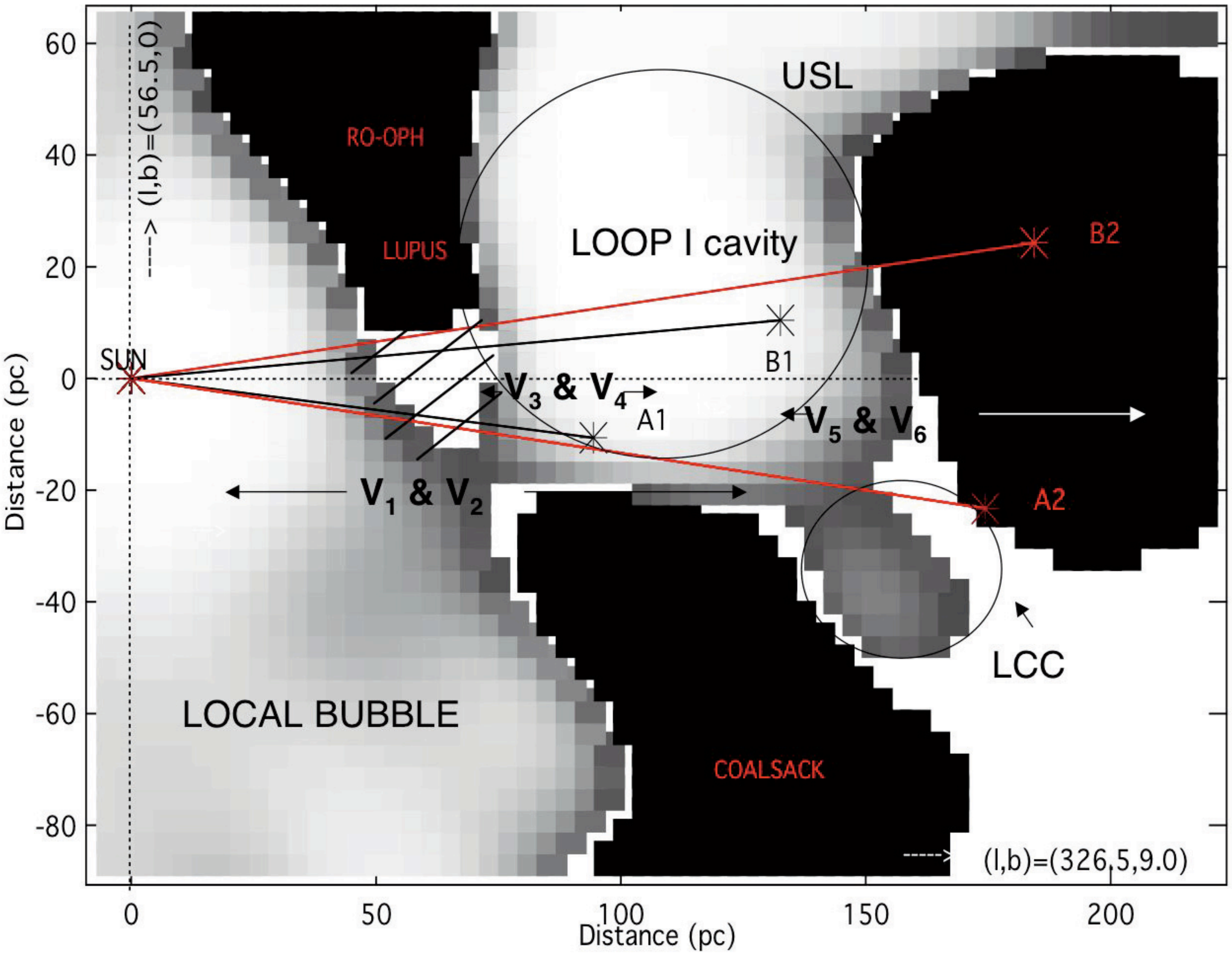

Welsh & Lallement 05

Local bubble
Loop I, …
← 20-40 SNe
at ~100 pc

Nearby SNRs surely affect the solar environments

SNR model (ATIC)

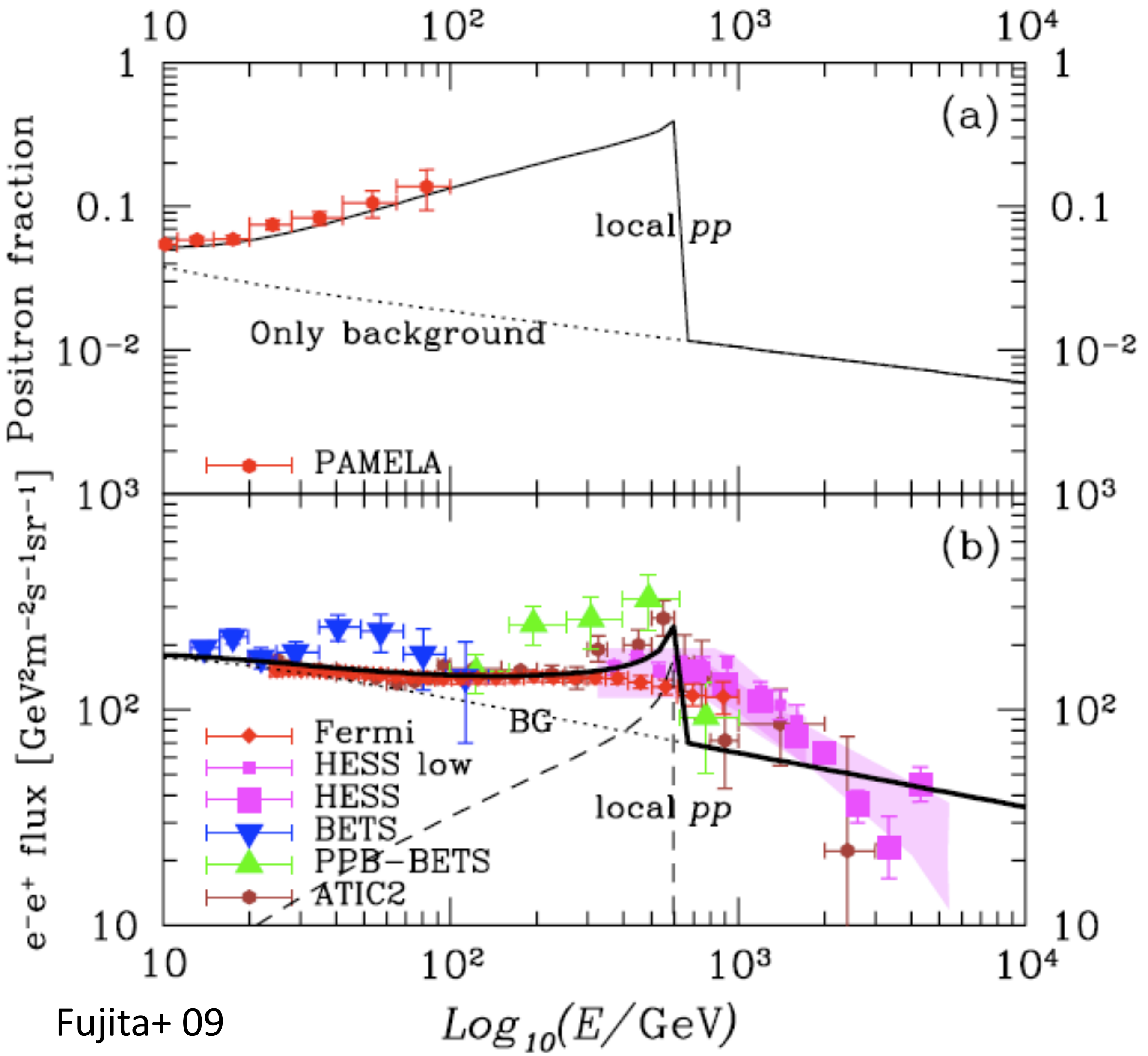

Fujita+ 09

Massive stars born in Dense Clouds

⇒ Supernova

⇒ Shock acc.

⇒ $pp \to e^+e^-$

$R \sim 40$pc,
$n \sim 100\,cm^{-3}$,
$d = 200$pc
$s = 1.4$,
$t_{pp} = 5 \times 10^5$yr,
$E_p = 3 \times 10^{50}$erg

SNR model (Fermi)

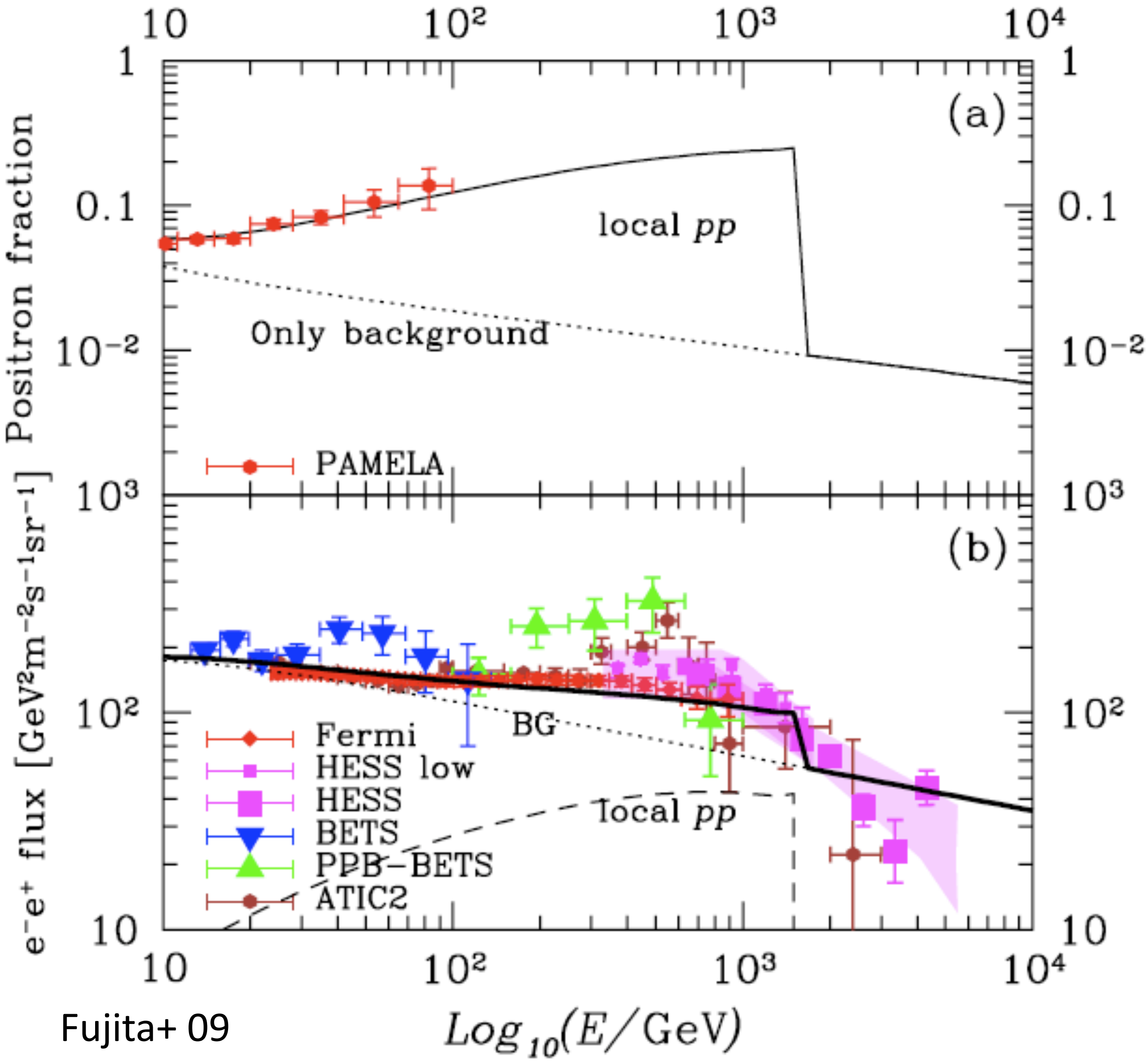

Fujita+ 09

Massive stars born in Dense Clouds
⇒ Supernova
⇒ Shock acc.
⇒ pp → e^+e^-

R~40pc,
n~$50cm^{-3}$,
d=200pc
s=1.75,
$t_{pp}=2x10^5yr$,
$E_p=3x10^{50}erg$

Hadronic v.s. Leptonic

Anti-proton fraction

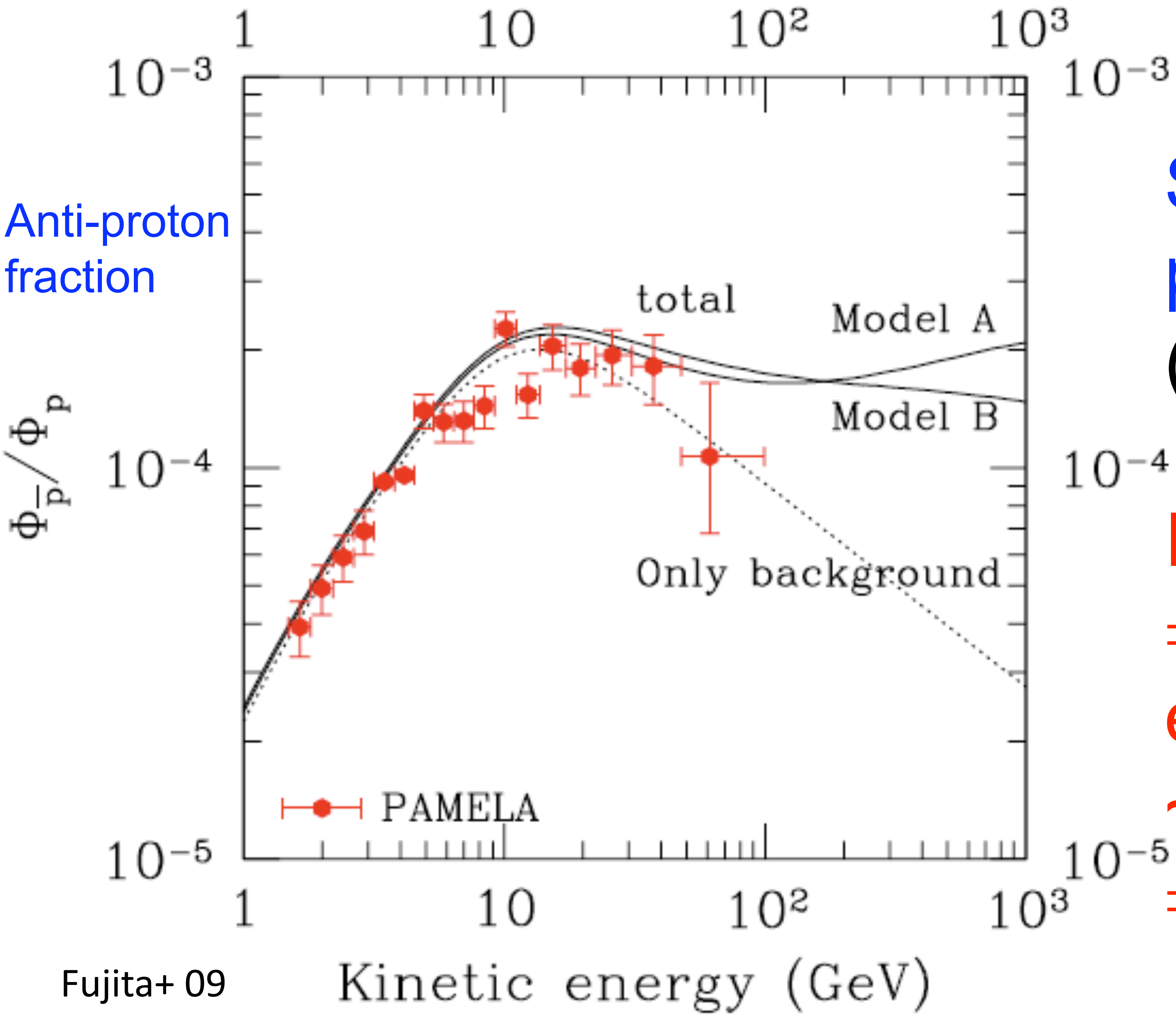

Fujita+ 09

SNR model:
pp → π^+ → e^+e^-
(w/ ISM/DC)

Inevitably
⇒ anti-proton excess above ~100 GeV
⇒ PAMELA

2nd Nuclei for Hadronic

Hadronic models ⇒ Secondary Nuclei Excesses

Titanium-to-iron ratio

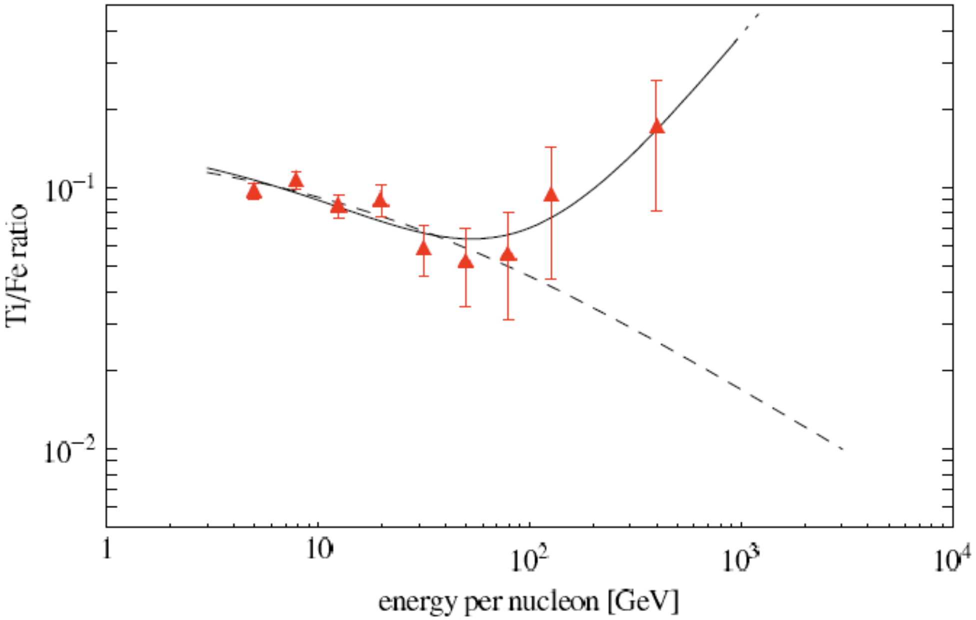

FIG. 1: The titanium-to-iron ratio in cosmic rays along with model predictions — the 'leaky box' model with production of secondaries during propagation only (dashed line), and including production and acceleration of secondaries in a nearby source (solid line - dotted beyond the validity of our calculation). The data points are from ATIC-2 [26].

Boron-to-carbon ratio

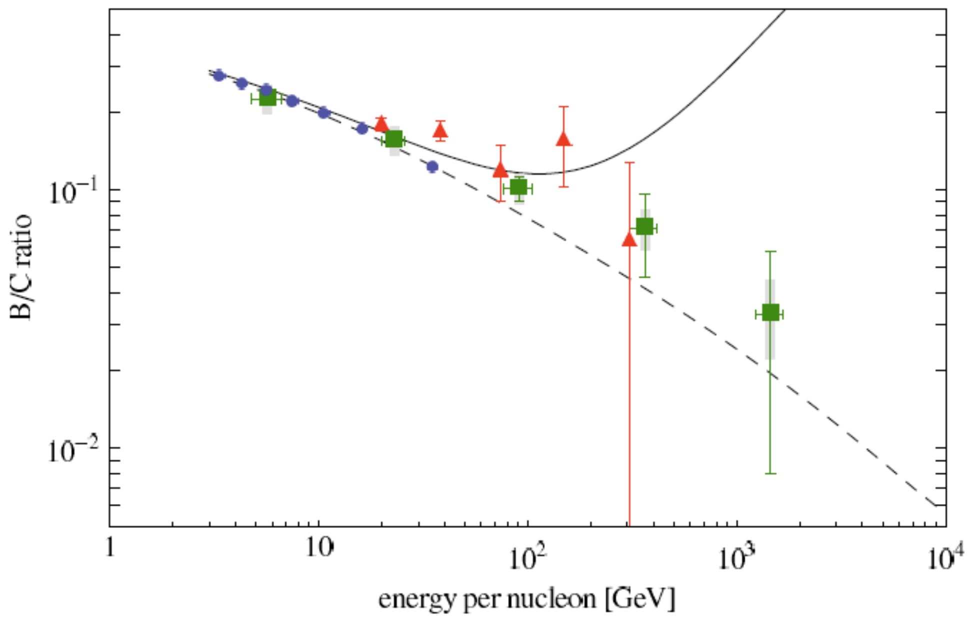

FIG. 2: The boron-to-carbon ratio in cosmic rays along with model predictions — the 'leaky box' model with production of secondaries during propagation only (dashed line), and including production and acceleration of secondaries in a nearby source (solid line). The data points are from HEAO-3 (circles) [30], ATIC-2 (triangles) [33] and CREAM (squares) [34].

Mertsch and Sarkar 09

SNR model features

Hard spectrum for e^+e^-

Radiative phase $t_{\rm age} > t_2 = 3.5 \times 10^3 E_{51}^{4/17} n_2^{-9/17}$ yr

$$N_p(E) \propto E^{-s} \exp(-E/E_{\rm max,p})$$

$$s = (r+2)/(r-1) < 2$$

$$E_{\rm max,p} = 1.6 \times 10^2 \ h^{-1} v_{s,8}^2 \left(\frac{B_{\rm d}}{10\ \mu{\rm G}}\right)\left(\frac{t_{\rm age}}{10^5 {\rm yr}}\right) \ {\rm TeV}$$

Low Gamma-ray and Neutrino Signals

The SNR destroyed the Dense Cloud

Anti-proton and Secondary Nuclei excess above ~100GeV

Inhomogeneous SNRs?

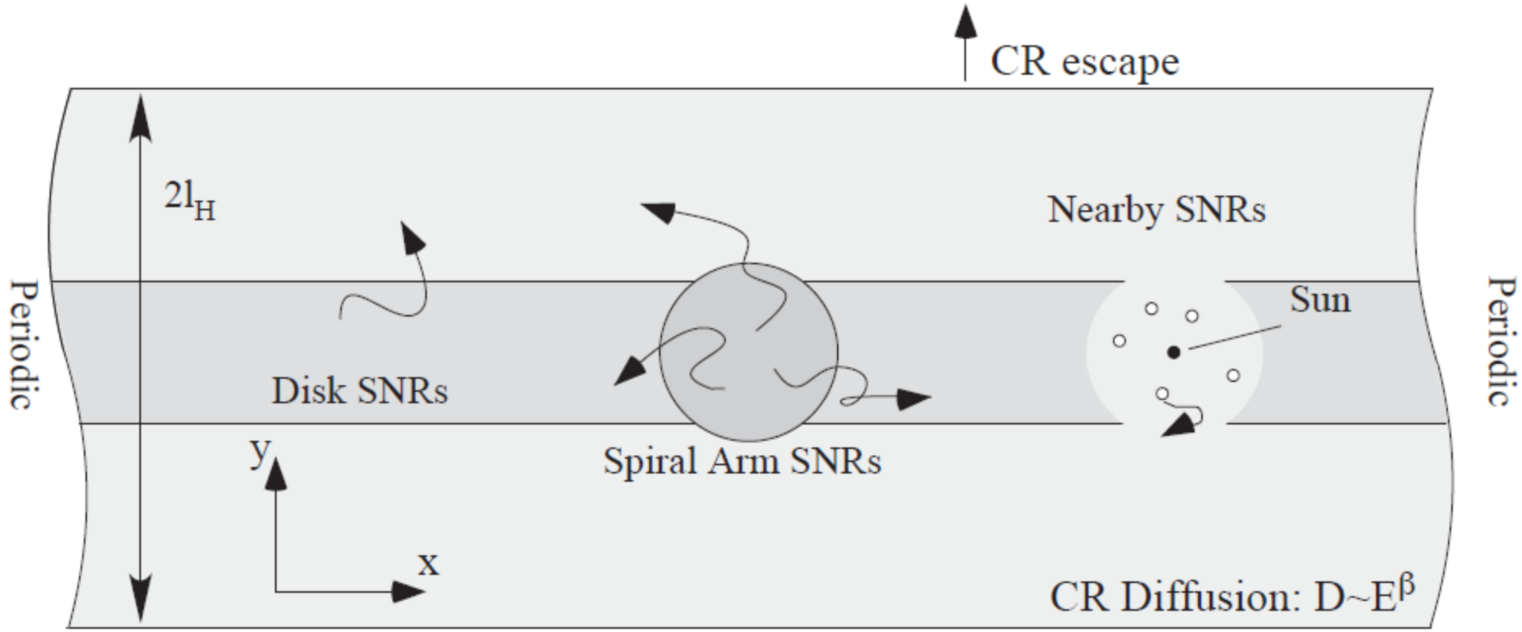

Shaviv+ 09

Figure 1: The CR flux diffusion model. We assume that the SNe remnant distribution has two components. The primary component resides in spiral arms with a Gaussian cross-section. Because the opening pitch angle i of the arms is small, they can be assumed to be long cylinders (with their main axis perpendicular to the plane of the figure), making the problem effectively 2D. The angle between the x-axis and the galactic radial axis, is the small pitch angle. A second component resides in the disk, with an exponential vertical decay. The arm and disk are assumed to have an energy dependent diffusivity D up to the "CR" halo at height $l_H = 1$ kpc, from which the CRs escape. The nearby source distribution is described as the sum of the known nearby SNR. Because nearby sources are considered, the smooth disk distribution is truncated for $r < 0.5$ kpc and $t < 0.5$ Myr.

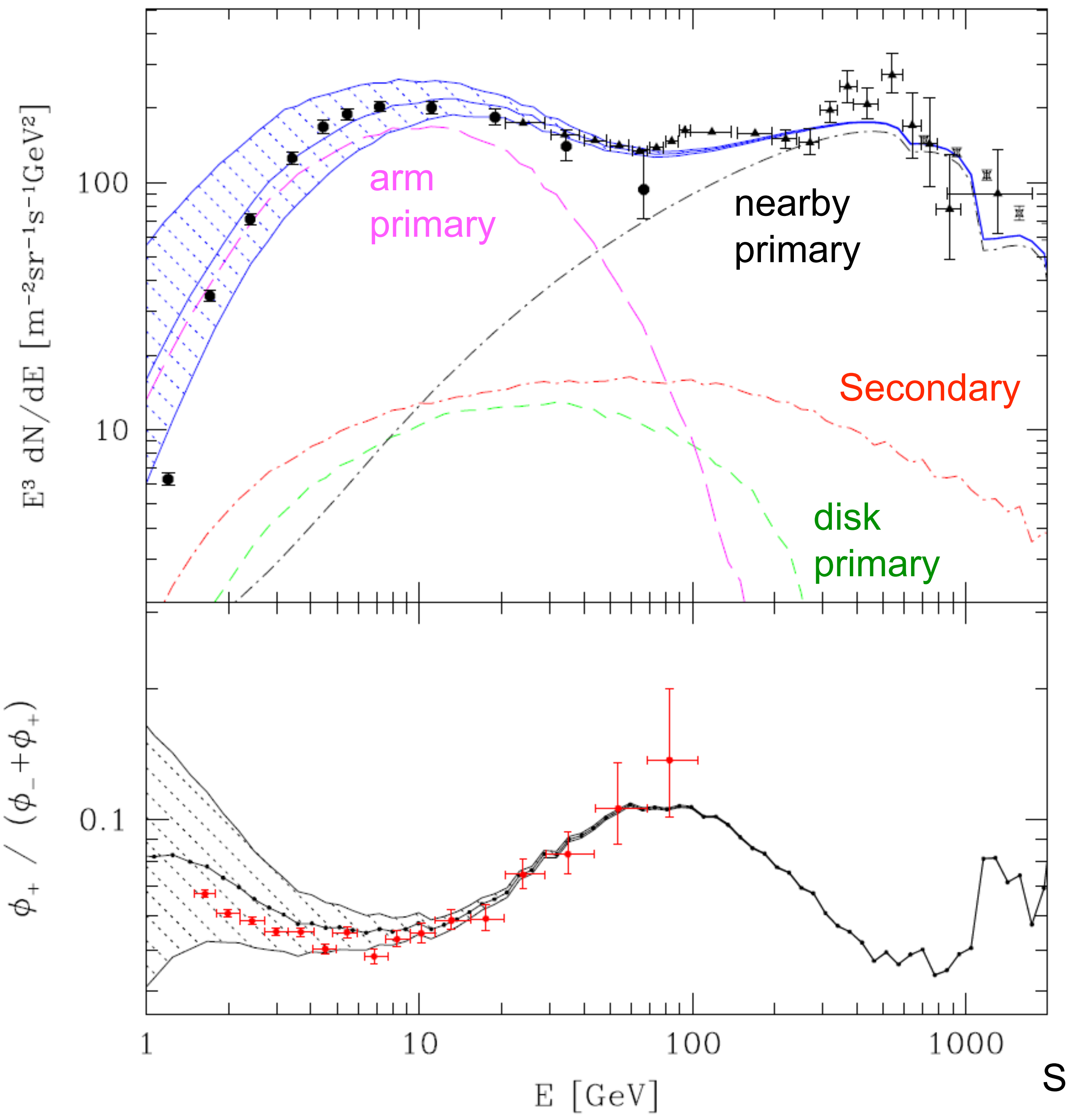

arm
primary
nearby
primary
Secondary
disk
primary
100
10
0.1
1
10
100
1000
E [GeV]

Shaviv+ 09

SNR w/ Reacceleration

$pp \rightarrow \pi \rightarrow e^+e^-$

$$Q_\pm(x,E) = \int dE' N_{CR}(E',x) \frac{d\sigma(E',E)}{dE'} n_{gas}(x) c,$$

Transport eq.

$$u\frac{\partial f_\pm}{\partial x} = D(p)\frac{\partial^2 f_\pm}{\partial x^2} + \frac{1}{3}\frac{du}{dx}p\frac{\partial f_\pm}{\partial p} + Q_\pm(x,p),$$

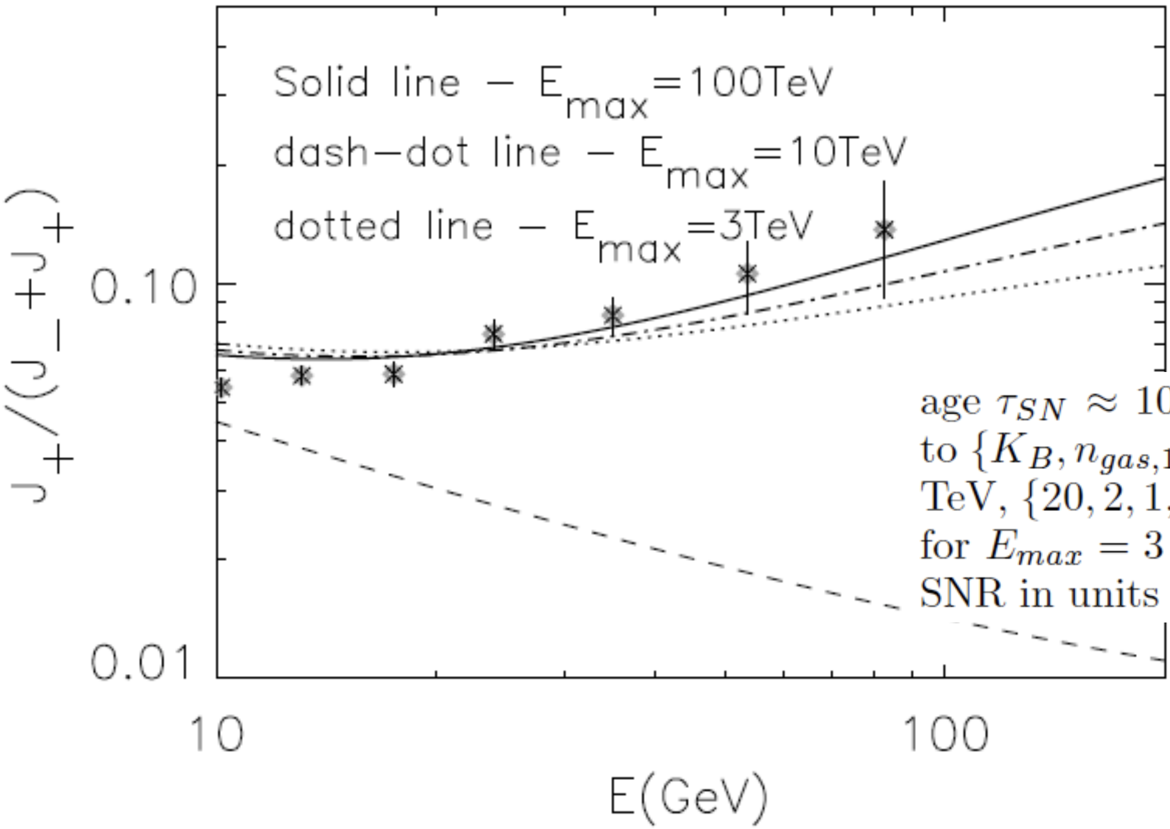

large p → large D → More return to the shock

age $\tau_{SN} \approx 10^4$ years for a SNR. The three curves refer to $\{K_B, n_{gas,1}, B_\mu, u_8\} = \{20, 1.3, 1, 0.5\}$ for $E_{max} = 100$ TeV, $\{20, 2, 1, 0.5\}$ for $E_{max} = 10$ TeV, and $\{20, 3, 1, 0.5\}$ for $E_{max} = 3$ TeV ($n_{gas,1}$ is the gas density close to the SNR in units of $1cm^{-3}$ and $u_8 = u_1/10^8 cm/s$). One can

Blasi 09

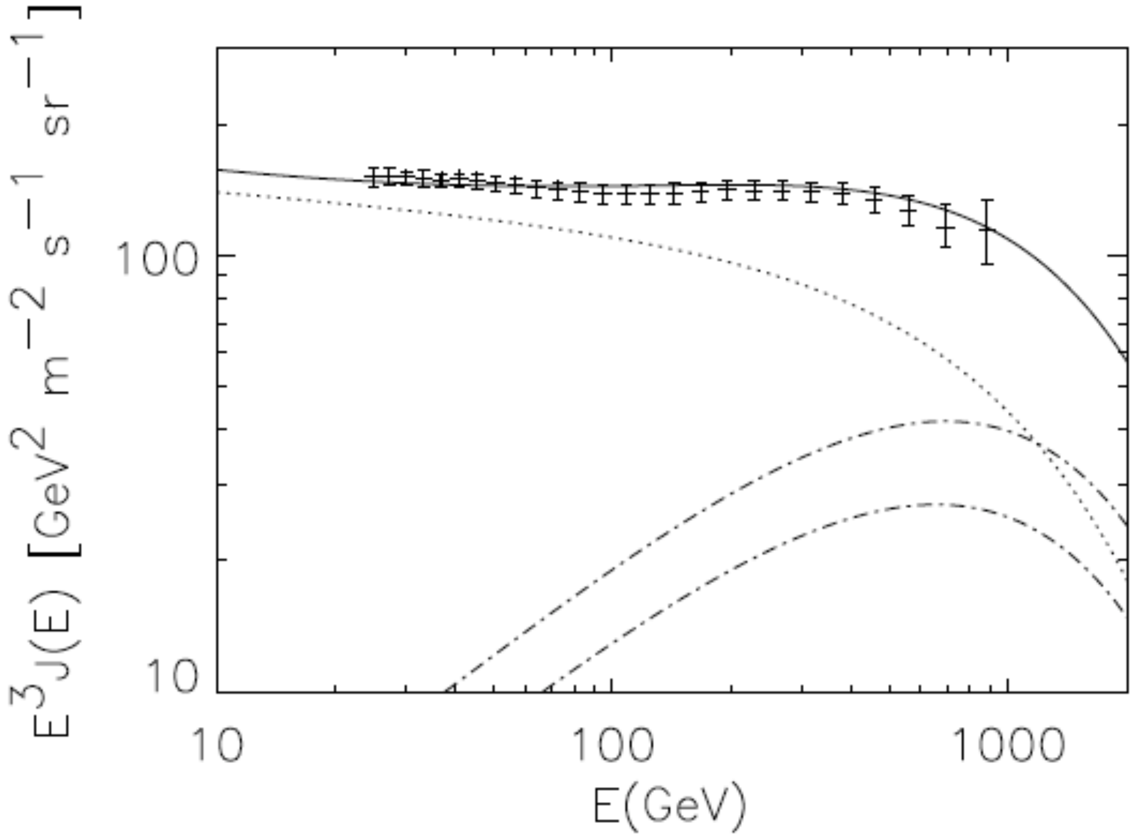

FIG. 2: Fluxes of e^- and e^+ at Earth for $E_{max} = 100$ TeV. The dotted line refers to primary electrons, the dashed lines are the fluxes of positrons (upper curve) and electrons (lower curve) from interactions of cosmic rays in the Galaxy. The dot-dashed lines are the fluxes of positrons (upper curve) and electrons (lower curve) from production in the sources. The thick solid line is the total flux. The data points are from Fermi/LAT [18].

Blasi 09

GRB summary

Luminosity: ~10^{51}erg/s (most luminous)
Energy: E_{iso}~10^{53}erg, E~10^{51}erg
Spectrum: ε_{peak}~200keV, Flat to TeV?
Event rate: ~1/10^5yr/galaxy
Optical flash: in some GRBs, why so rare?
Dark GRB: ~1/2 GRBs, dust absorption?

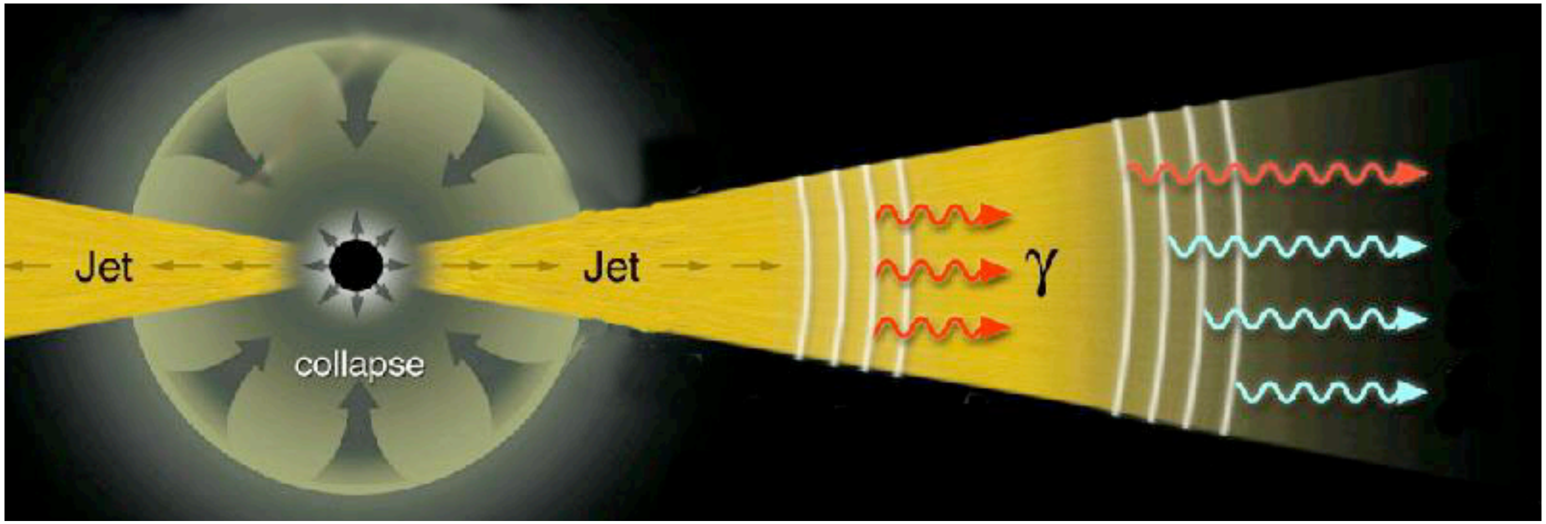

Galactic GRB

Energy: E~10^{51}erg

E(MeV)~E(GeV-TeV)

$$\gamma\gamma \rightarrow e^{+}e^{-}$$

Event rate: ~1/10^5yr/galaxy

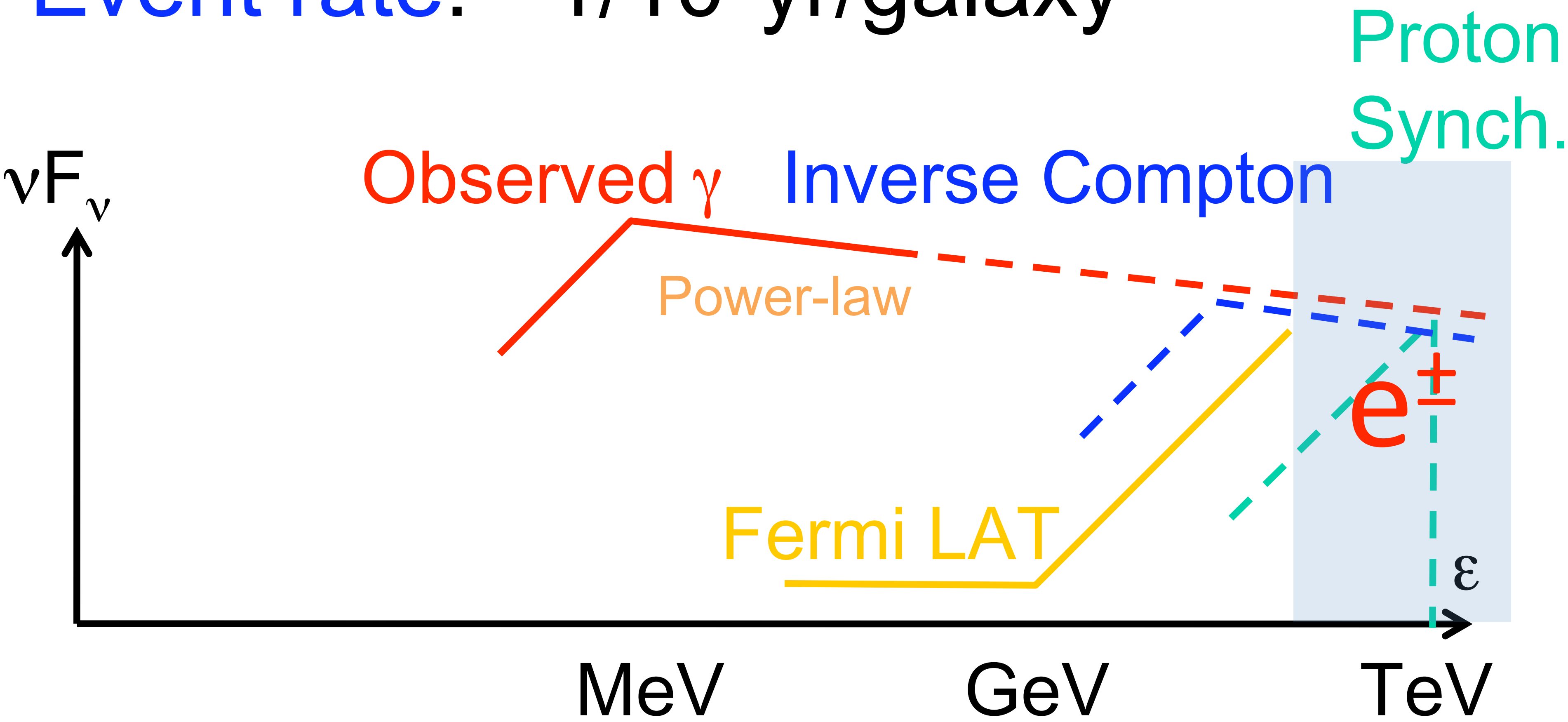

GRB 080916C

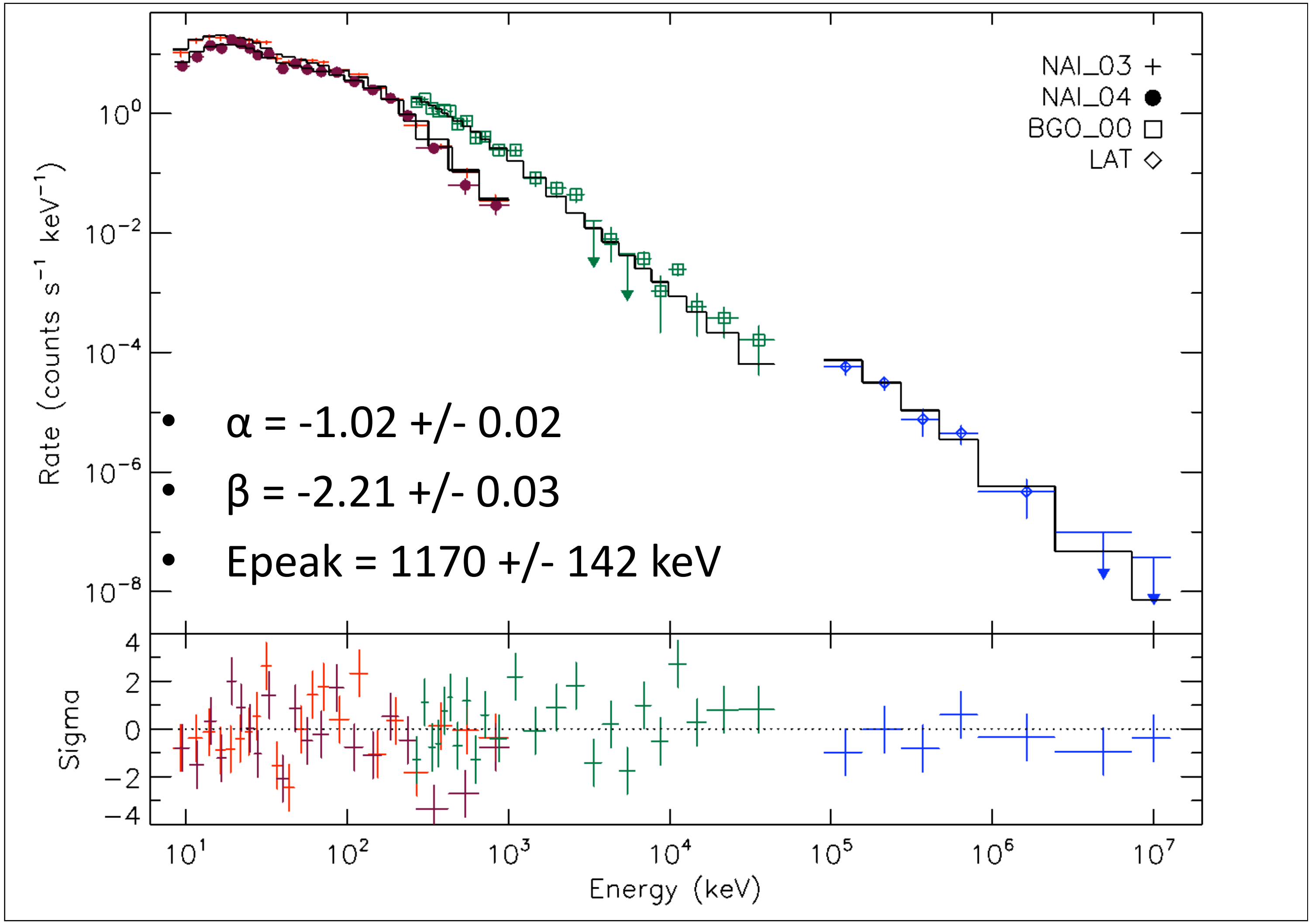

- α = -1.02 +/- 0.02
- β = -2.21 +/- 0.03
- Epeak = 1170 +/- 142 keV

Band function over 6 decades in energy

Adiabatic cooling

Important for compact sources

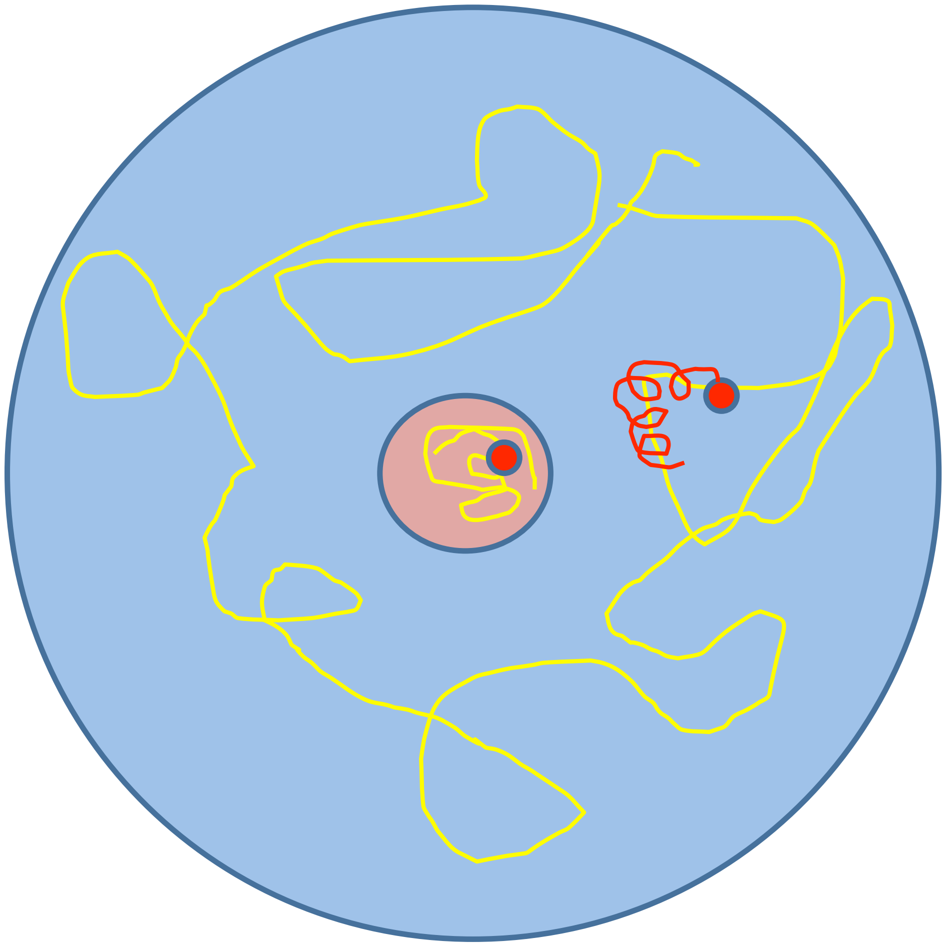

Trapped e± have adiabatic invariant

$$\frac{p_\perp^2}{B} \sim \text{const}$$

$$B \propto V^{-2/3}$$

⇒ e± lose energy

⇒ Old (>10^5yr) pulsars

How about GRBs?

Possible mechanism

$e^{\pm}$ production far outside the remnant

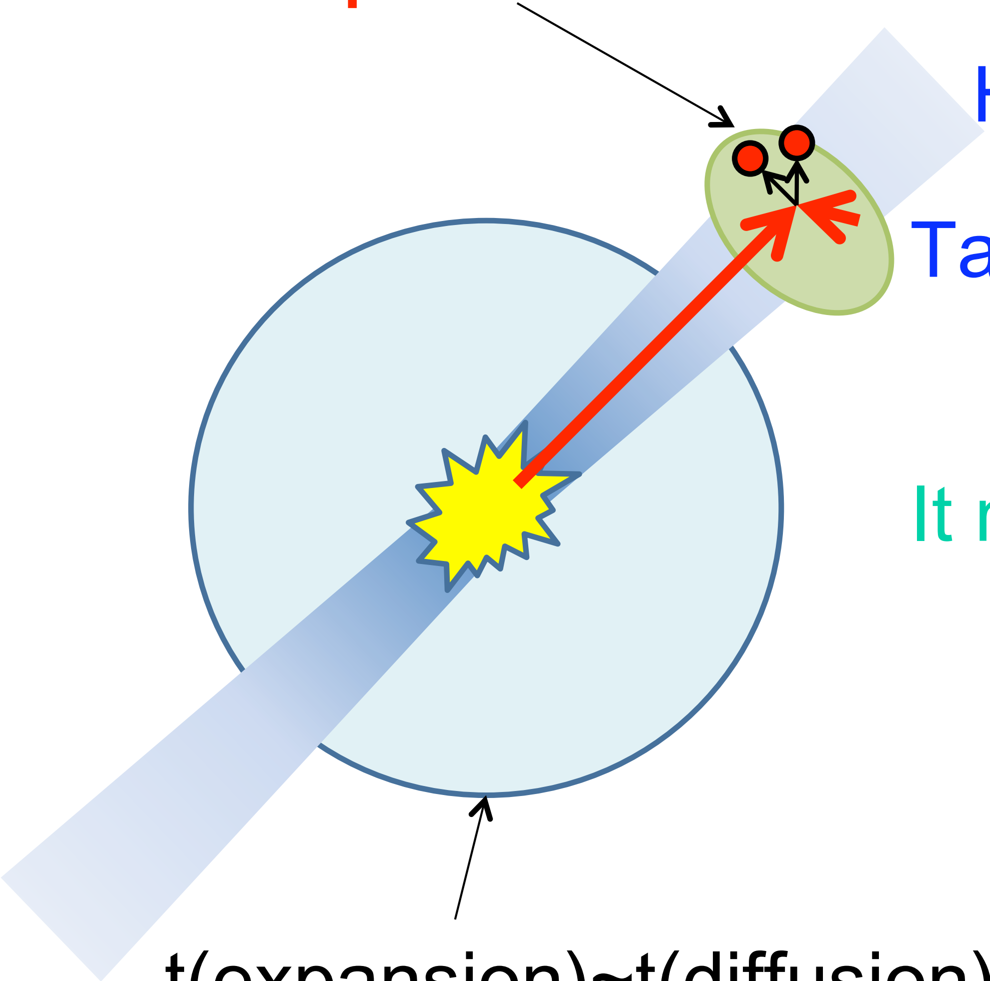

High energy photon ε_g

Target photon ε_t

$\varepsilon_g \, \varepsilon_t > (m_e c^2)^2$

It needs many target photons

$$n_t \sim \frac{1}{\sigma_T R_e} \sim 10^6 \text{ cm}^{-3} \left(\frac{R_e}{1\text{pc}} \right)^{-1}$$

$$\varepsilon_t n_t R_e^3 \sim 10^{50} \text{erg} \left(\frac{\varepsilon_t}{1\text{eV}} \right) \left(\frac{R_e}{1\text{pc}} \right)^2$$

~ GRB energy

t(expansion)~t(diffusion)

R~10^{18}cm~0.3pc

Dust echo

$e^{\pm}$ production far outside the remnant

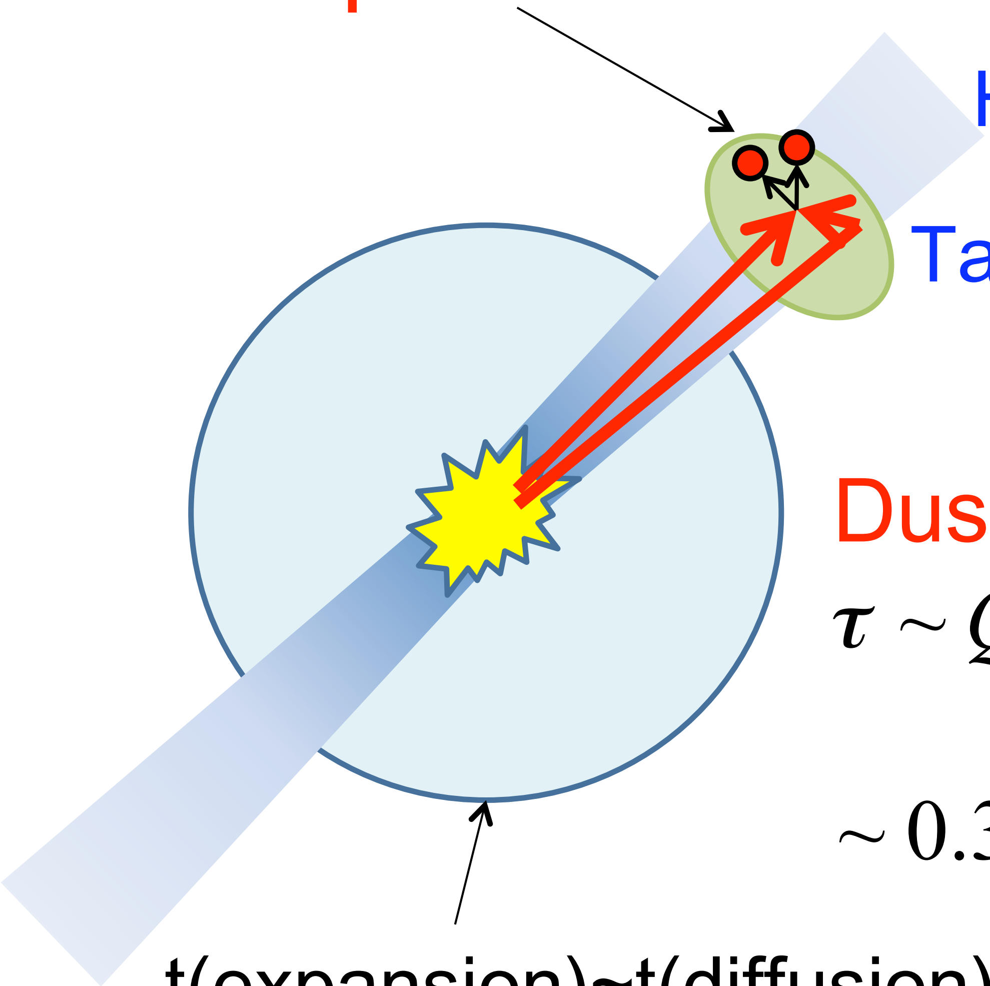

High energy photon ε_g>1TeV

Target photon ε_t~1eV

$\varepsilon_g\ \varepsilon_t > (m_e c^2)^2$

Dust scattering

$$\tau \sim Q_{scatter} n_d \pi a_d^2 R_e$$

$$\sim 0.3 \left(\frac{a_d}{10^{-5}\,\mathrm{cm}} \right)^{-1} \left(\frac{n_H}{10^2\,cm^{-3}} \right) \left(\frac{R_e}{1\mathrm{pc}} \right)$$

Typical for molecular cloud

Naked-eye GRB

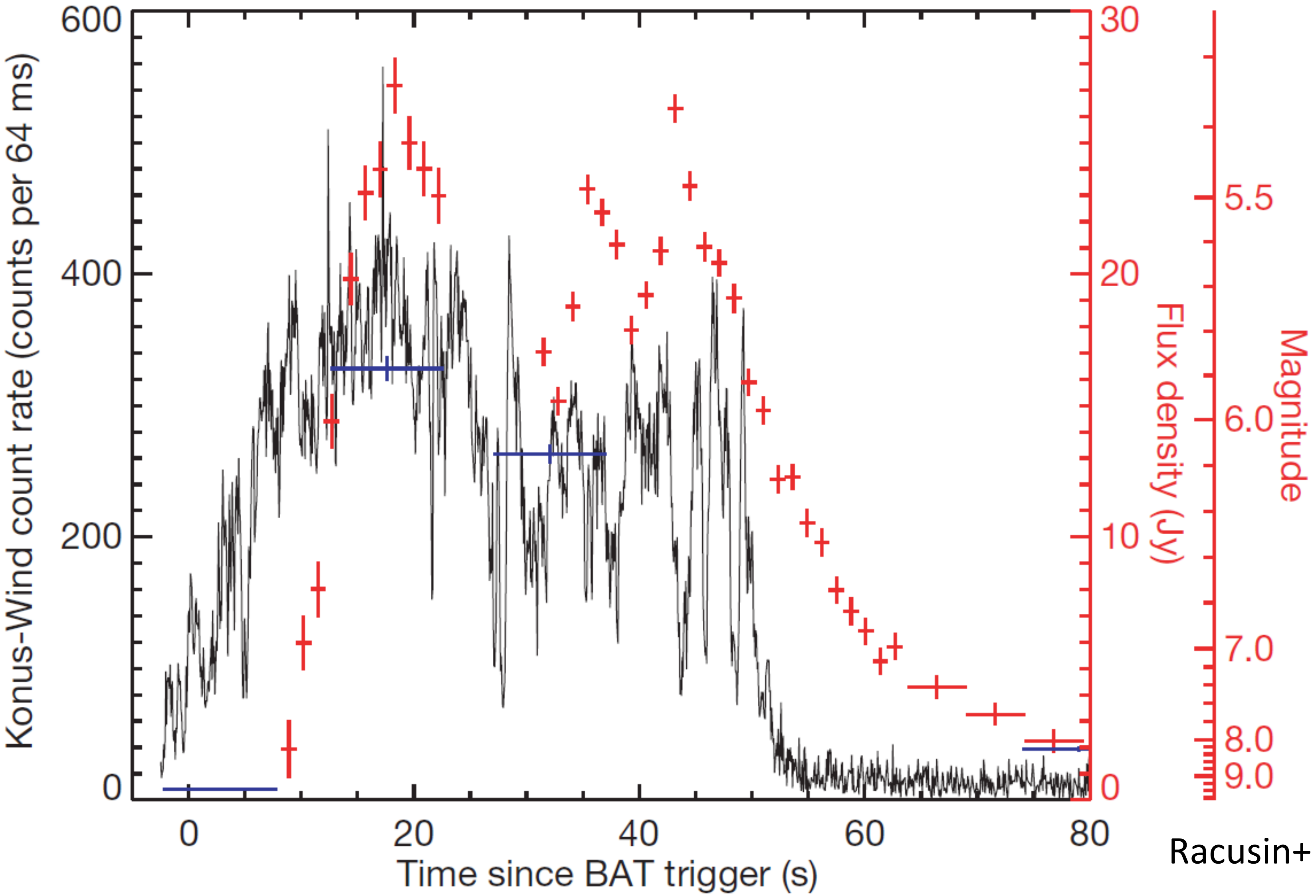

Racusin+ 08

GRB080319B peaked at V_{mag}~5.3, E_{eV}~10%E_{MeV}

$e^{\pm}$ spectrum

$e^{\pm}$ production far outside the remnant

High energy photon ε_g>1TeV

Target photon ε_t~1eV

$\varepsilon_g\ \varepsilon_t > (m_e c^2)^2$

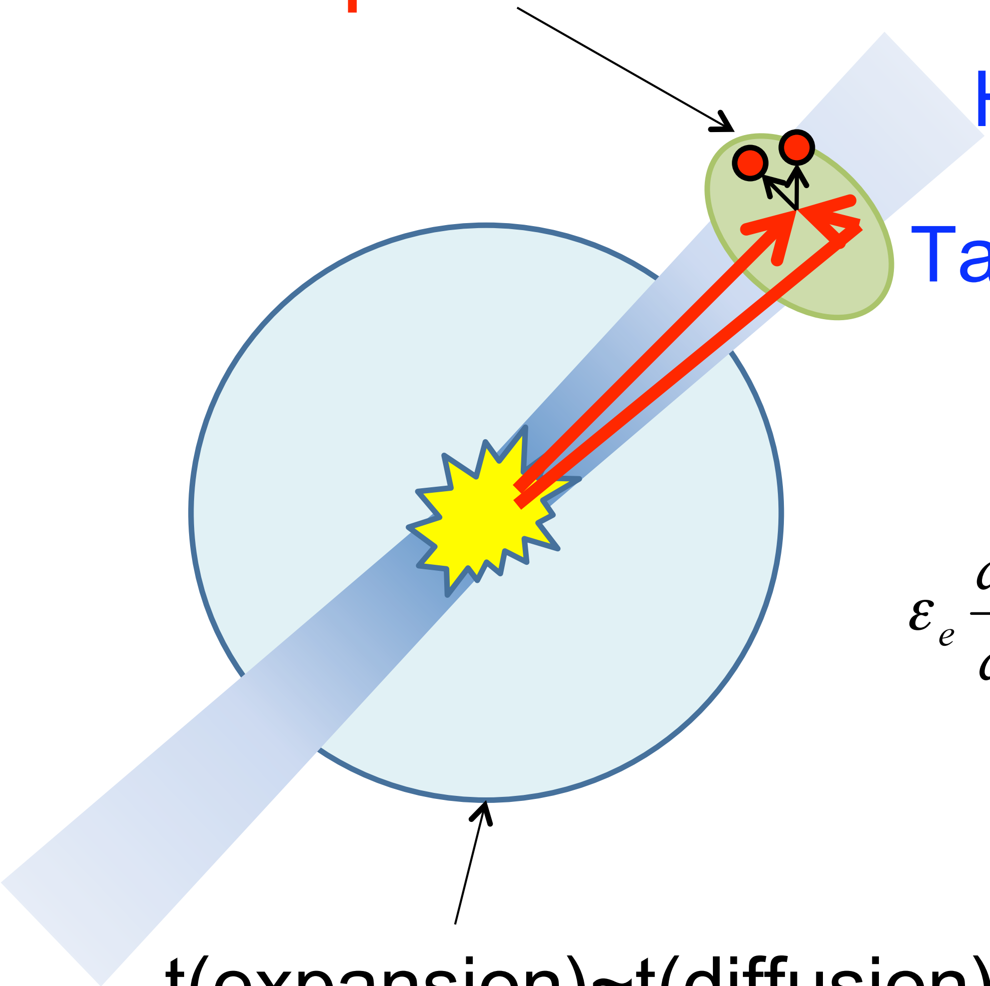

t(expansion)~t(diffusion)

R~10^{18}cm~0.3pc

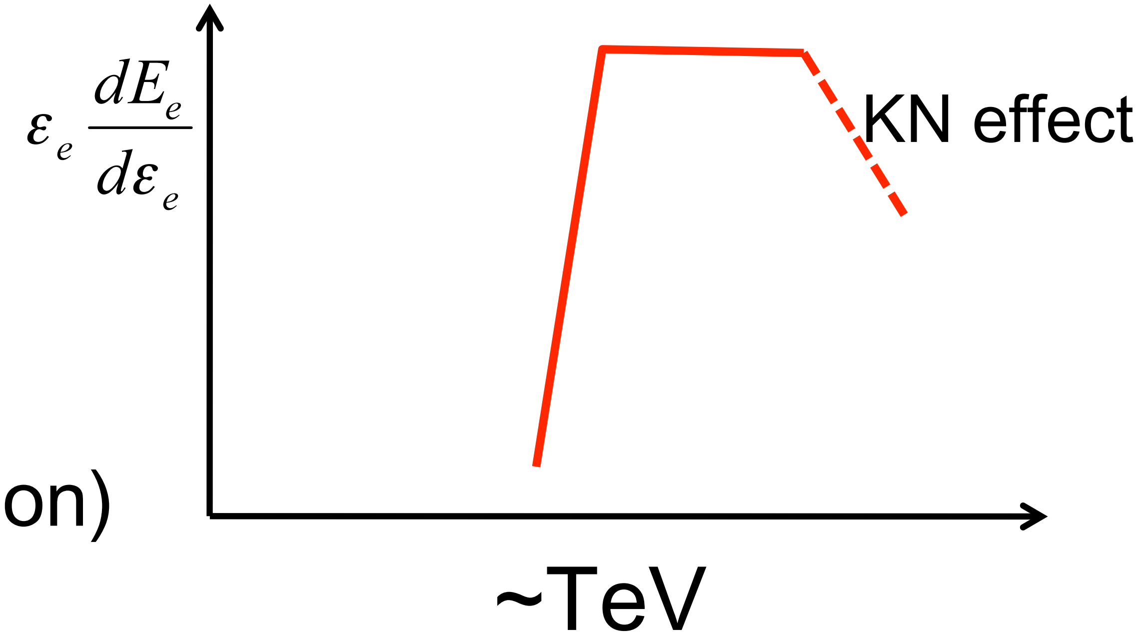

Spectral conversion

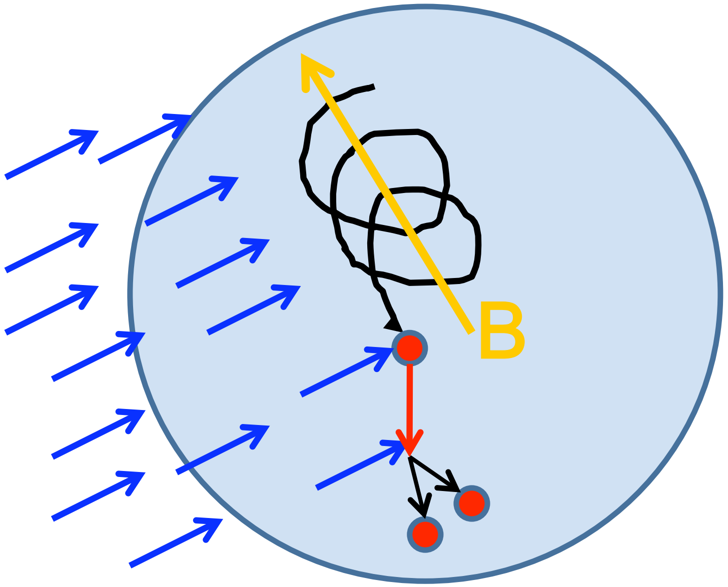

$$t_{cool} \sim \frac{3m_e^2c^4}{4\sigma_T c U_a \varepsilon_e}$$

$$U_a \sim \frac{E}{4\pi R_e^2 ct}$$

$$\Rightarrow \varepsilon_e \sim \frac{3\pi R_e^2 m_e^2 c^4}{\sigma_T E} \sim 1\,\mathrm{TeV}$$

To isotropic distribution

$$R_L \sim \frac{\varepsilon_e}{eB} \sim 10^{15}\,\mathrm{cm}\left(\frac{\varepsilon_e}{1\mathrm{TeV}}\right)\left(\frac{B}{1\mu G}\right)^{-1}$$

Scatter afterglow photons

⇒ $e^{\pm}$ cooling & creaction

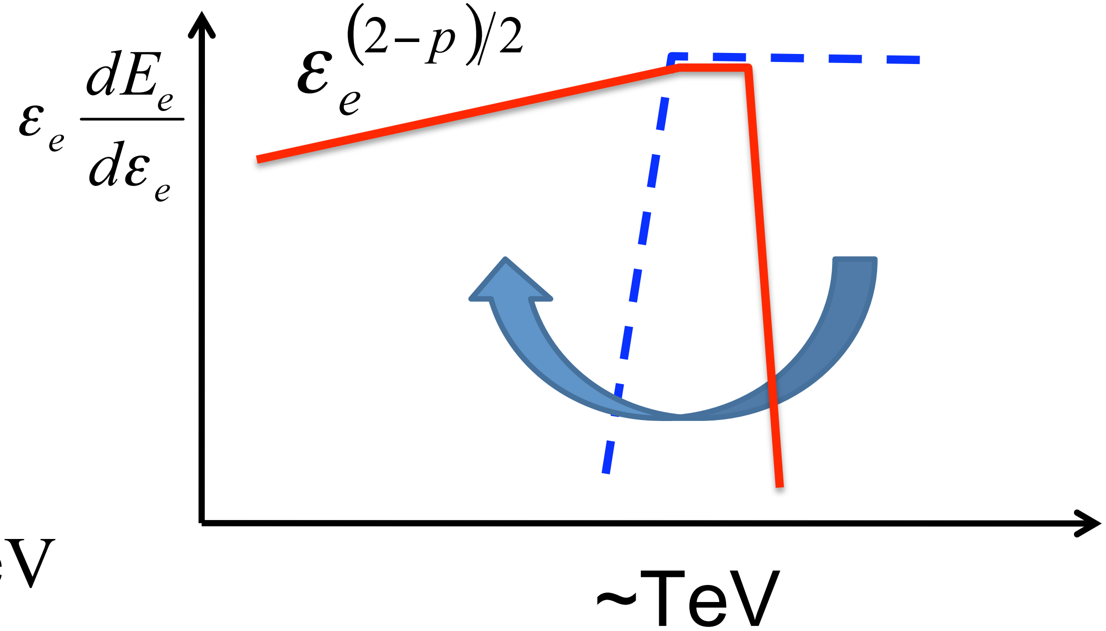

Microquasar

$L_{Eddington}\ (10^{38}\mathrm{erg/s}) \times 10^{5}\mathrm{yr} \sim 10^{50}\mathrm{erg}$

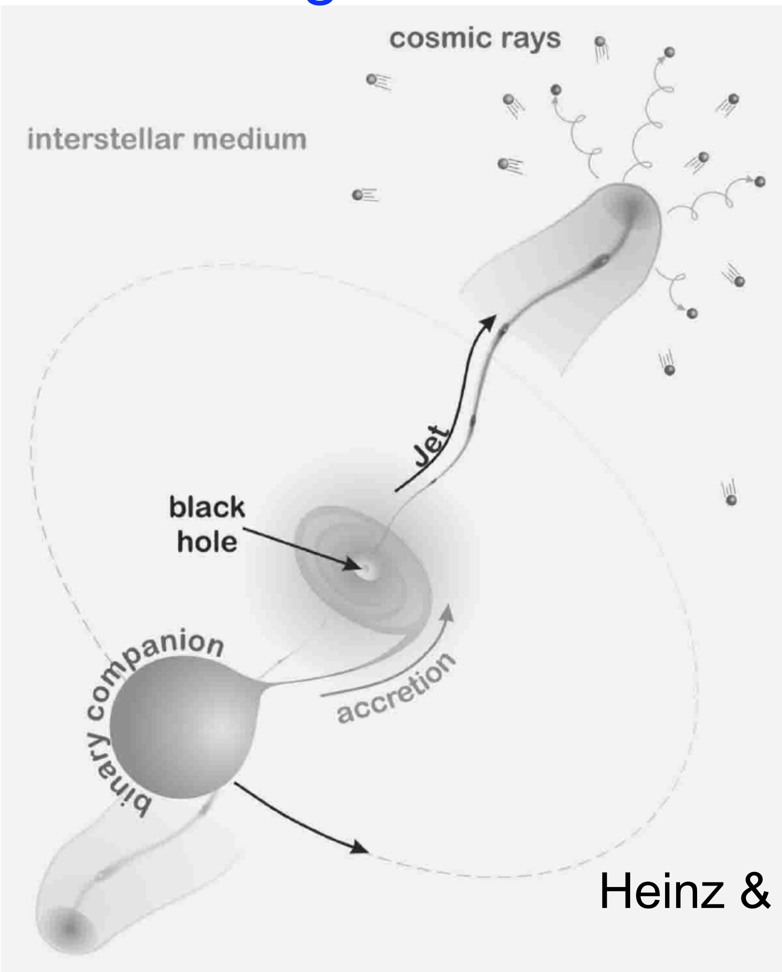

Fig. 1. Cartoon of the proposed model of CR production in microquasars: The interface between the relativistic jet and the ISM is a natural site for the production and release of relativistic particles.

Heinz & Sunyaev 02

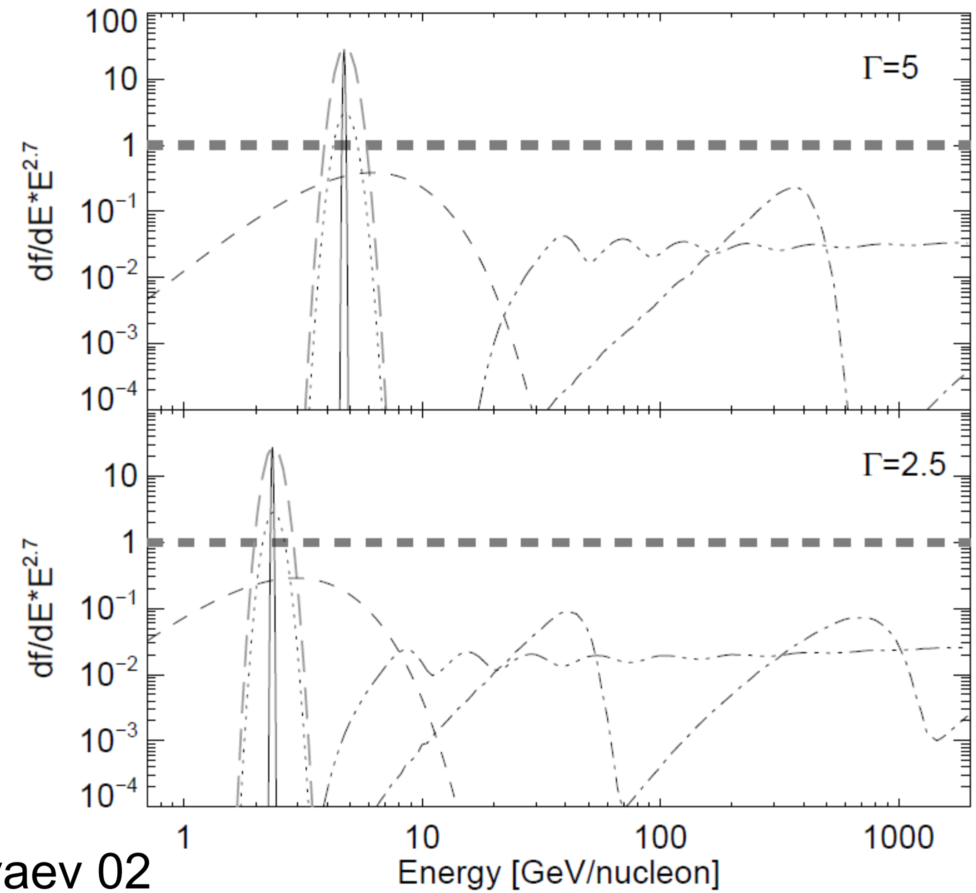

Fig. 7. Toy model of the microquasar contribution to the CR spectrum, for a *single* microquasar situated in a low mass X-ray binary, active for $\tau \gtrsim 1.5 \times 10^{7}$ yrs on the level of 3×10^{38} ergs s^{-1} (similar to GRS 1915+105), and at a distance of 1 kpc. For simplicity, we assumed the source was operating with uniform bulk Lorentz factor

Theoretical uncertainty

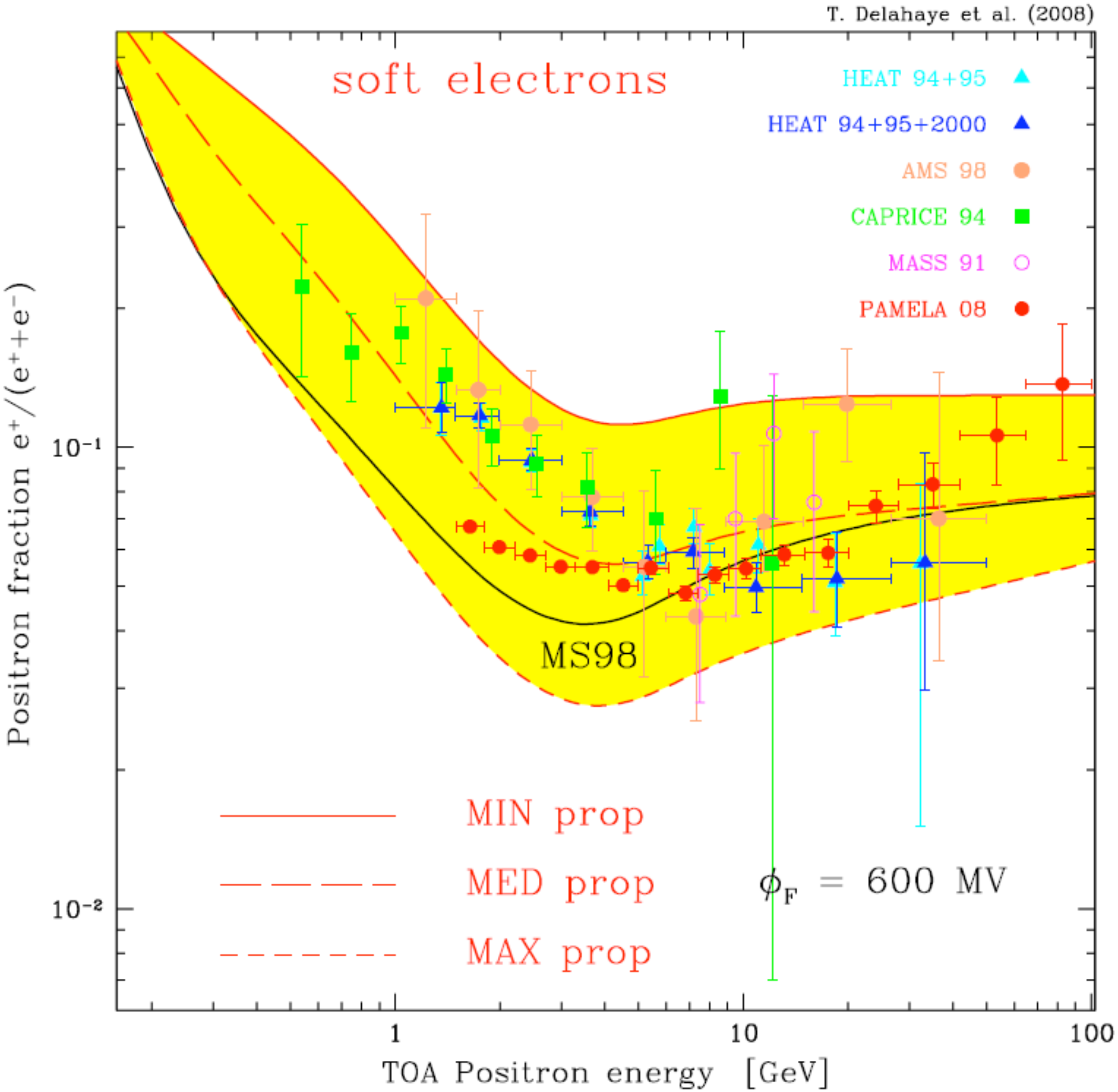

Theoretical uncertainty ~1 order-of-mag.

⇒ It could be just secondary

Delahaye+ 08

Nested Leaky Box

$$\left.\begin{array}{ll} \tau_s(E) \sim \tau_B(E) - \tau_G & for\ 1\ GeV < E < 10\ GeV \\ \tau_G(E) \sim\ constant & for\ 1\ GeV < E < 10^6\ GeV \end{array}\right\} (Model\ C).$$

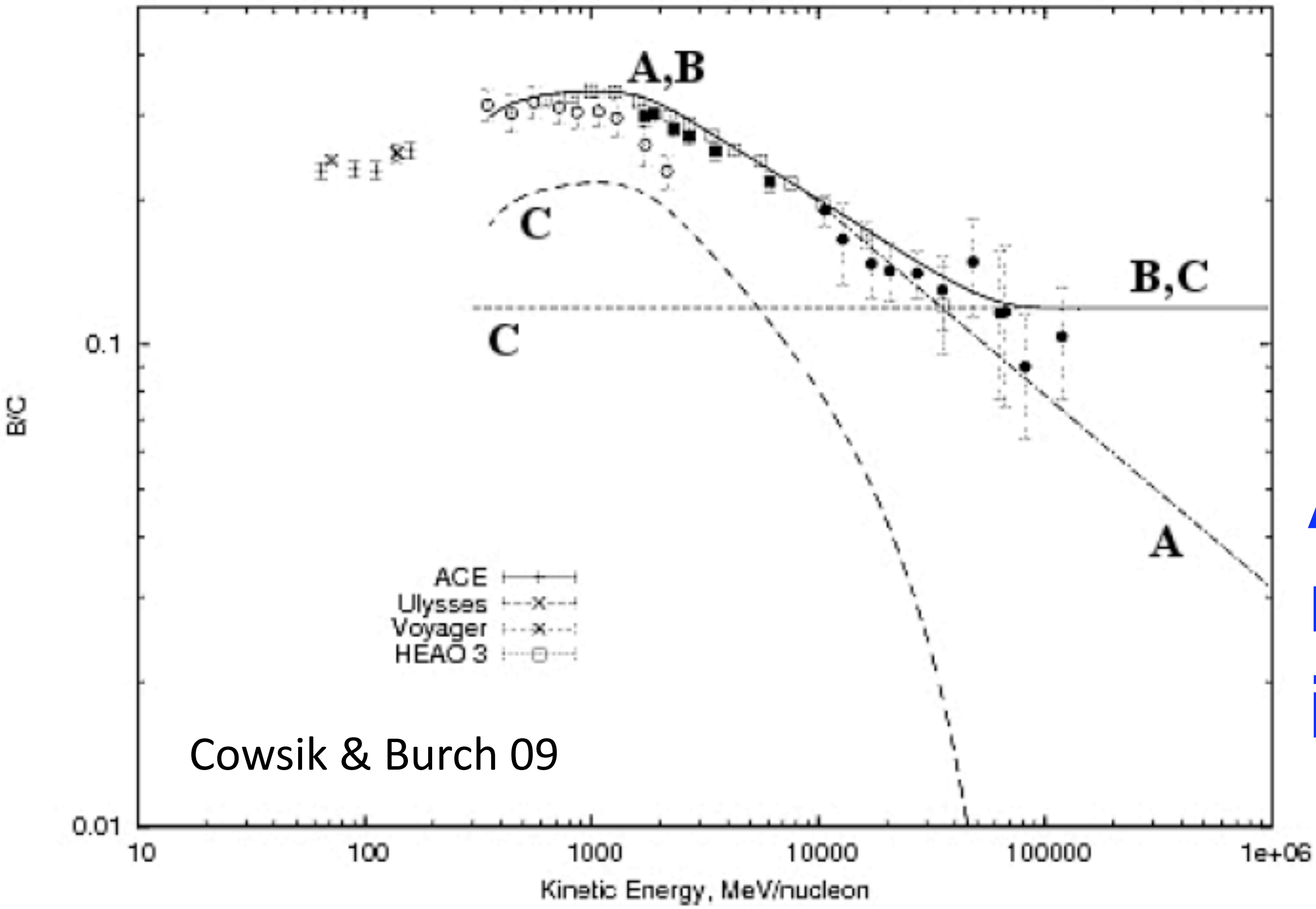

CRs spend some time $\tau_s(E)$ near the source

After that, residence time in ISM is const.

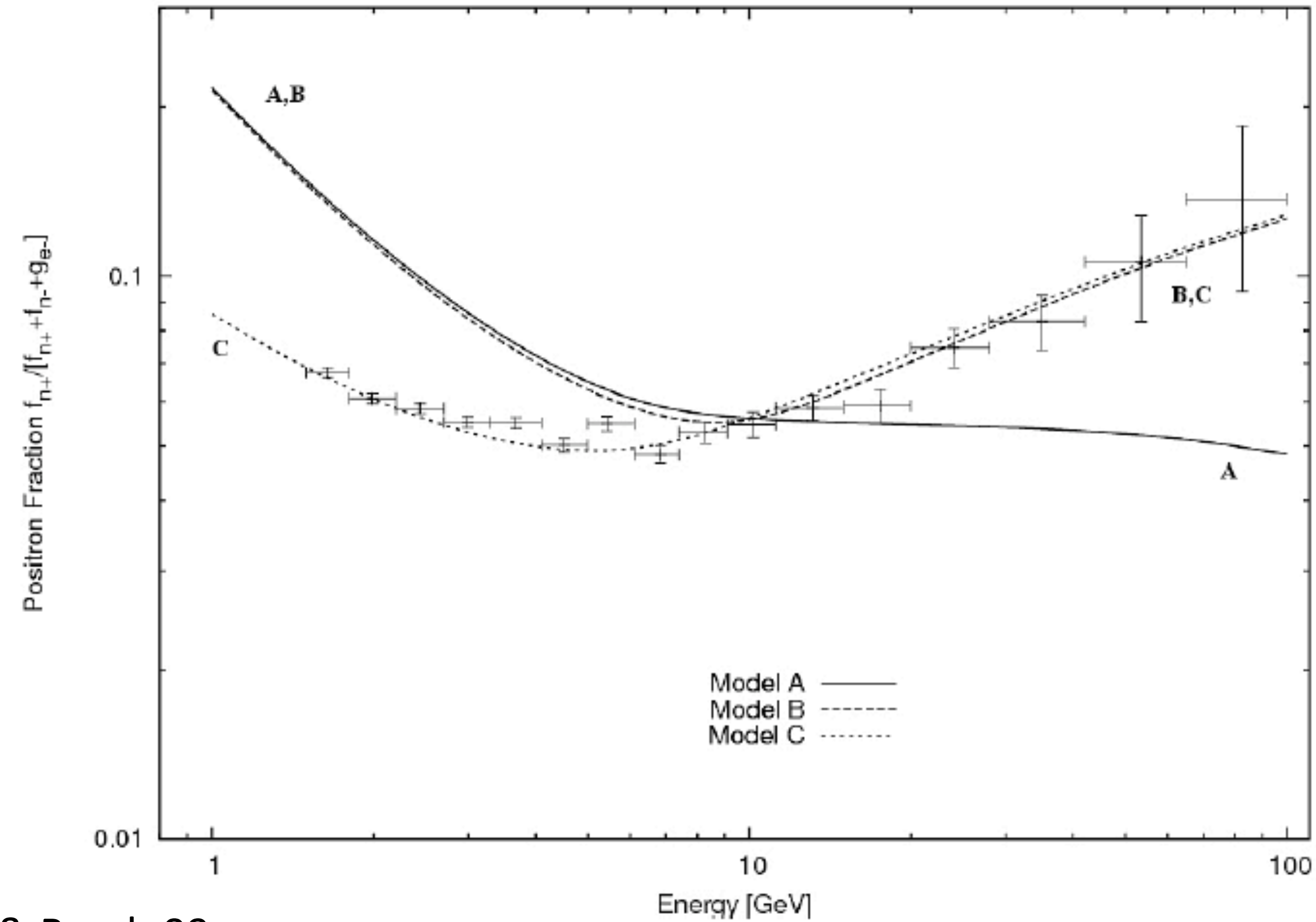

Cowsik & Burch 09

FIG. 6: The theoretically calculated positron fraction in models A (similar to that of [10] as shown in fig. 2), B, and C are compared with the observations. All calculations are normalized at ~ 10 GeV

Diffuse γ-ray background

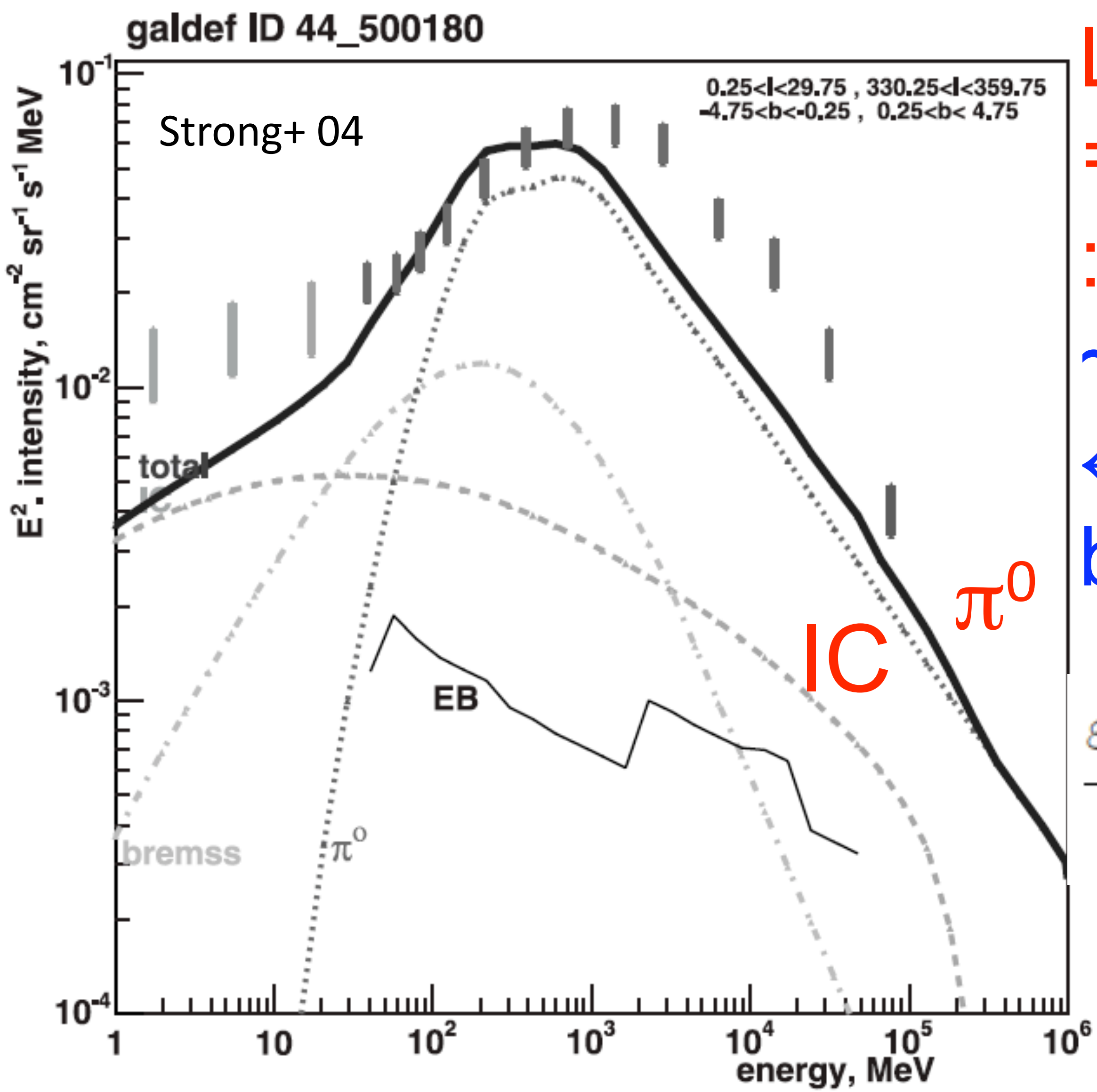

Locally obs. electron
⇒ Minor role of IC
:conventional model

~10-10^3 GeV γ
←Inverse Compton
by ~10^2-10^3 GeV e

$$\frac{\varepsilon_\gamma^2 \Phi_\gamma(\varepsilon_\gamma)}{\varepsilon_e^2 \Phi_e(\varepsilon_e)} \sim 2 \left[\frac{K(\varepsilon_e) b \varepsilon_e}{c^2}\right]^{1/2}$$

$$\sim 0.05 \left(\frac{\varepsilon_e}{10^3\,\mathrm{GeV}}\right)^{2/3}$$

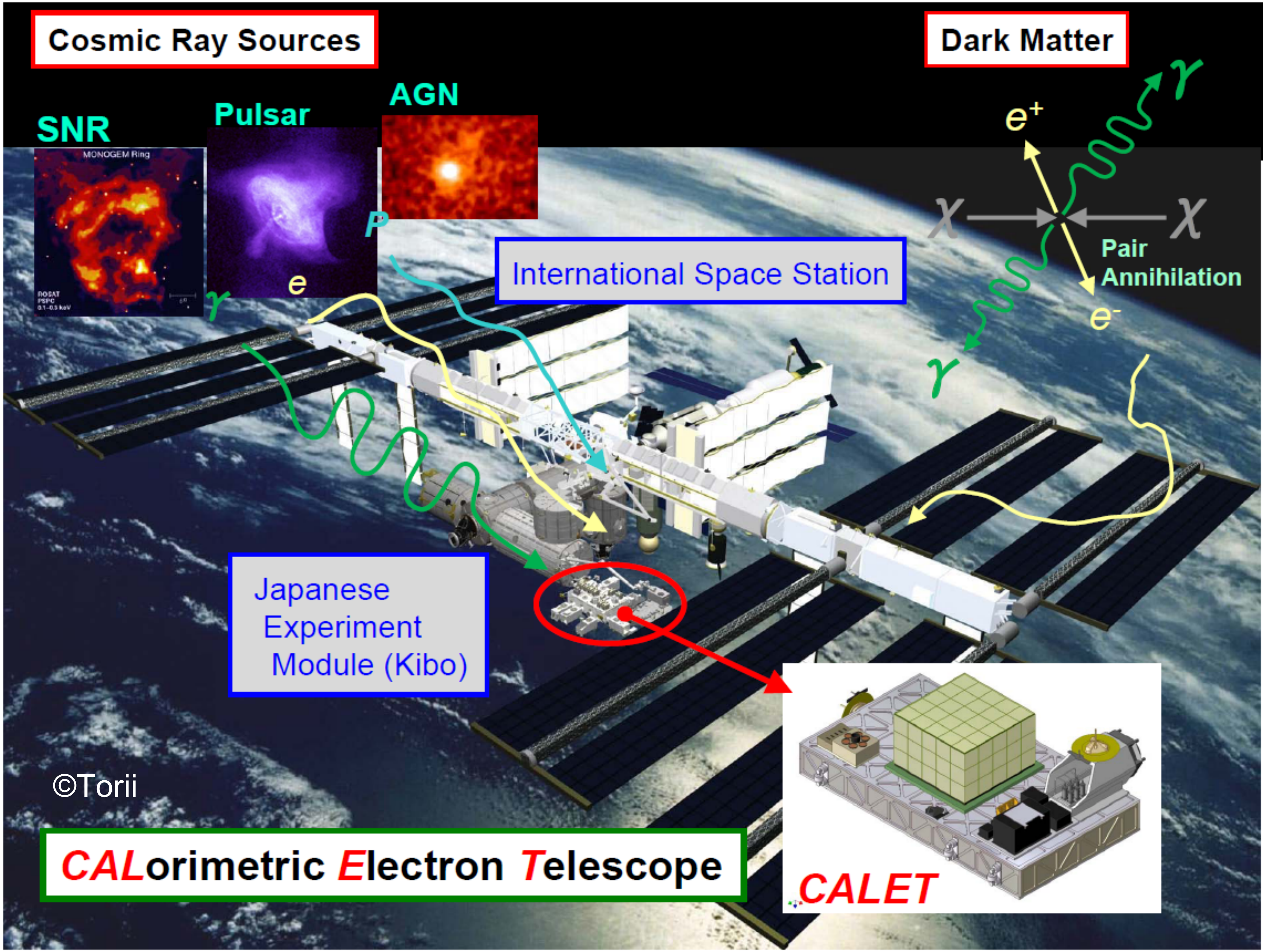

Cosmic Ray Sources
Dark Matter
SNR
MONOGEM Ring
ROSAT PSPC 0.1–0.3 keV
Pulsar
AGN
P
e
γ
e+
e-
χ
χ
γ
γ
Pair Annihilation
International Space Station
Japanese Experiment Module (Kibo)
©Torii
CALorimetric Electron Telescope
CALET

CALET

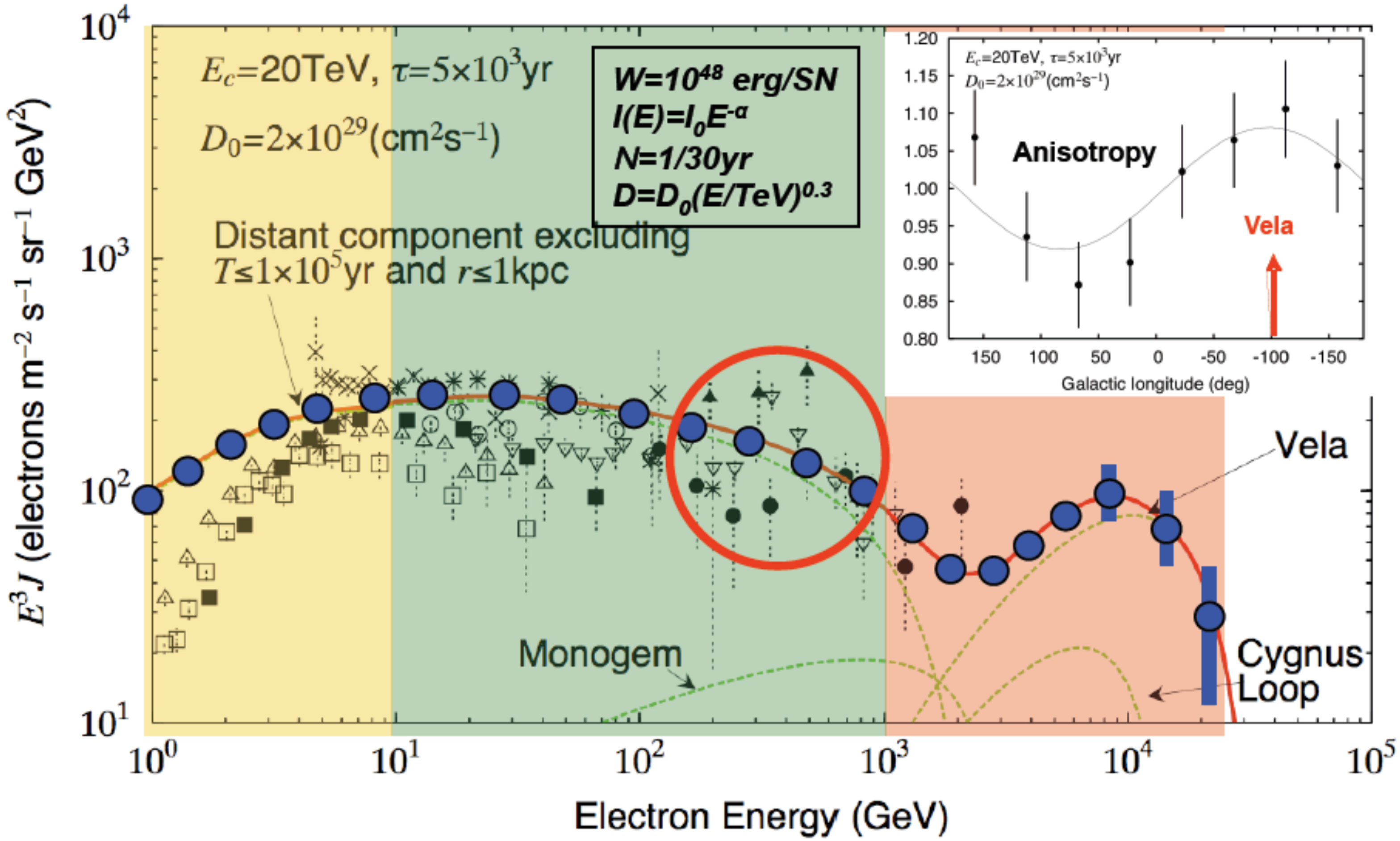

$$\boxed{\frac{\Delta\varepsilon_e}{\varepsilon_e} \approx 2-3\%\,(\varepsilon_e > 100\mathrm{GeV})}$$

©Torii

Summary

Electron/Positron excess

Dark Matter?

Pulsar? SNR: pp? GRB: TeV γ + dust eV γ?

Astrophysical sources

$\sim 10^{49\text{-}50}$erg $e^{\pm}$ $\sim 10^{5\text{-}6}$yr ago

Fit spiky ATIC as well as Smooth Fermi

Spectral cutoff similar to DM case ($\Rightarrow$CALET)

Anisotropy (CR & Diffuse γ)

Anti-proton, 2^{nd} Nuclei: Hadronic models

γ of Pulsar Wind

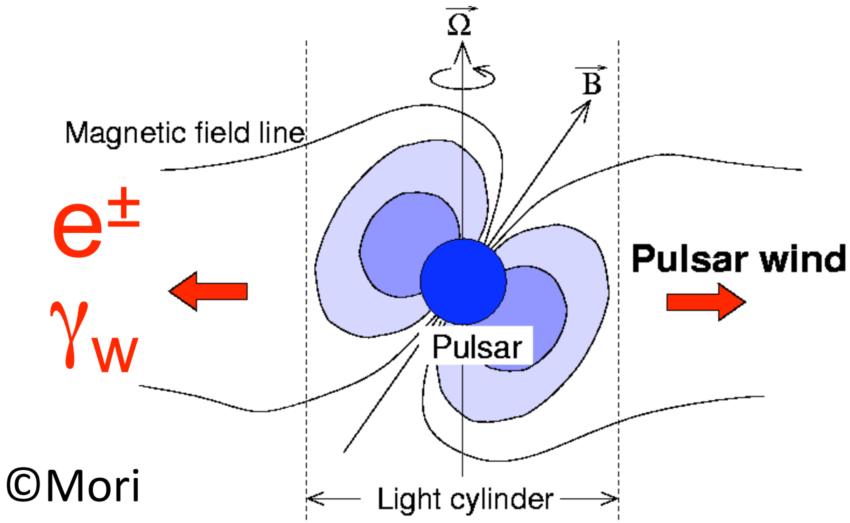

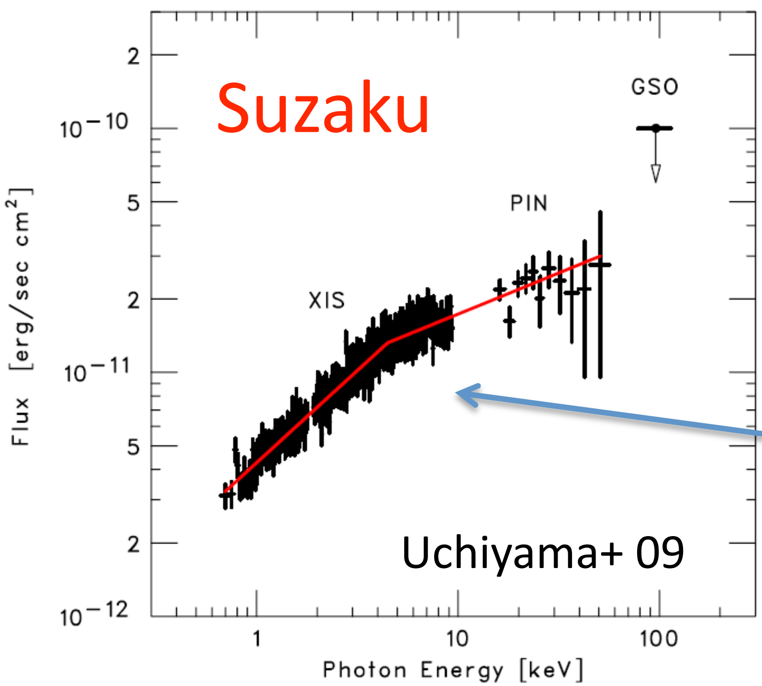

PAMELA excess

requires 10^{49} $e^{\pm}$ per SN

$$\Rightarrow 10^{49} \times \gamma_{\mathrm{w}} m_e c^2 \text{ erg}$$

$$\sim 10^{49} \left(\frac{\gamma_{\mathrm{w}}}{10^6} \right) \text{ erg per SN}$$

$$\Leftrightarrow E_{\mathrm{rotation}} \sim 10^{50} \text{erg } P_{10\mathrm{ms}}^{-2}$$

So far only $\gamma_{\mathrm{w}} \sim 10^6$ for Crab

$\gamma_{\mathrm{w}} \sim 4\mathrm{x}10^5$ for PSR B1259

$$\varepsilon_{\mathrm{br}} = \sqrt{\frac{3}{2} \frac{e\hbar}{m_e c^2}} B \gamma_1^2 \simeq 4 \left(\frac{B}{1.8 \text{ G}} \right) \left(\frac{\gamma_1}{4 \times 10^5} \right)^2 \text{ keV.}$$

Remnants of e± Sources

~10^{50}erg e± ~$10^{5\text{-}6}$yr ago ⇒ Old remnant
⇒ X-ray dim via cooling ~ TeV unID

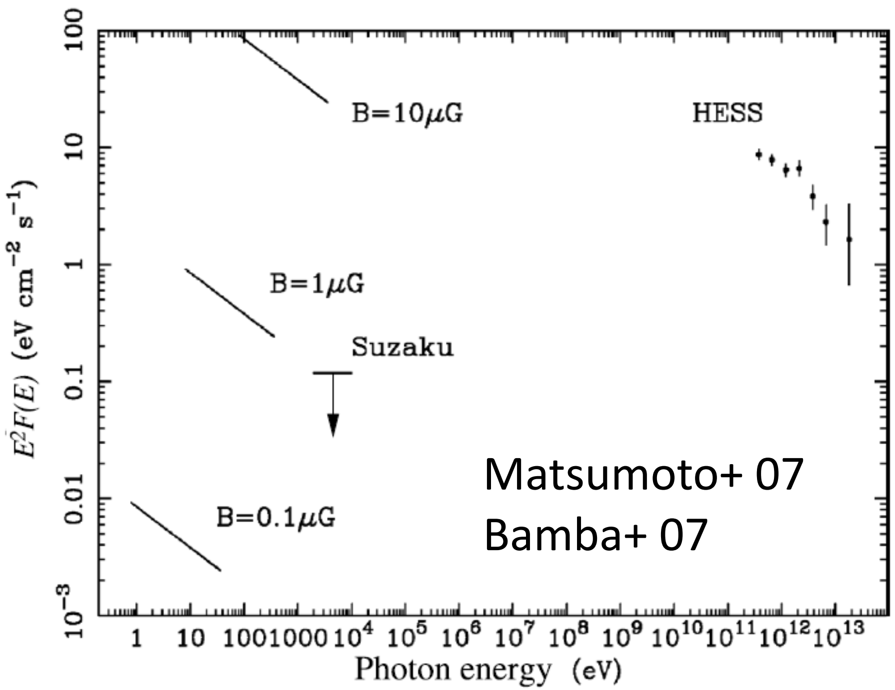

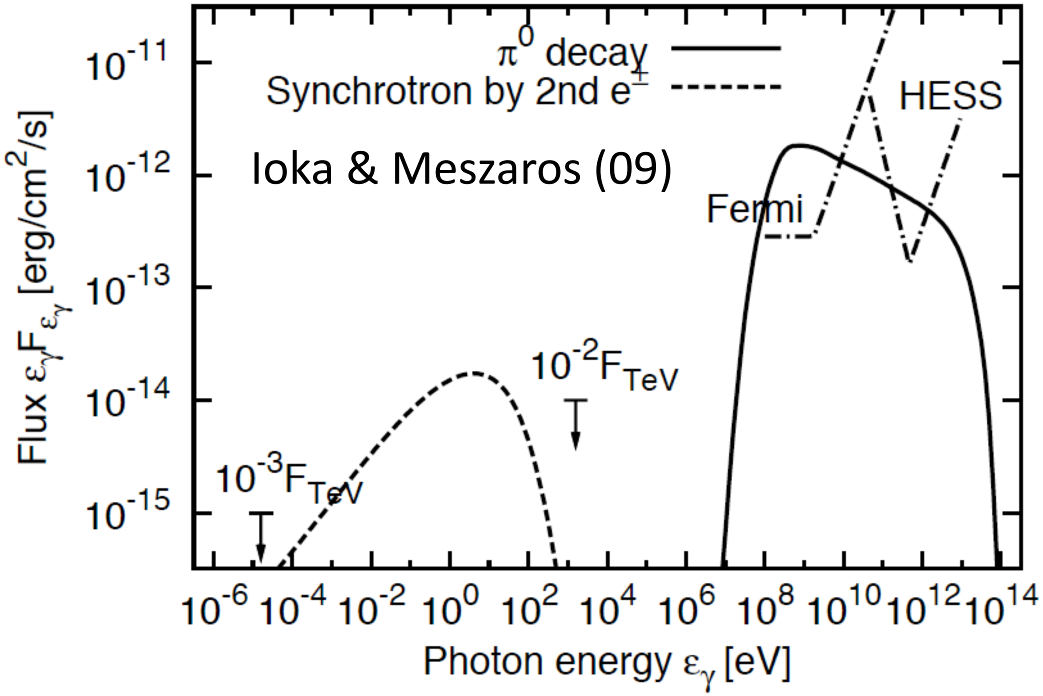

Many TeV unIDs

HESS J1616: TeV/X>55 (Matsumoto+ 07)
HESS J1804: TeV/X>13 (Bamba+ 07)
Westerlund 2: TeV/X>2.7 (Fujita+ 09)

GRB/Hypernova Remnants
~ 10 ~ Observed TeV unID

Bamba: GeV ~ pion?

Metal in SNR

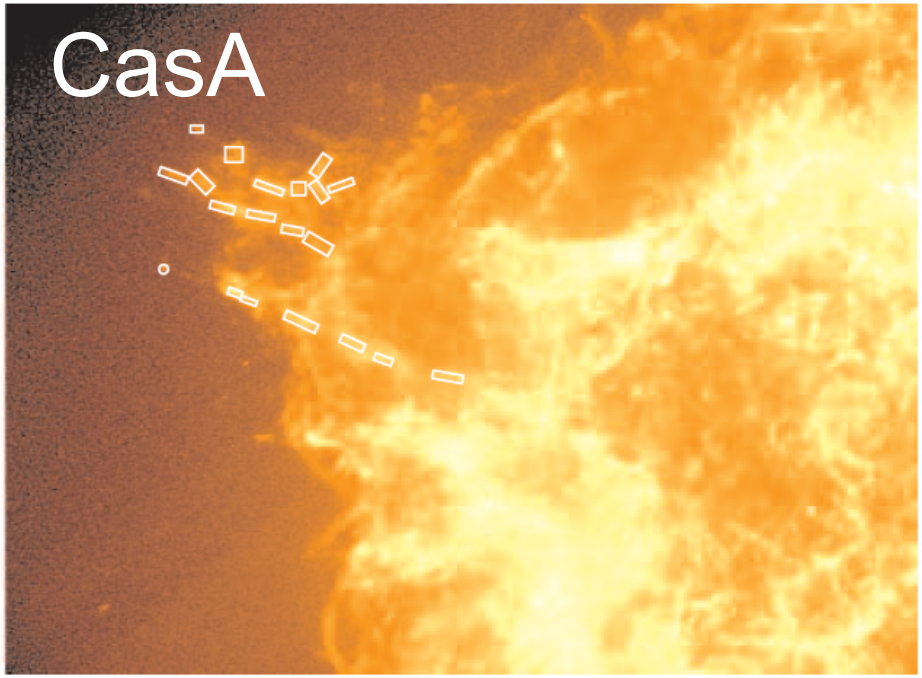

FIG. 1.—Regions of the three filaments (north, middle, and south) of the northeast jet used for spectral analysis.

Laming+(06)

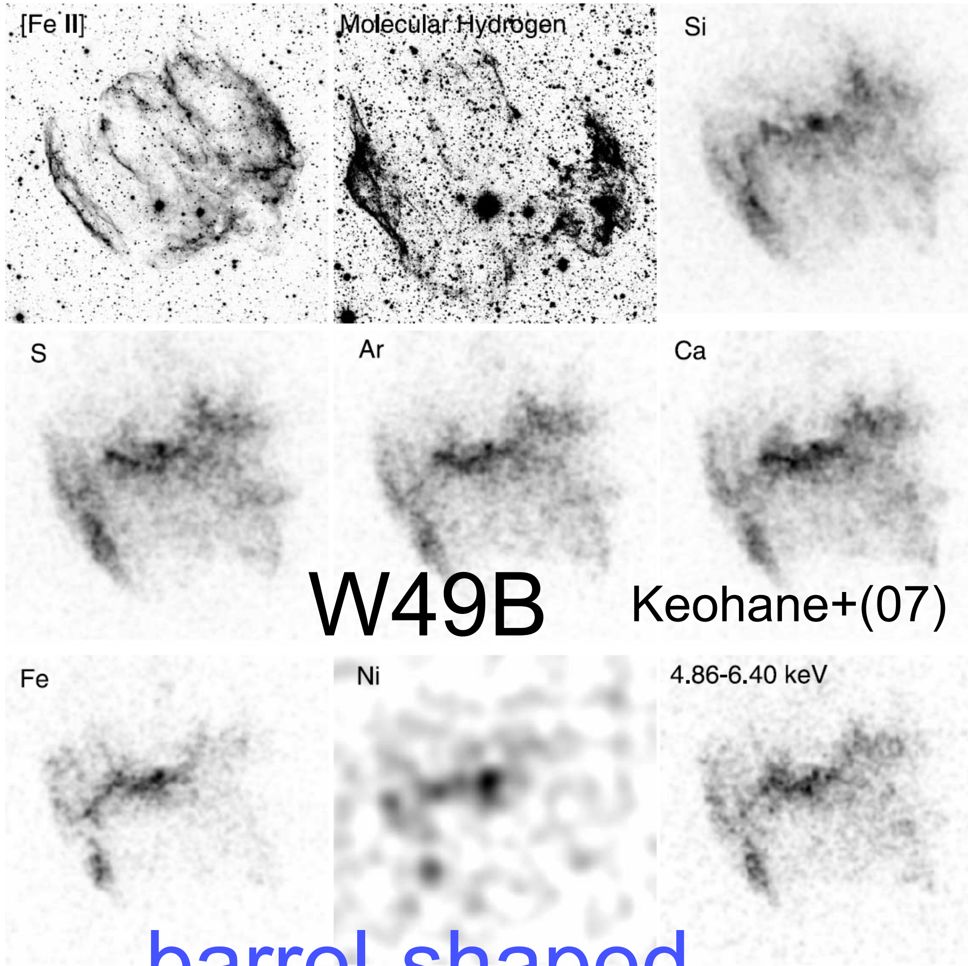

"Jet" region
X-ray Spec.⇒2×10^{52}erg
~7° Jet⇒10^{50}erg?

barrel-shaped
Ni & Fe in the jet
⇒ GRB-like jet?

Candidates

Dark Matter

Annihilation

$\langle\sigma v\rangle \sim 3\times10^{-24}\mathrm{cm}^3/\mathrm{s}$

$> 3\times10^{-26}\mathrm{cm}^3/\mathrm{s}$

boost factor ~100

Decay

$\tau_{decay} \sim 10^{26}\mathrm{sec}\ (> H^{-1})$

Many (>100) papers

Astrophysical Model

$10^{-3} \times \overbrace{10^{50}\mathrm{erg/SN}}^{\text{Cosmic-ray energy}}$

$\sim 10^{47}\mathrm{erg/SN}$

~ (1sec Pulsar)/SN

~ (10^{-3} x SNR)/SN

~ (1 GRB)/10^3SN

~ (1 Microquasar)/10^3SN

~30 papers

Cutoff width by inhomo.

$$\Delta\varepsilon_{\rm cut}/\varepsilon_{\rm cut} = -\Delta b/b - \Delta t/t$$

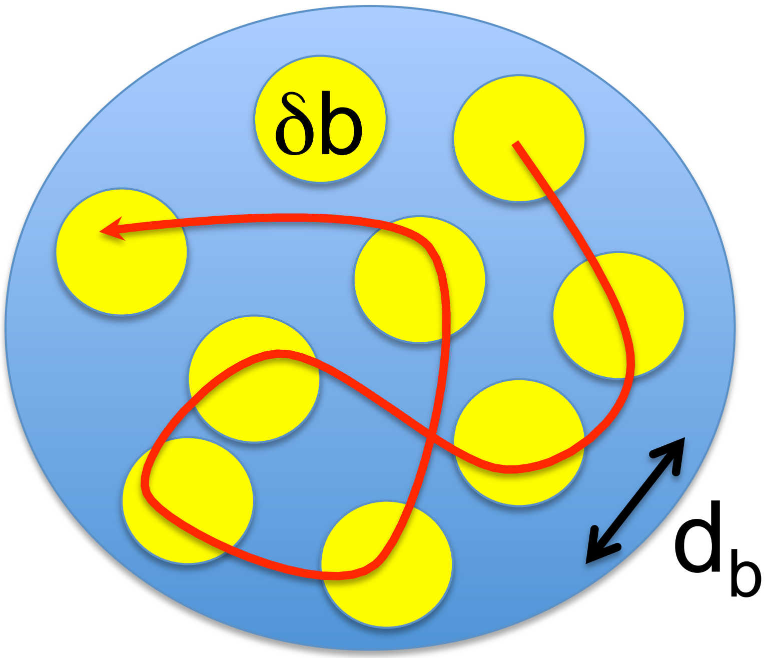

$$N_b \sim c t_{\rm age}/d_b$$

$$\Delta b \sim \delta b/\sqrt{N_b}$$

$$\left(\frac{\Delta\varepsilon_{\rm cut}}{\varepsilon_{\rm cut}}\right)_{\Delta b} \sim 6\% \left(\frac{\delta b}{b}\right)\left(\frac{d_b}{1{\rm kpc}}\right)\left(\frac{t_{\rm age}}{10^6{\rm yr}}\right)^{-1/2}$$

Short Summary

Electron/Positron excess

PAMELA

ATIC/PPB-BETS ⇔ Fermi/HESS

Dark matter? Astrophysical sources?

Astrophysical source

$\sim 10^{50}$erg $e^{\pm}$ $\sim 10^{5\text{-}6}$yr ago

Fit spiky ATIC as well as Smooth Fermi

Spectral cutoff similar to DM case

Cutoff energy ~ 300GeV$(10^6$yr/t)

Cutoff width $\Delta\varepsilon/\varepsilon \sim \Delta t/t$

PAMELA e/h separation

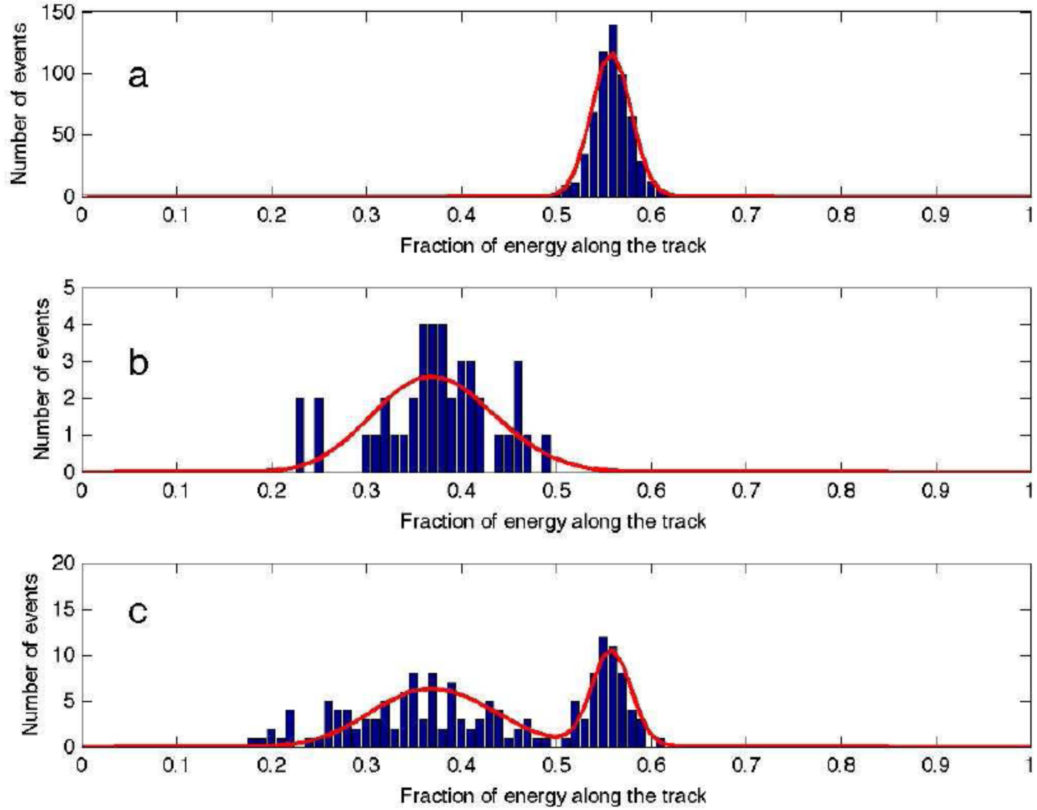

FIG. 2: **Calorimeter energy fraction $\mathcal{F}$: 28–42 GV.** Panel **a** shows the distribution of the energy fraction for negatively charged particles, selected as electrons in the upper part of the calorimeter. Panel **b** shows the same distribution for positively charged particles selected as protons in the bottom part of the calorimeter. Panel **c** shows positively charged particles, selected in the upper part of the calorimeter, i.e. protons and positrons.

Antiproton as predicted

No excess for antiproton

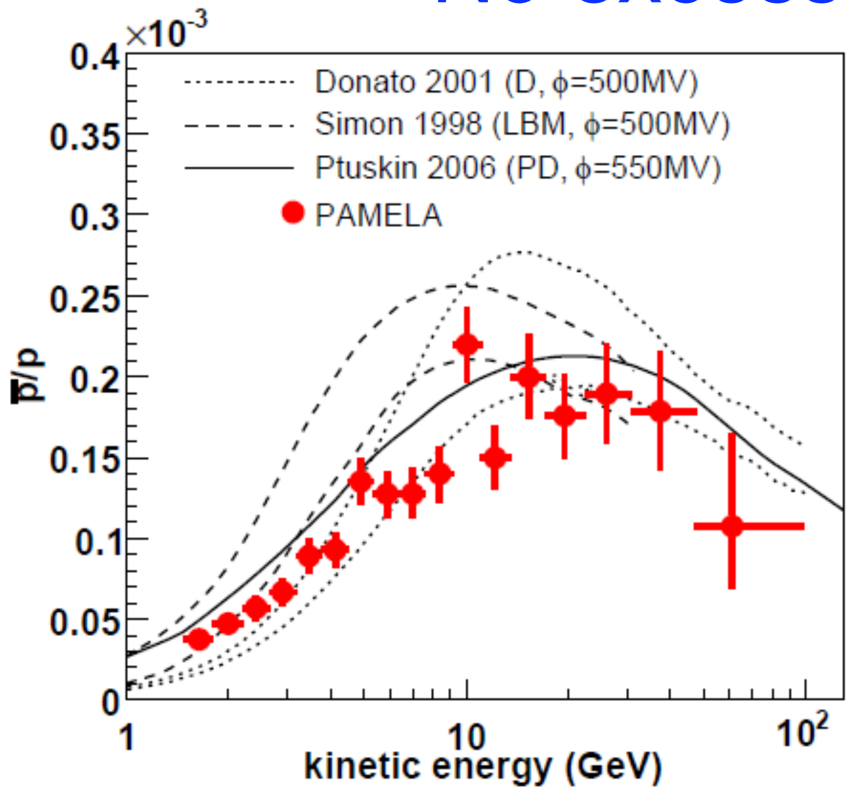

FIG. 3: The antiproton-to-proton flux ratio obtained in this work compared with theoretical calculations for a pure secondary production of antiprotons during the propagation of cosmic rays in the galaxy. The dashed lines show the upper and lower limits calculated by Simon et al. [17] for the standard Leaky Box Model, while the dotted lines show the limits from Donato et al. [18] for a Diffusion model. The solid line shows the calculation by Ptuskin et al. [19] for the case of a Plain Diffusion model. The curves were obtained using appropriate solar modulation parameters (indicated as ϕ) for the PAMELA data taking period.

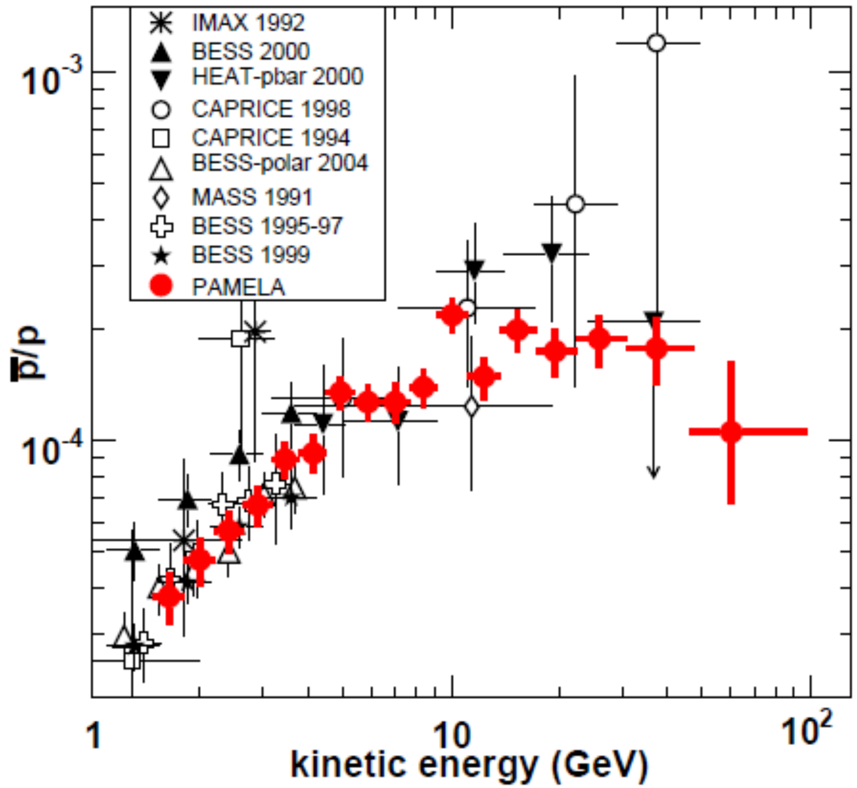

Adriani+(PAMELA) 08

Fermi $\Delta\varepsilon_e$

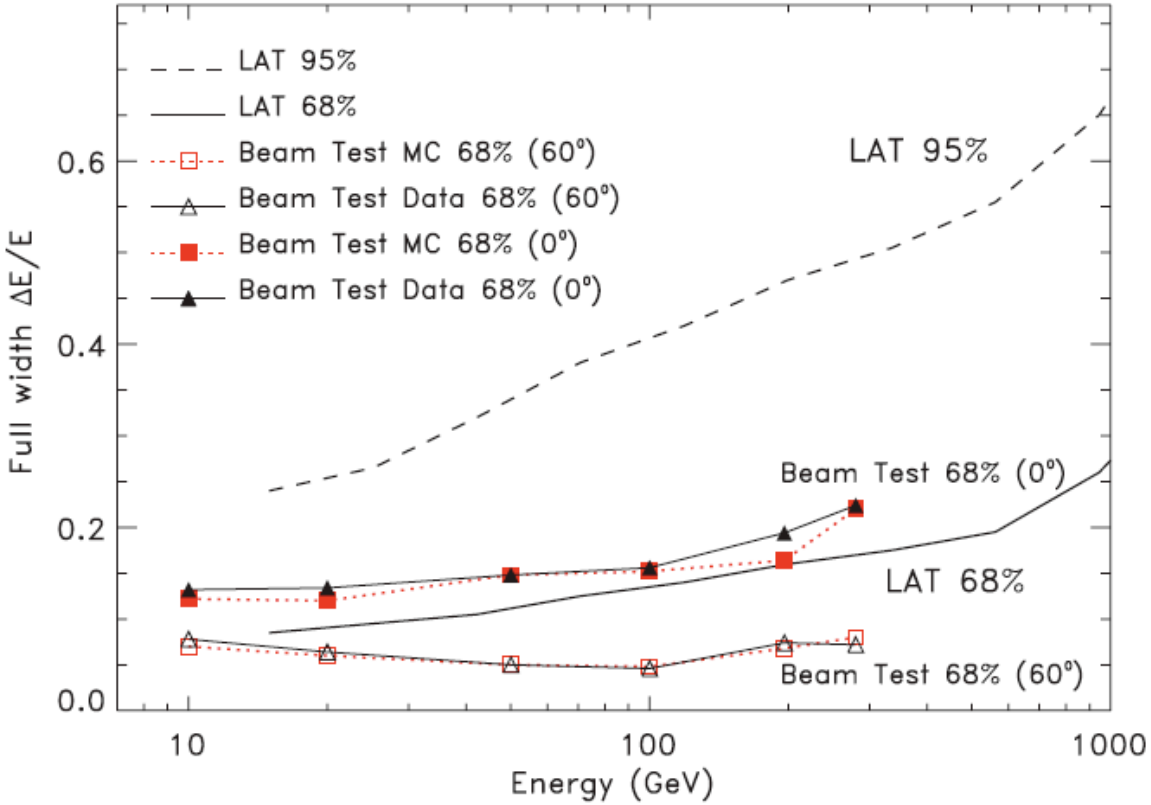

FIG. 1 (color online). Energy resolution for the LAT after electron selection; the full widths of the smallest energy window containing the 68% and the 95% of the energy dispersion distribution are shown. The comparison with beam test data up to 282 GeV and for on-axis and at 60° incidence shown in the figure indicates good agreement with the resolution estimated from the simulation.

Abdo+ 09

Fermi e/h separation

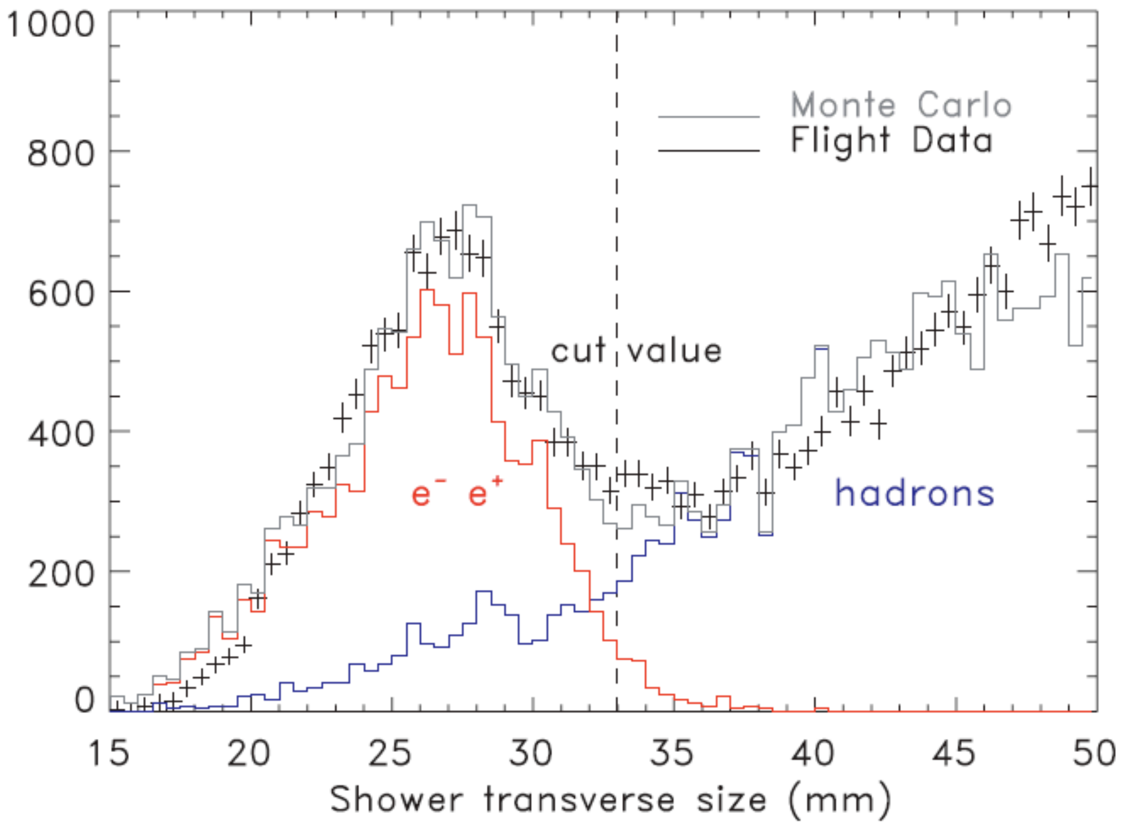

FIG. 2 (color online). Distribution of the transverse sizes of the showers (above 150 GeV) in the CAL at an intermediate stage of the selection, where a large contamination from protons is still visible. Flight data (black points) and MC simulation (gray solid line) show very good agreement; the underlying distributions of electron and hadron samples are visible in the left (red) and the right (blue) peaks, respectively.

Abdo+ 09

Fermi e/h separation

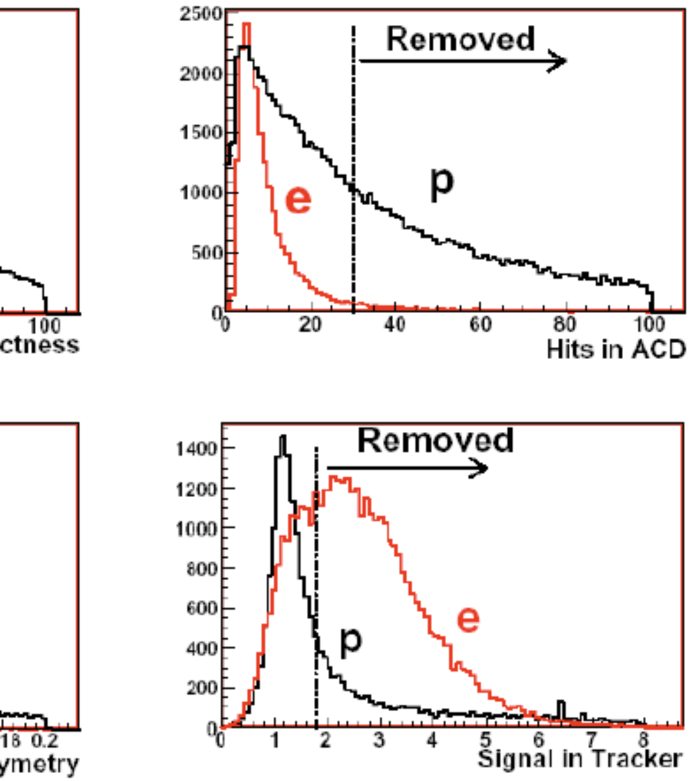

or the analysis. Number of protons
to the number of electrons (red

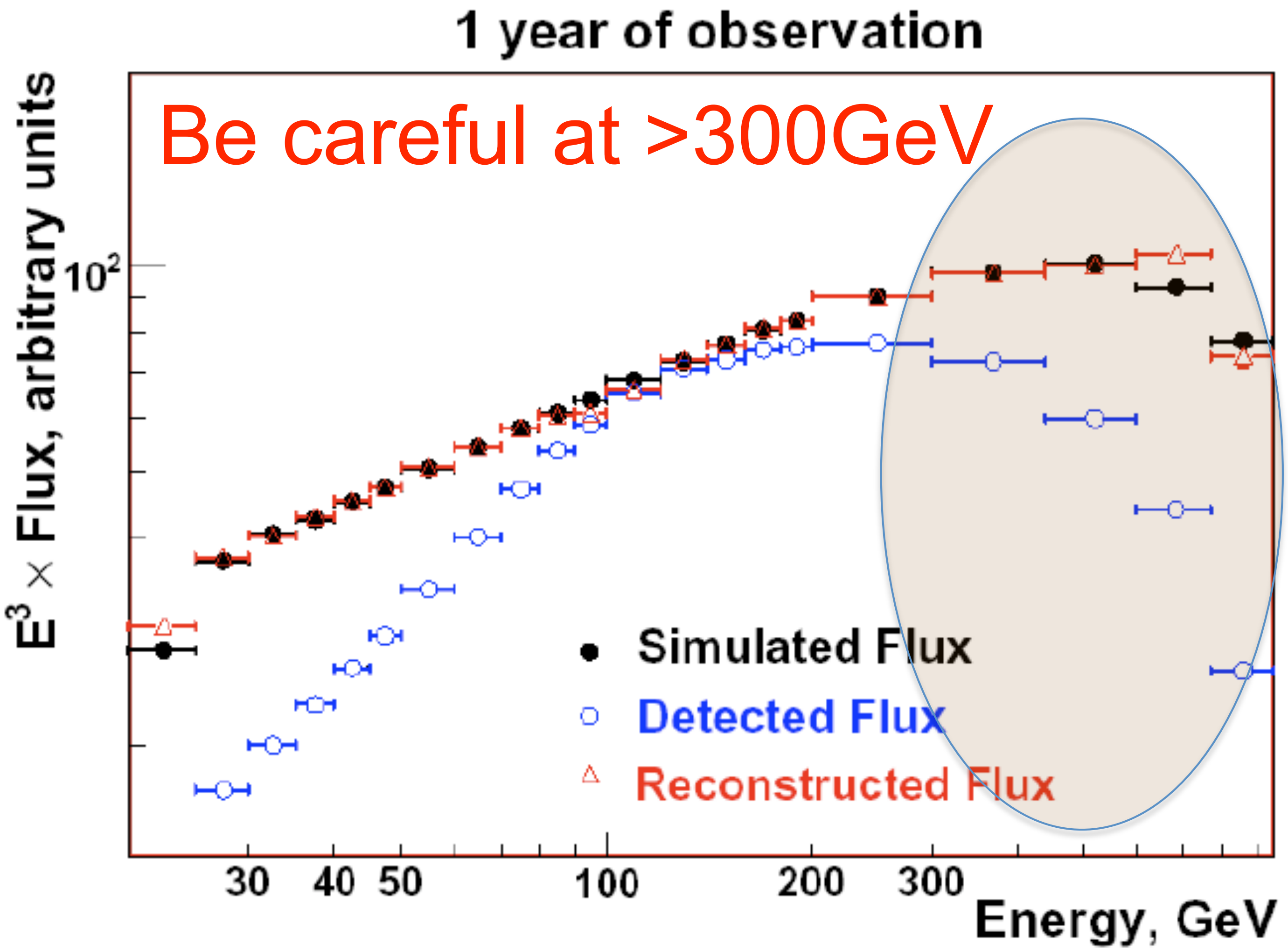

Figure 4. Electron flux reconstruction (see details in the text)

Moiseev+ 07

HESS 08

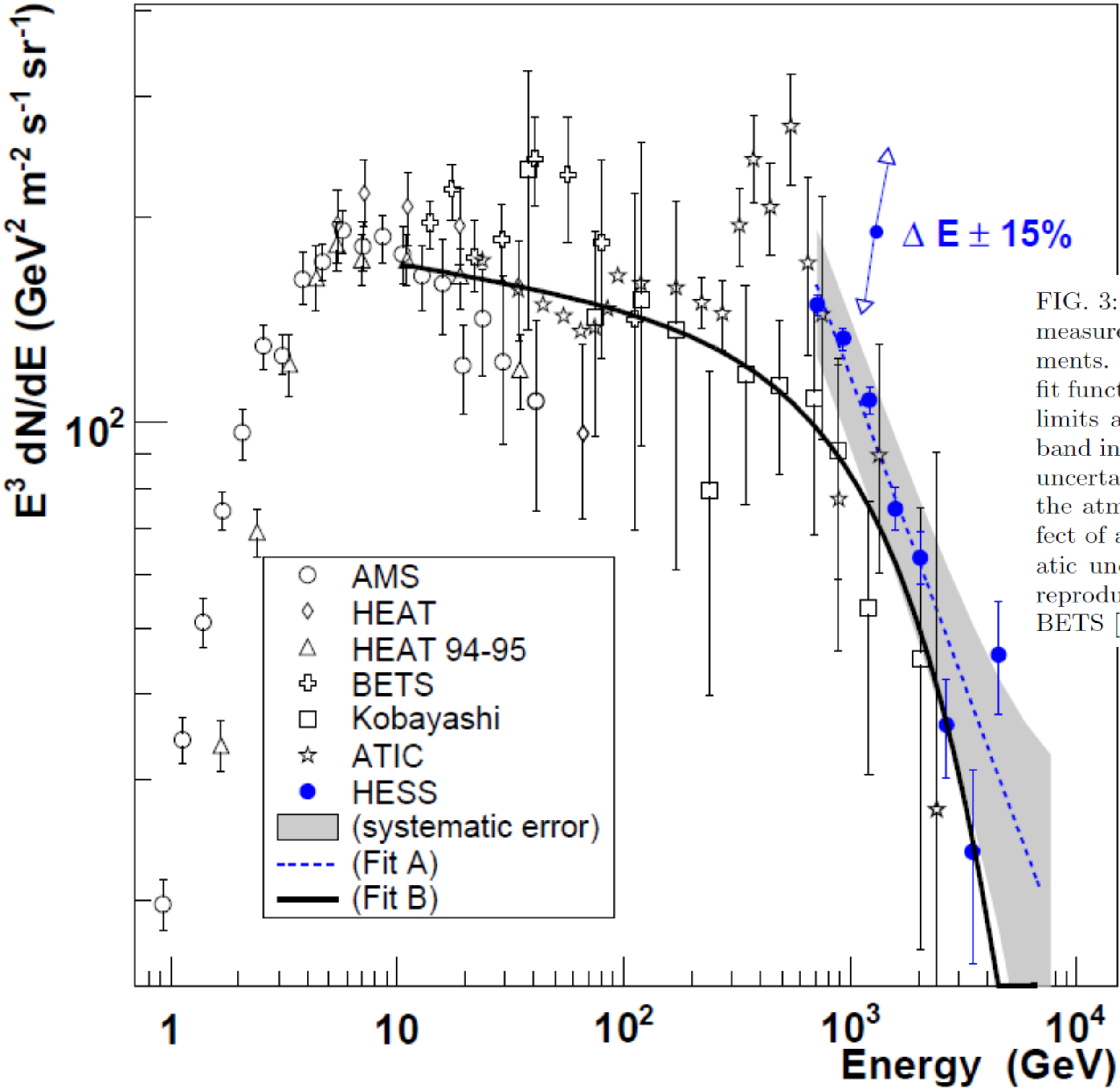

FIG. 3: The energy spectrum E^3 dN/dE of CR electrons as measured by H.E.S.S. in comparison with previous measurements. The H.E.S.S. data are shown as solid points. The two fit functions (A and B) are described in the main text. Upper limits are given for a confidence level of 95%. The shaded band indicates the approximate systematic error arising from uncertainties in the modeling of hadronic interactions and in the atmospheric model. The double arrow indicates the effect of an energy scale shift of 15%, the approximate systematic uncertainty on the H.E.S.S. points. Previous data are reproduced from: AMS [18], HEAT [19], HEAT 94-95 [20], BETS [21], Kobayashi [2] and ATIC [22].

Polarcap

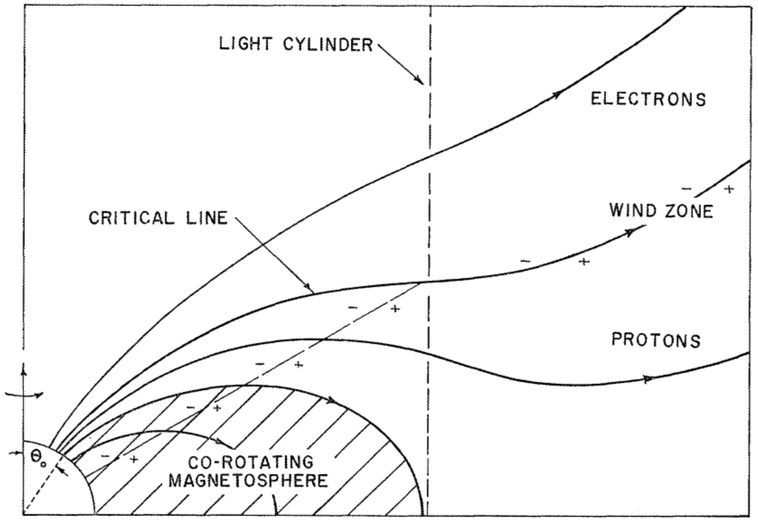

FIG. 1.—Schematic diagram showing the corotating magnetosphere and the wind zone. Star is at lower left.

Goldreich&Julian 69

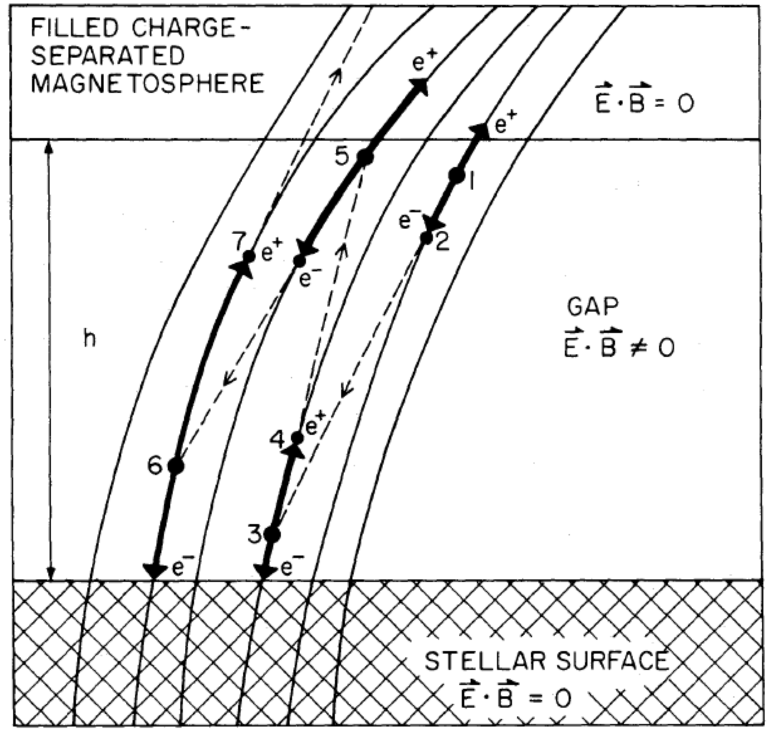

FIG. 3.—Breakdown of the polar gap. The solid lines are polar field lines of average radius of curvature ρ; for a pure dipole field $\rho \sim (Rc/\Omega)^{1/2} \sim 10^8 P^{1/2}$ cm, but for a realistic pulsar one expects $\rho \sim 10^6$ cm if many multipoles contribute near the surface. A photon (of energy $> 2\,mc^2$) produces an electron-positron at *1*. The electric field of the gap accelerates the positron out of the gap and accelerates the electron toward the stellar surface. The electron moves along a curved field line and radiates an energetic photon at *2* which goes on to produce a pair at *3* once it has a sufficient component of its momentum perpendicular to the magnetic field. This cascade of pair production—acceleration of electrons and positrons along curved field lines—curvature radiation—pair production results in a "spark" breakdown of the gap.

$$\Delta V \approx \frac{\Omega^2 B_s R^3}{c^2} = 10^{16}\left(\frac{\Omega}{10^2\ \mathrm{s}^{-1}}\right)^2\left(\frac{B_s}{3\times10^{12}\ \mathrm{G}}\right)\left(\frac{R}{10^6\ \mathrm{cm}}\right)^3 \mathrm{V}\,, \tag{2.1}$$

Ruderman&Sutherland 75

Outergap

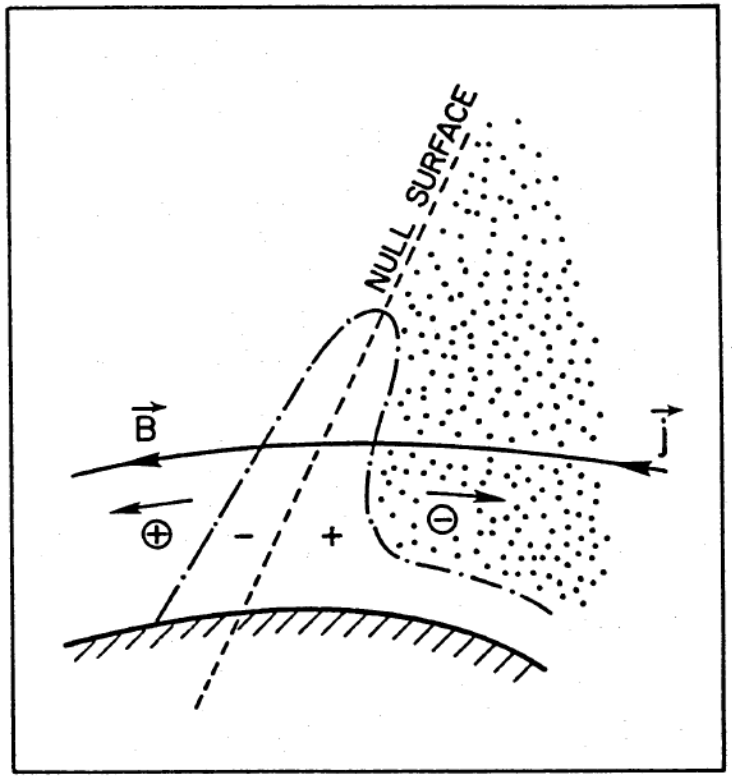

FIG. 2.—A growing charge-deficient region ($\rho \approx 0$) in the outer magentosphere near a null surface. Negative charge is assumed to flow out, leaving behind a partial void near that surface (labeled + for the equivalent electrostatic effect of the absence of −). The Coulomb field of $\rho - \rho_0 \approx -\rho_0$ pushes positive charge + on the other side of the null surface toward the star, leaving behind a partial void which acts as a negative charge region (as labeled).

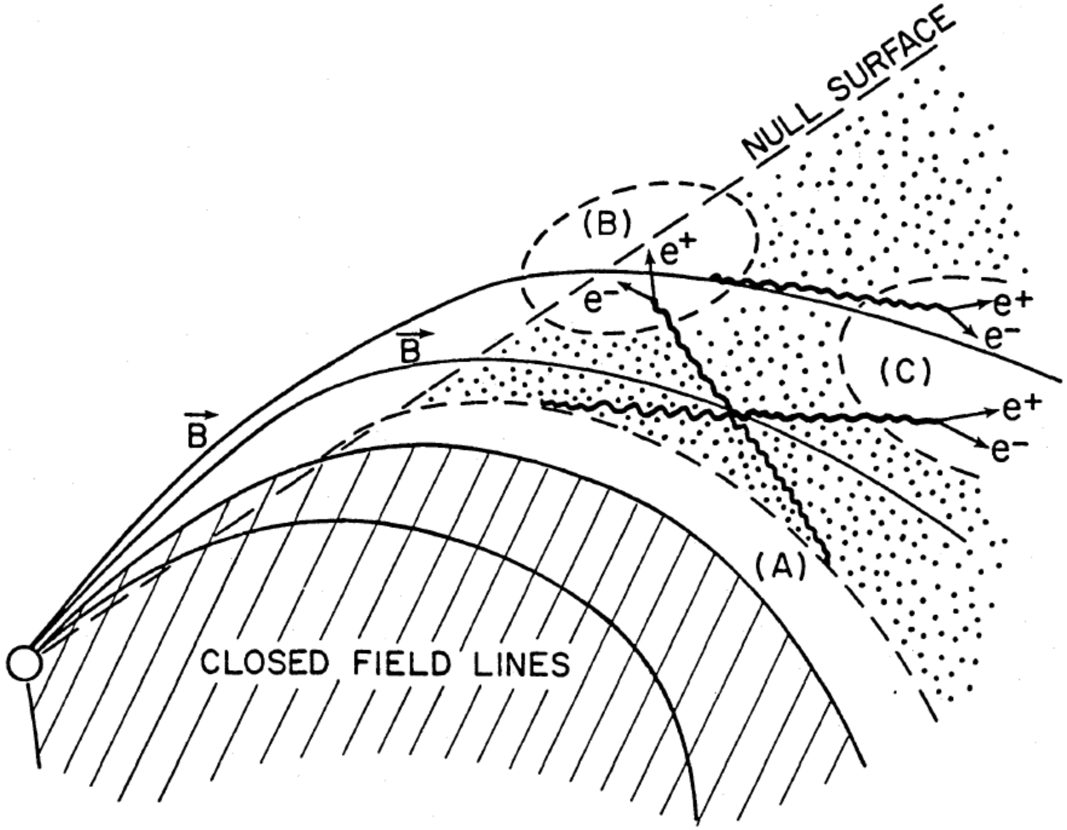

Chen,Ho & Ruderman86

High Energy γ

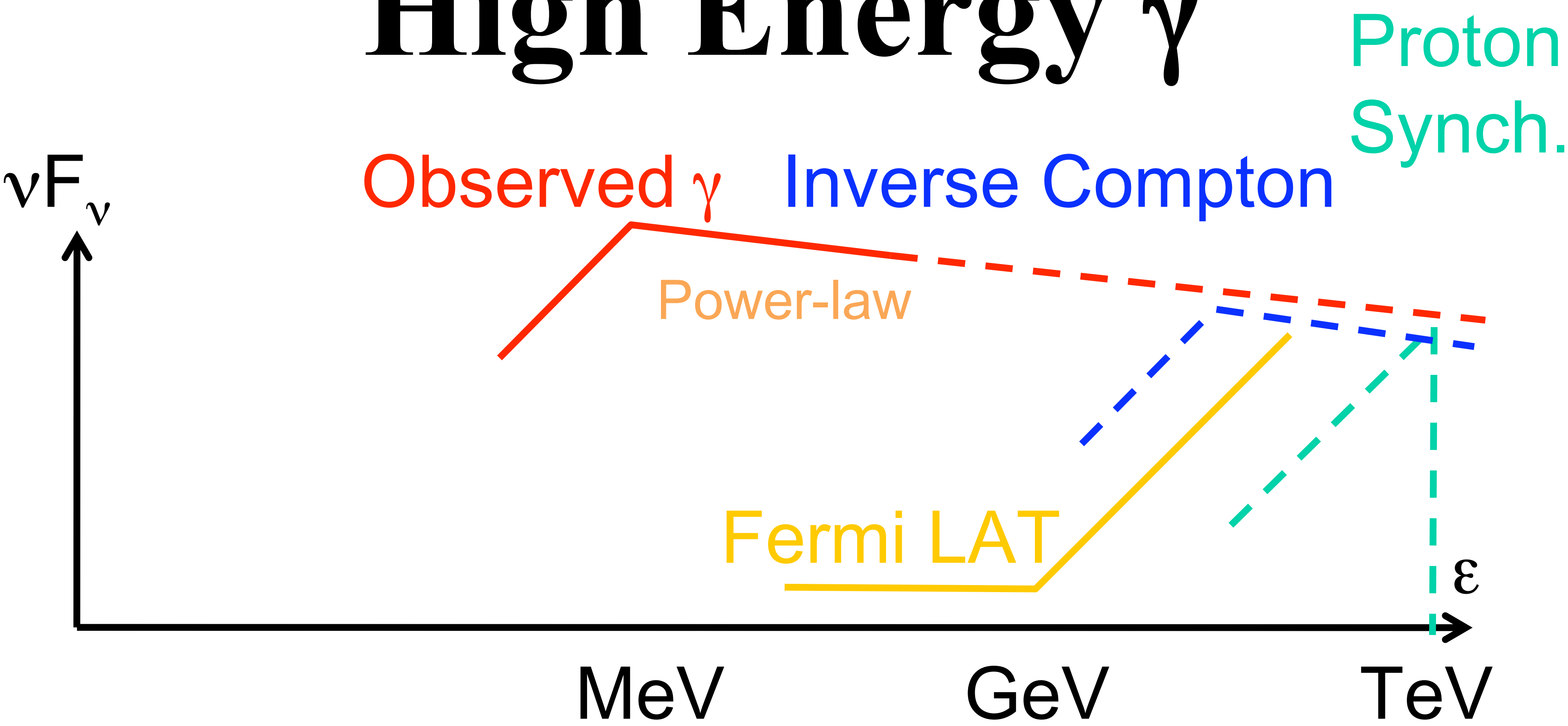

If extrapolate to TeV ⇒ E(MeV)~E(GeV-TeV)

Other components are also expected

Fermi LAT: 080825C (<35sec, 14γ <GeV),
080916C (14γ >GeV), 081024B (Short, <3GeV)
090510 (short, high Epeak)

$e^{\pm}$ cutoff and line

1. $e^{\pm}$ cutoff energy ⇒ Jet velocity

$e^+e^- \to \gamma\gamma$ 2. $e^{\pm}$ line ⇒ $e^{\pm}$ abundance

(⇒ Jet properties ⇒ Central engine)

KI+ 07
Murase&KI 08

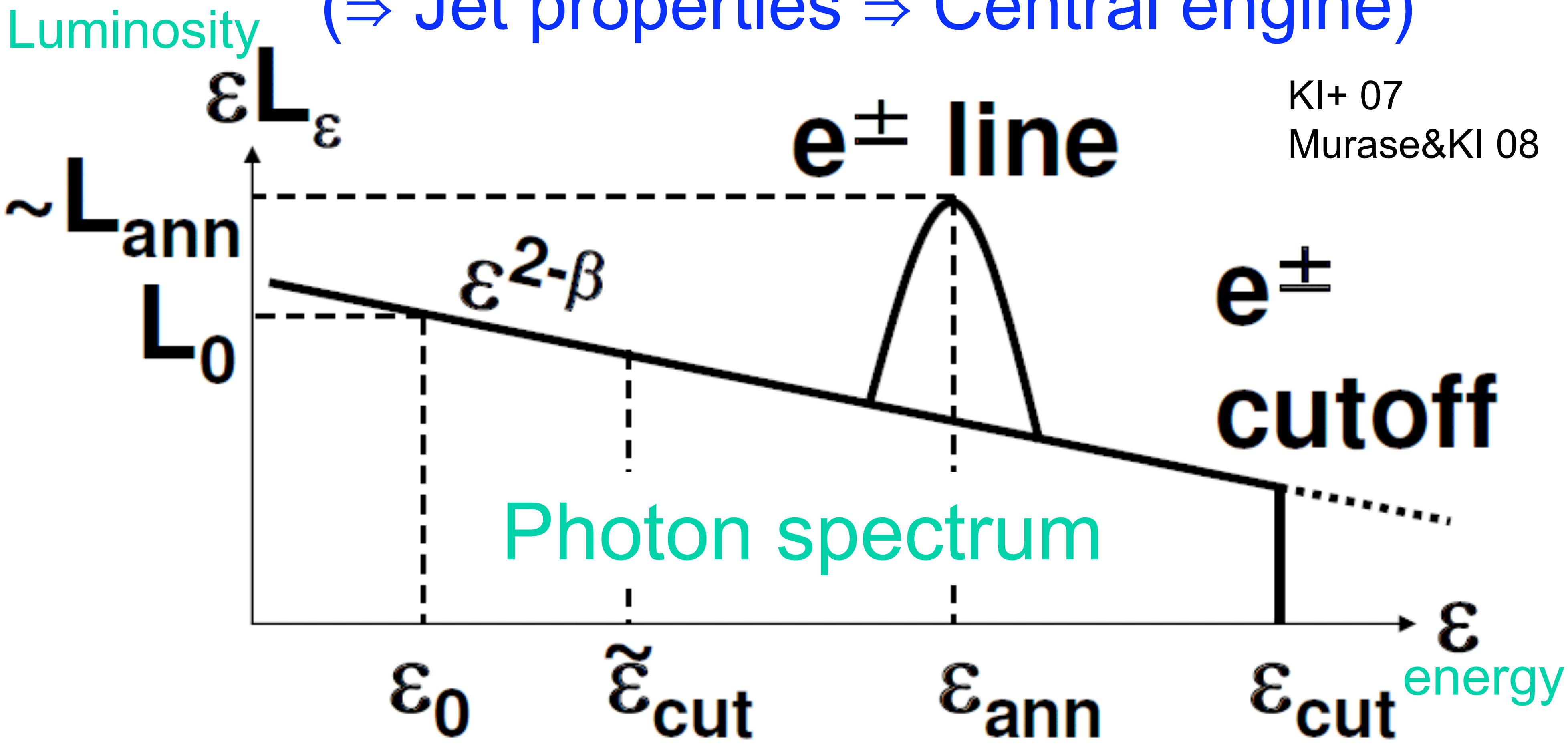

Low Energy γ

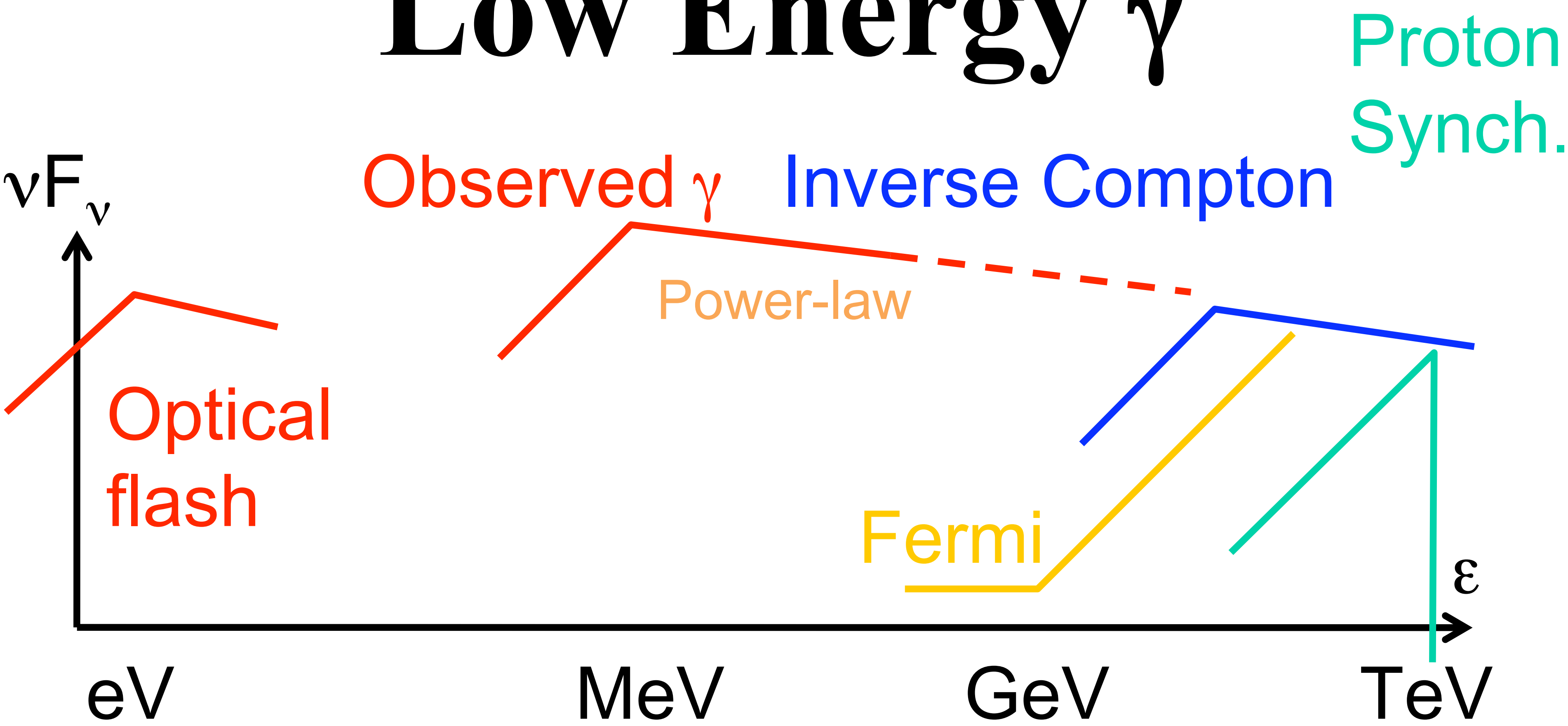

Some GRBs have ~eV photon (optical) flashes

Optical flash was theoretically expected

⇒ Absorption/Scattering by dust?

(~1/2 GRBs are dark without optical afterglow)

Dust sublimation

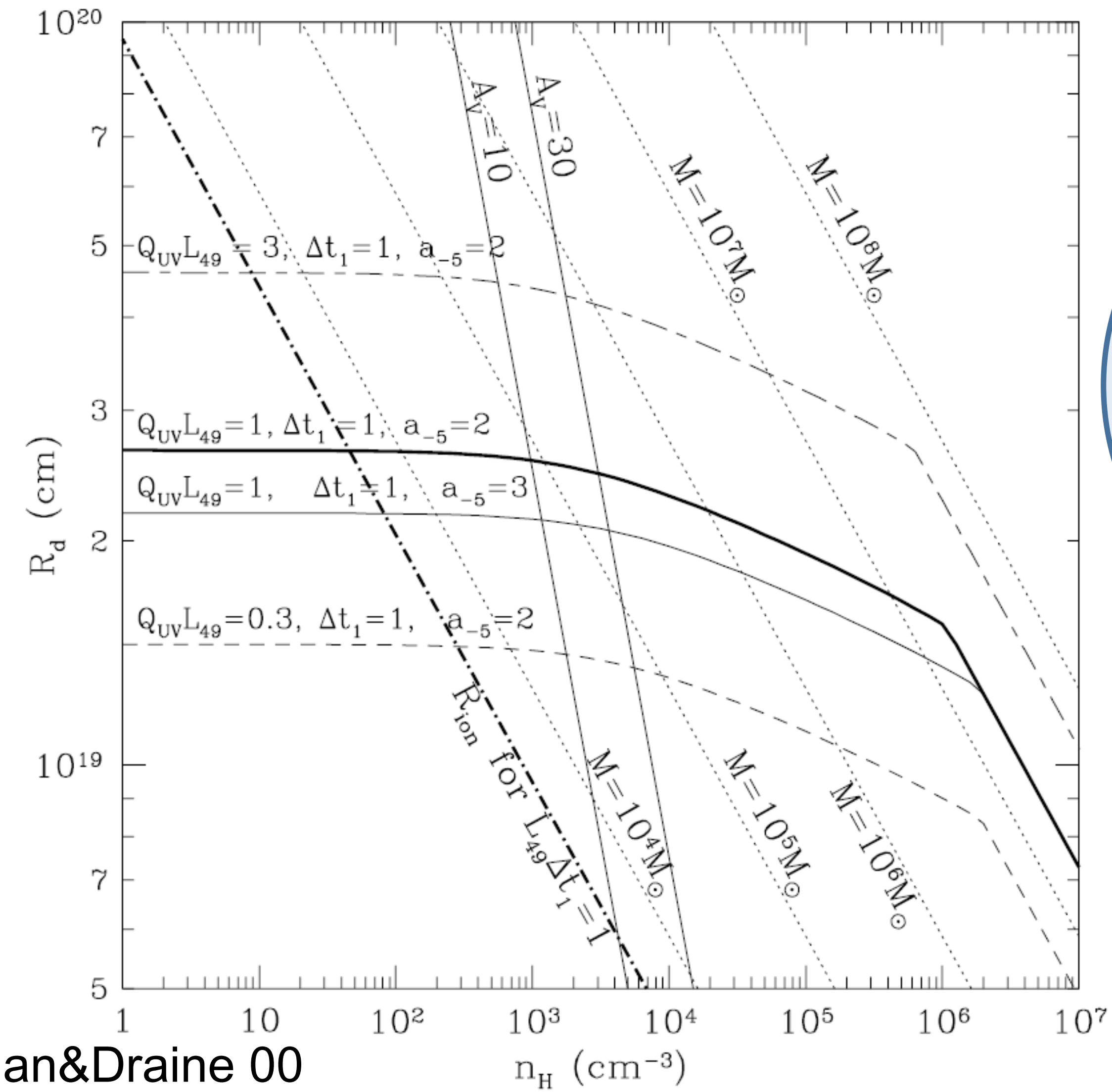

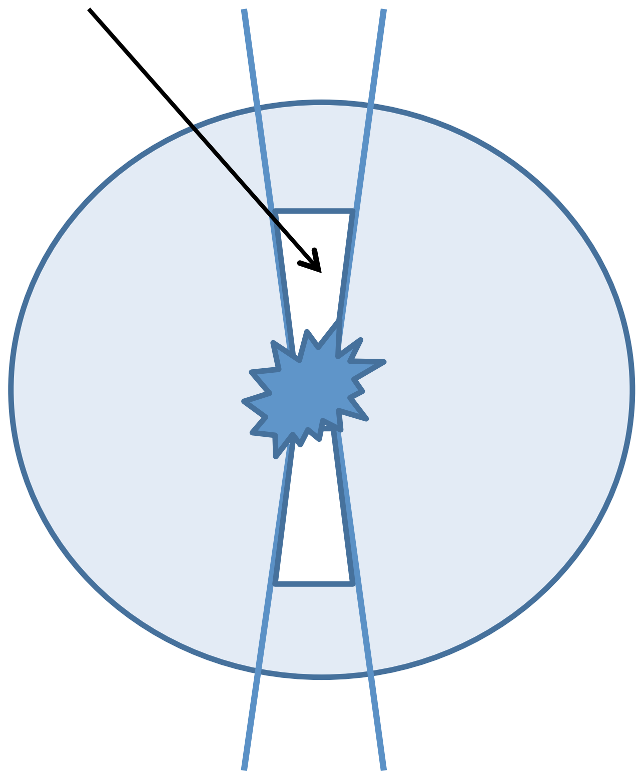

Scattering only at the outside

Waxman&Draine 00

FIG. 1.—Radius R_d out to which grains are destroyed by thermal sublimation, as a function of cloud density n_H, for different values of L_{49}, Δt_1, and a_{-5}. The heavy curve is for "typical" GRB parameters. The lines $A_V = 10$ and $A_V = 30$ show the radius of a cloud having $A_V = 10$ and 30 from center to edge. Also shown (*dot-dashed line*) is the radius R_{ion} out to which the gas is photoionized by a flash with $L_{49}\Delta t_1 = 1$. Dotted lines indicate radii with enclosed gas mass from 10^4 to 10^8 $M_\odot$.

Old SNR

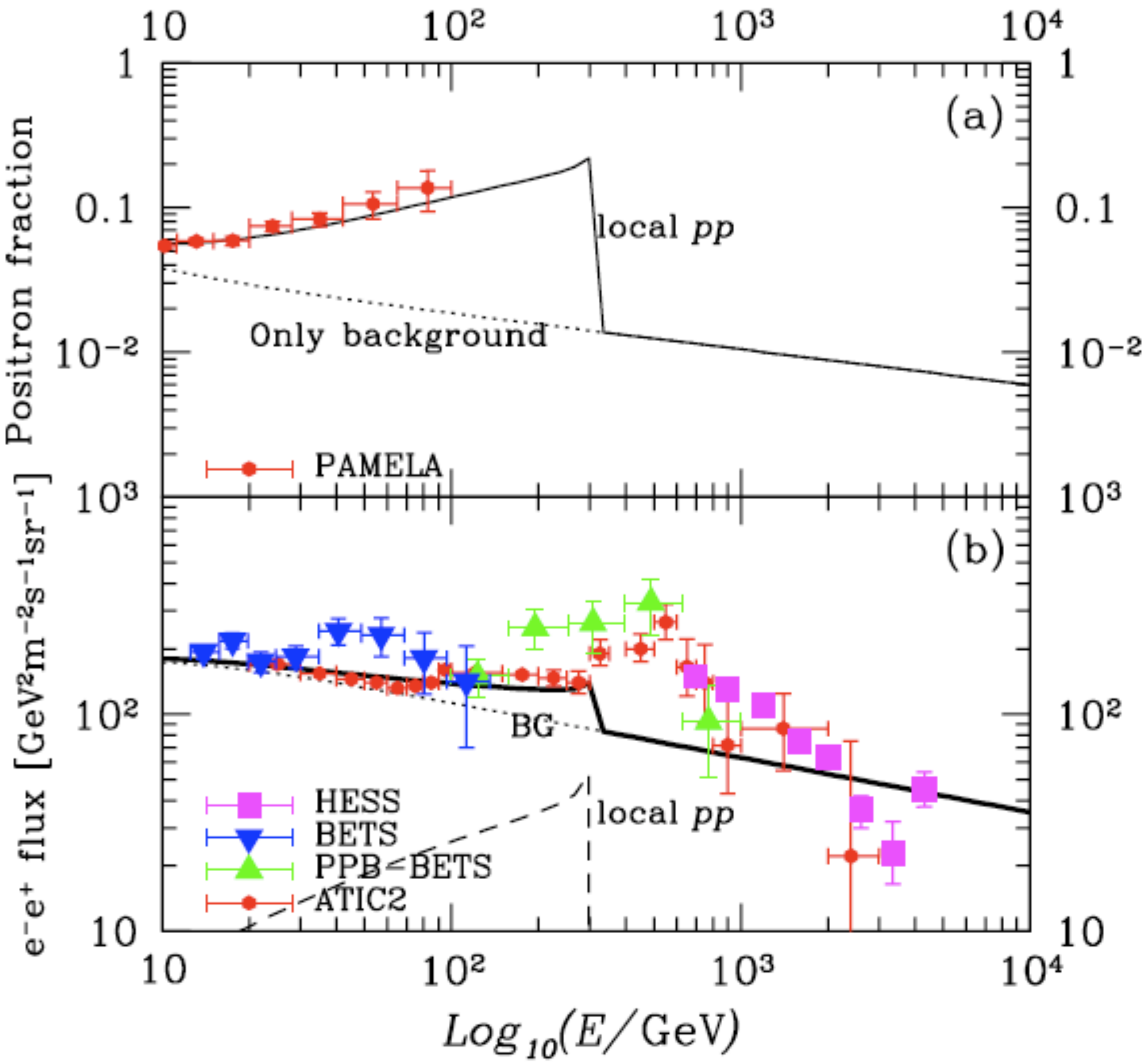

SN in
Dense Cloud

$R \sim 40$pc,
$n \sim 100\mathrm{cm}^{-3}$,
$d = 200$pc,
$s = 1.6$,
$t_{pp} = 10^6$yr,
$E_p = 3\mathrm{x}10^{50}$erg

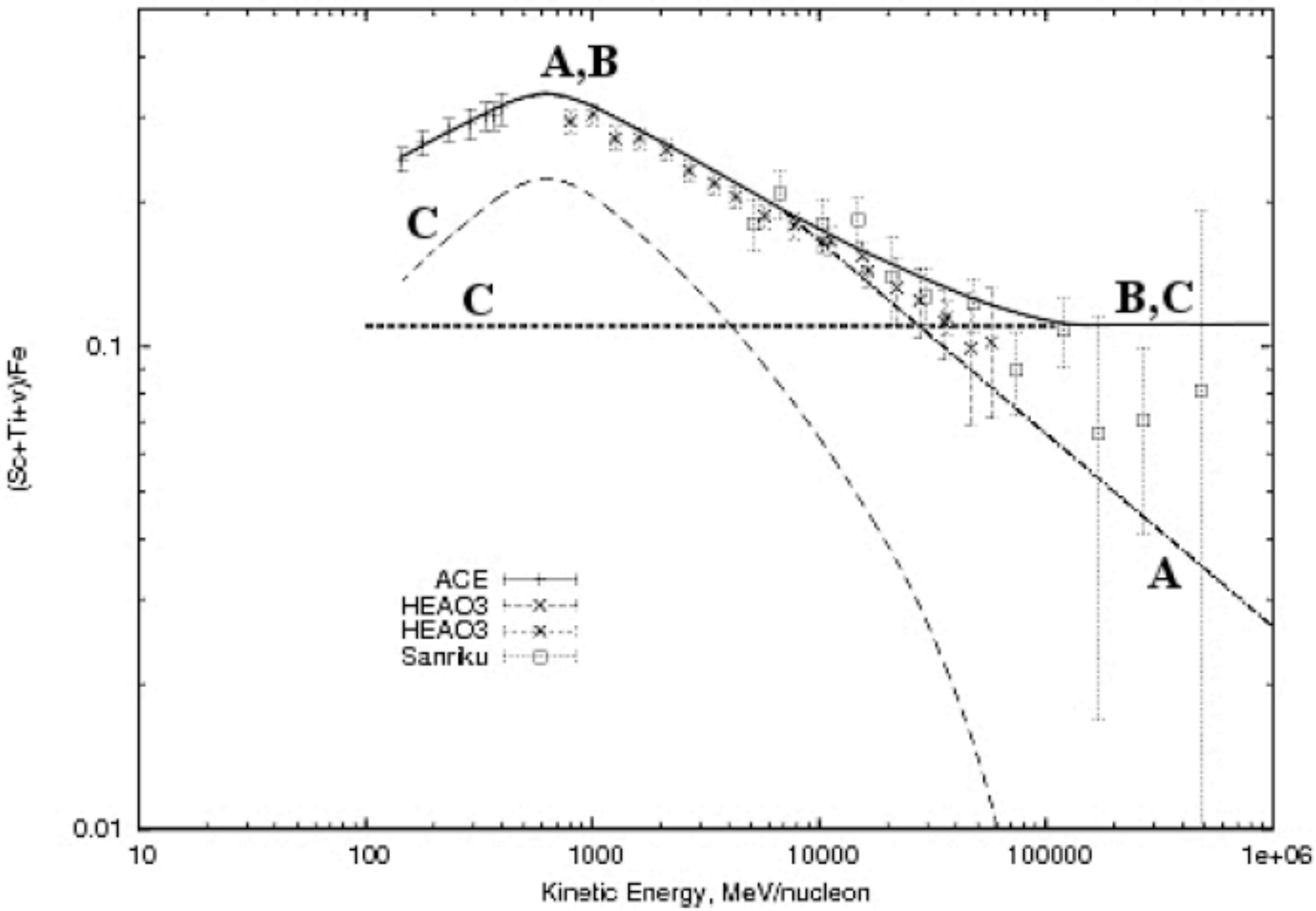

Cowsik & Burch 09

FIG. 4: The observed (Sc+Ti+ν)/Fe secondary to primary ratio is plotted (points from a compilation in [11]) along with the power law extrapolation at high energies (dot-dashed line, Model A), a constant extrapolation (solid line, Model B), and a two-component fit (dotted lines, Model C).

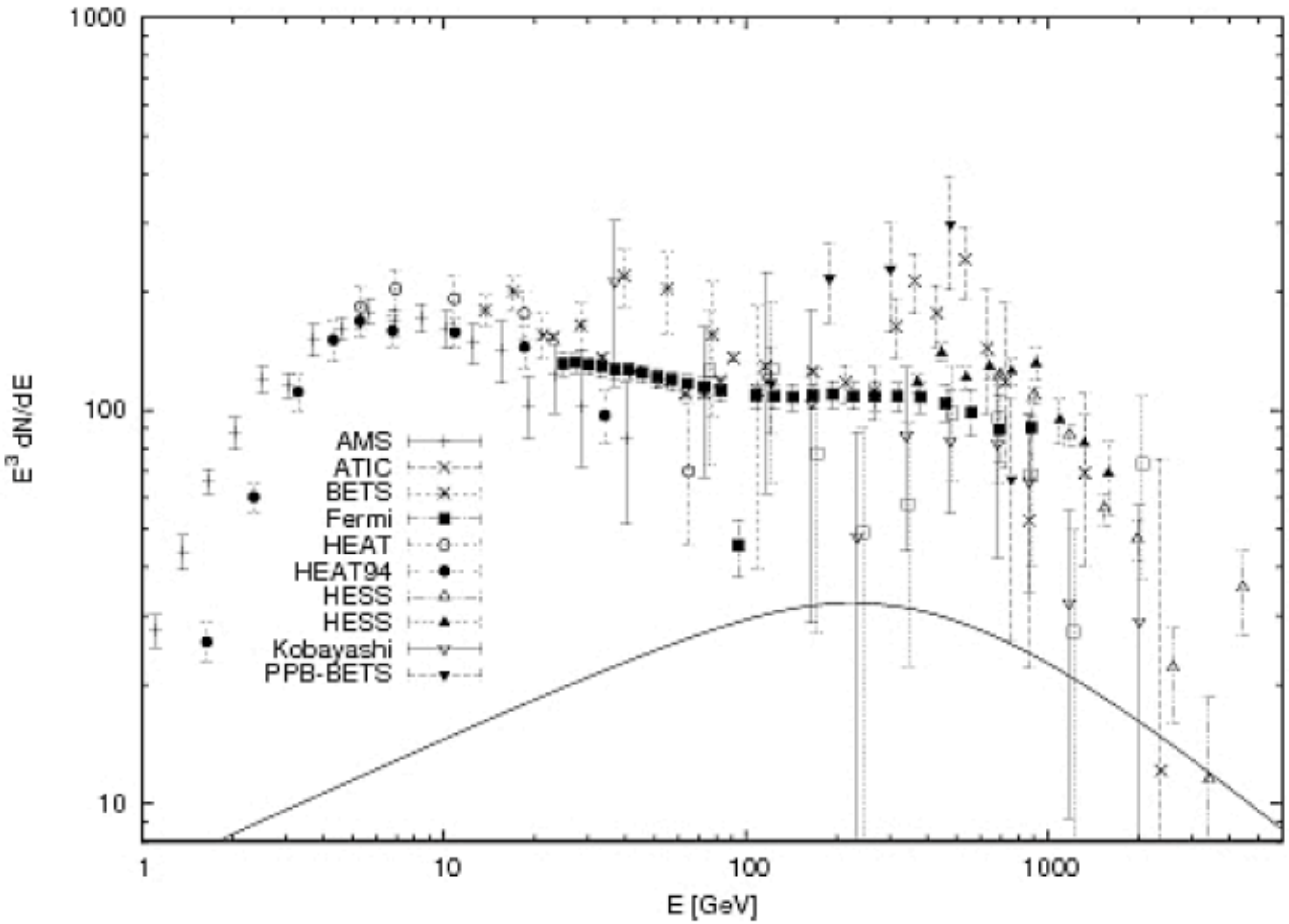

Cowsik & Burch 09

FIG. 5: Here we have subtracted $f_{n^+}(E)$ and $f_{n^-}(E)$ from the total spectrum of the electronic component and have shown $g_e(E)$, the spectrum of electrons generated by the cosmic ray sources. The primary electron component $g_e(E)$ is plotted for the HESS, FERMI, ATIC and other data using $\eta = 0.45$. The positron spectrum from the nested leaky box model C is plotted as well (solid line).

Other possibilities

Simple model $\Rightarrow$ $E \sim 10^{50}$erg~(GRB)

1. 10msec pulsar has a rotational energy of $E \sim 10^{50}$erg (Kawanaka,KI+09)
2. $L_{Eddington}$ (10^{38}erg/s) x 10^{5}yr ~ 10^{50}erg
   e.g., Black hole + Disk + Jet
   (Microquasar)
3. Supernova remnant (Fujita+KI 09)
   $pp \rightarrow \pi \rightarrow e^{+}$

$e^{\pm}$ cooling

Lavalle+ 07

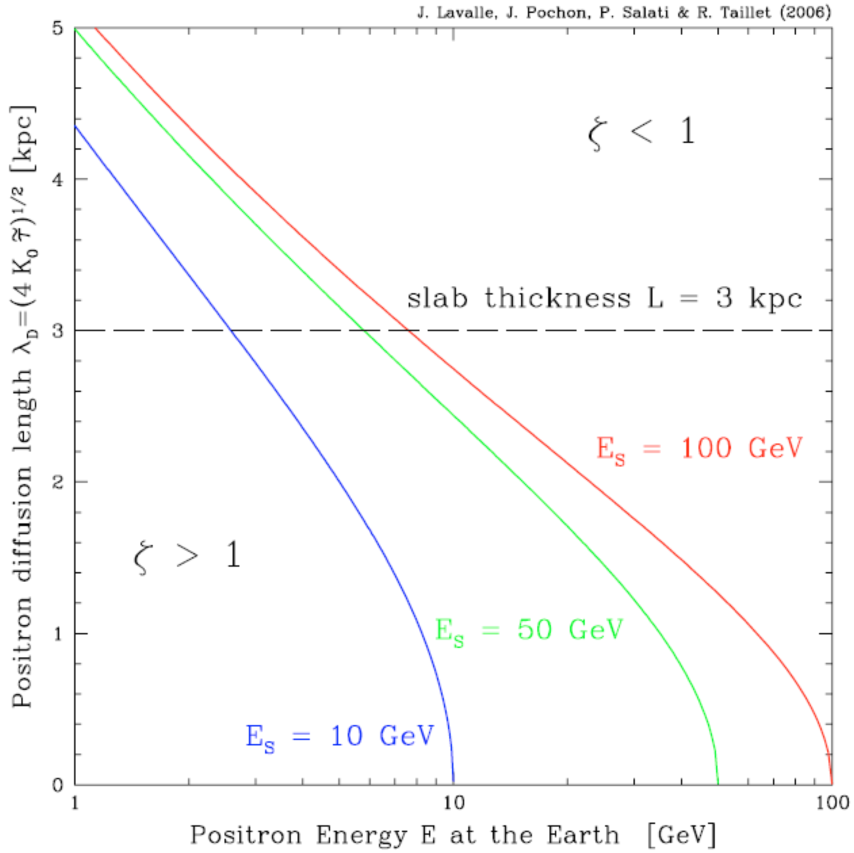

Fig. 6. The positron diffusion length λ_D decreases as the energy E at the Earth approaches the energy E_S of the line. The long-dashed horizontal line corresponds to a diffusion length λ_D equal to the thickness L of the diffusion layers. Below that limit, positron propagation is not sensitive to the vertical boundaries and the infinite 3D approximation is valid. This regime corresponds to large values of the parameter ζ – see the definition (42).

$e^{\pm}$ lose energy (cool) via inverse Compton and synchroton

Sources should be within R_d~kpc < Galactic disk~10kpc

Diffusion time ~R_d^2/K~10^7yr
⇒ Galactic Rate >1/10^5yr

Cosmic Ray

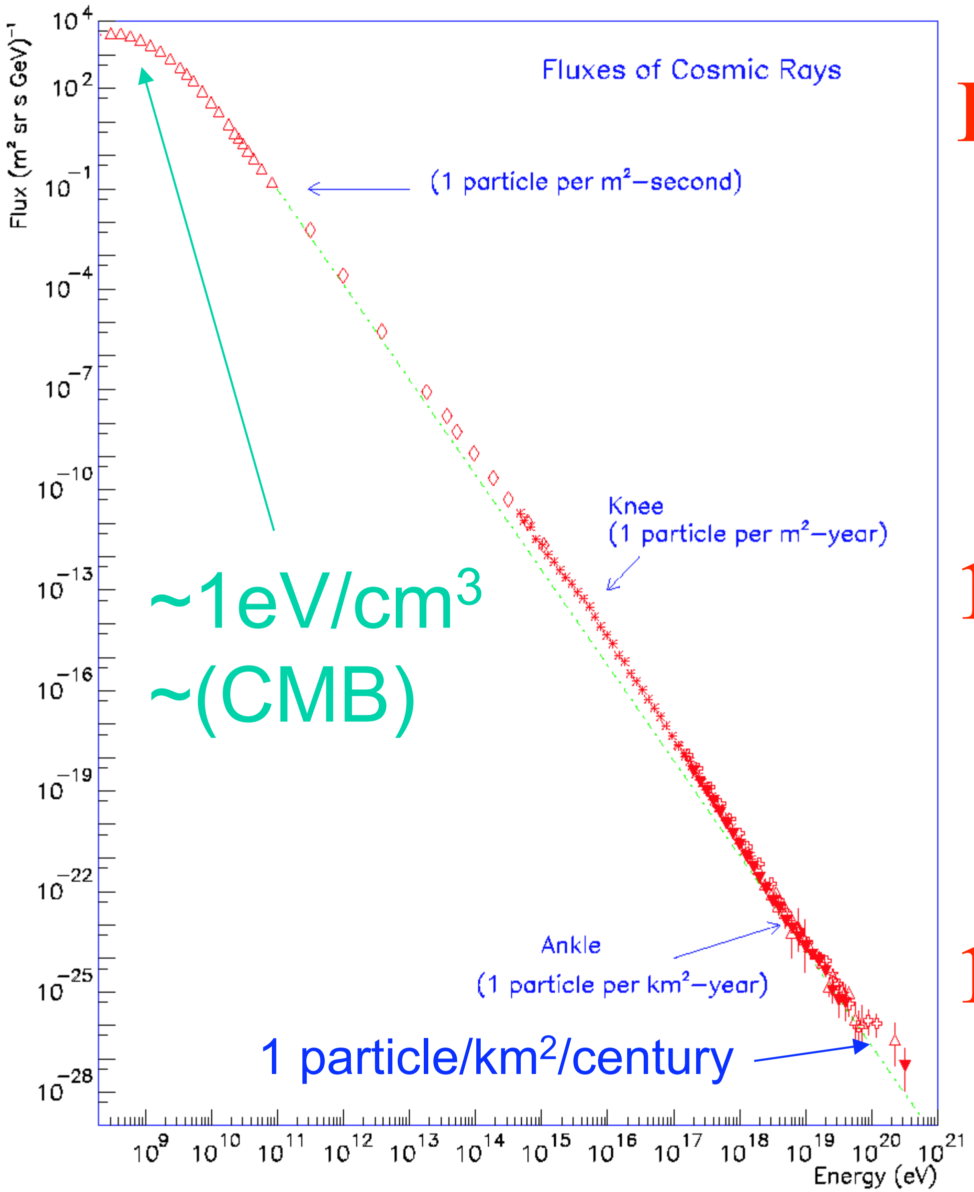

Bhattacharjee&Sigl(00)

$E<10^{15\text{-}16}$eV (Knee)

$F \propto E^{-2.7}$

Probably Galactic SNR

$L_{CR} \sim 10^{41}$erg/s$\sim 0.1 E_{SN}/t_{SN}$

No direct evidence

$10^{15\text{-}16}<E<10^{18}$eV (Ankle)

$F \propto E^{-3\text{-}3.2}$

Galactic origin??

Simple SNR: $E<10^{14}$eV

10^{18}eV$<E$

$F \propto E^{-2.7}$

Extragalactic AGN? GRB?

Cutoff/Line at ~600 GeV

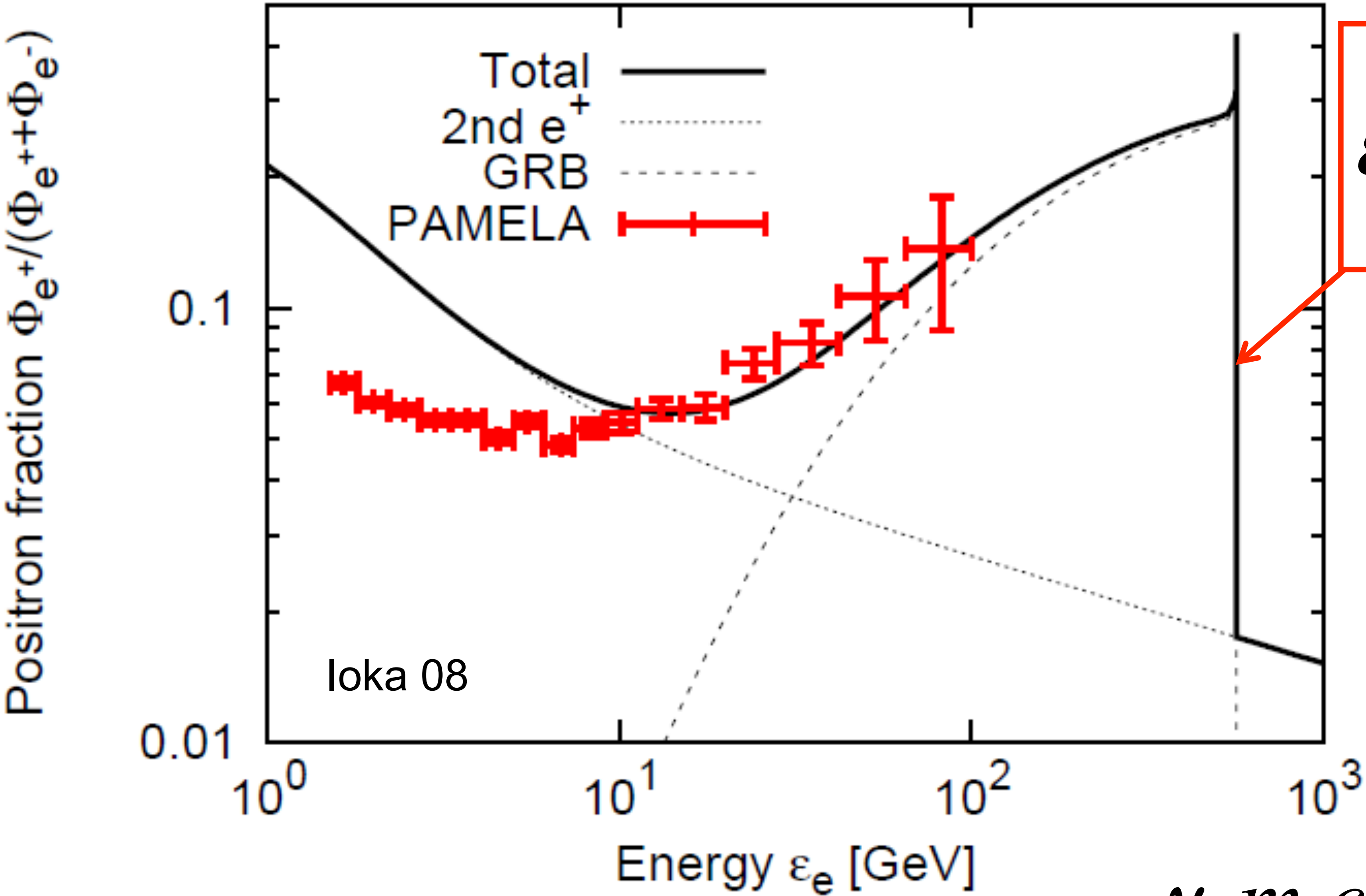

$$\boxed{\varepsilon_{\max} \sim \frac{1}{bt}}$$

Due to cooling

600GeV
⇔t~10^6yr

$$t_{cool} \sim \frac{\gamma_e m_e c^2}{\sigma_T c U_{\gamma+B} \gamma_e^2} \propto \gamma_e^{-1}$$

Multiple pulsars

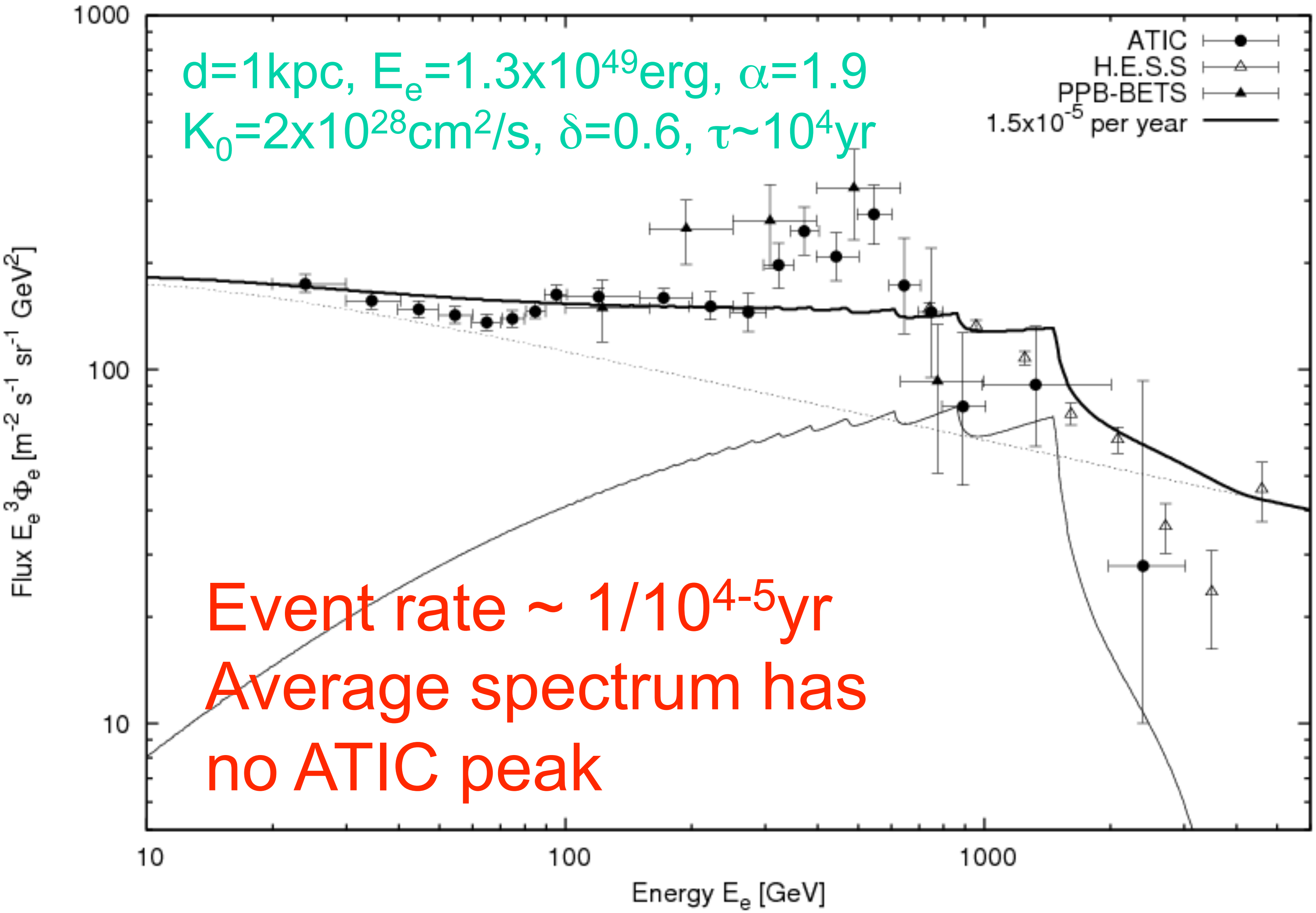

Positron Fraction

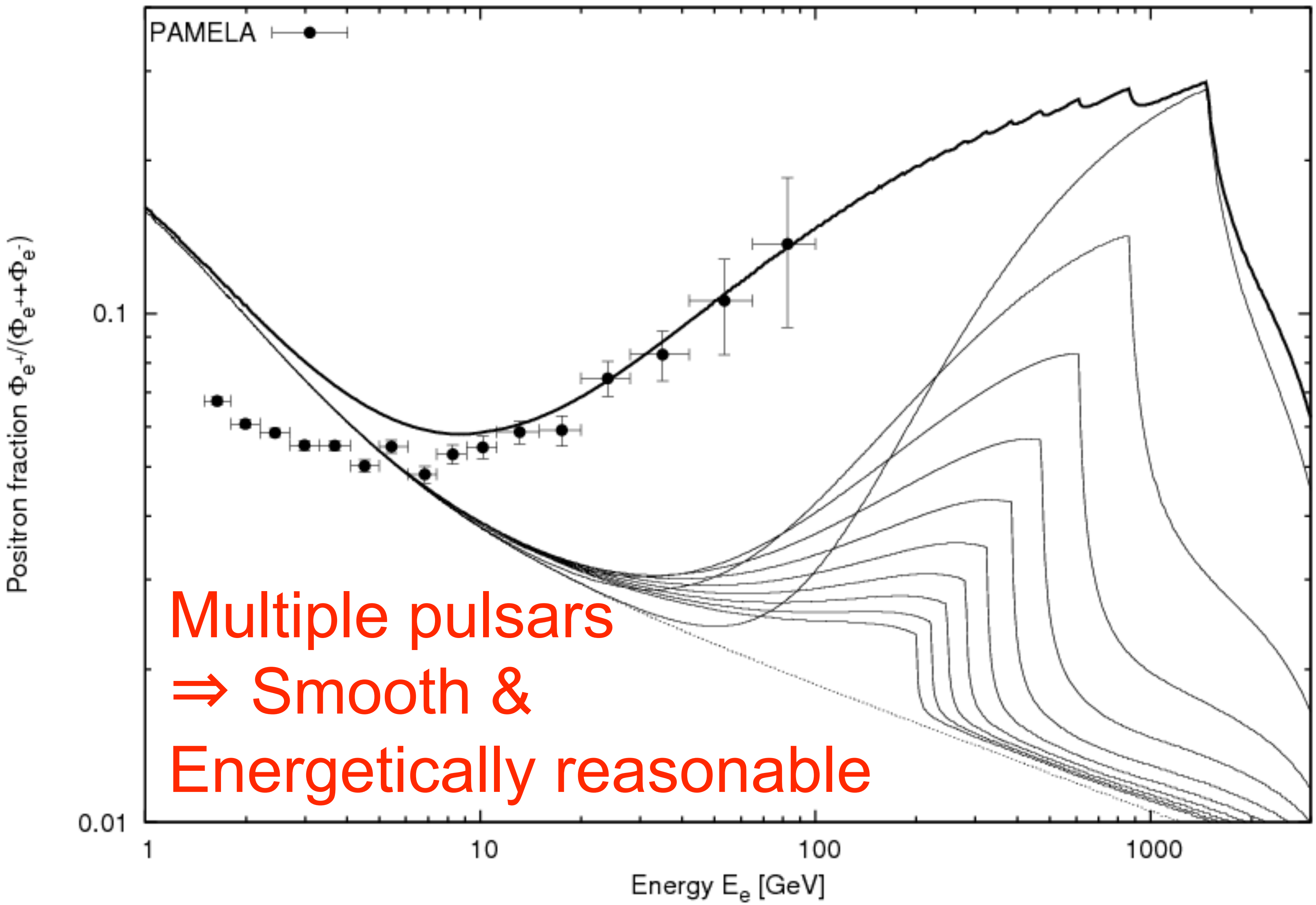

Expected Performance of LAT

- LAT will be able to precisely reconstruct the e-spectrum in **20 GeV –1 TeV**. (still working on extending this range in both directions).
- LAT should detect **> 10^7 electrons above 20 GeV per year** of operation. LAT will be able to check at much better statistics and with much smaller systematic errors on various spectral features !

All currently available experimental results. Not much can be said about spectral features

$$\frac{\Delta\varepsilon_e}{\varepsilon_e} \approx 10\%$$

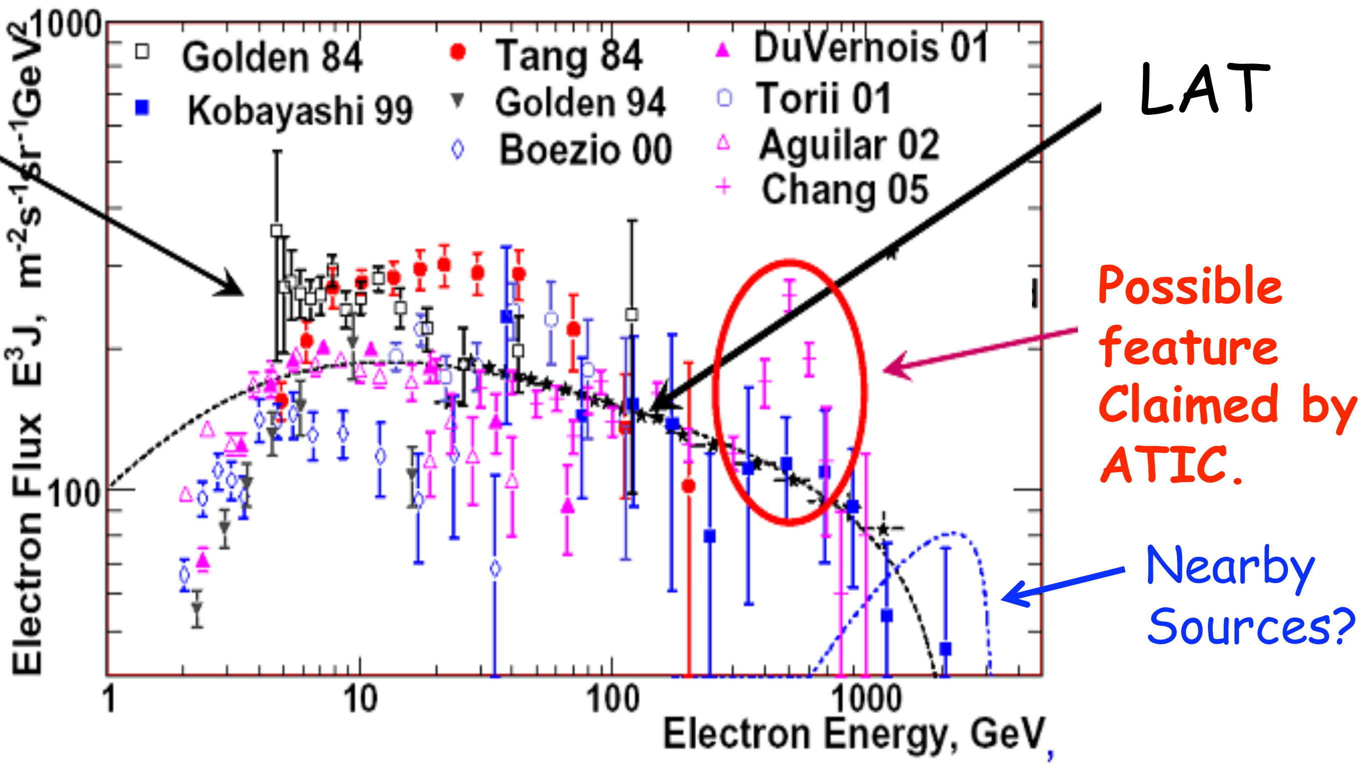

Anisotropy

GRB case (b)

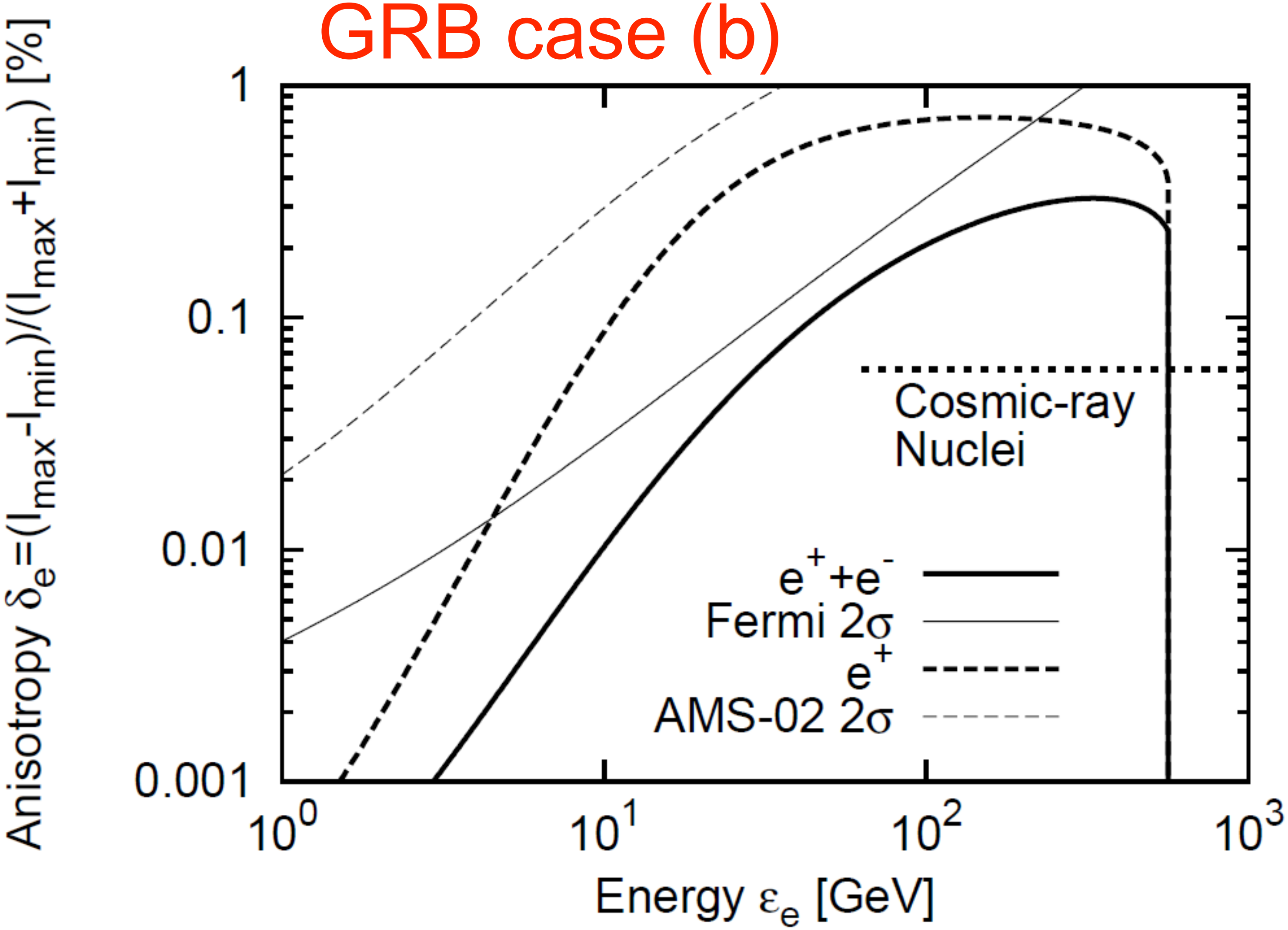

$$\delta = \frac{I_{\max} - I_{\min}}{I_{\max} + I_{\min}}$$

$$= \frac{3K|\nabla f|}{cf}$$

$$\sim \frac{3d}{2ct} @ \varepsilon_e \sim \varepsilon_{\max}$$

⇔ DM case (~0?)

A COSMIC-RAY POSITRON ANISOTROPY DUE TO TWO MIDDLE-AGED, NEARBY PULSARS?

I. BÜSCHING,[1,2] O. C. DE JAGER,[1,2,3] M. S. POTGIETER,[1,2] AND C. VENTER[1,2]

Received 2007 October 23; accepted 2008 March 20; published 2008 April 10

Geminga and B0656+14 are the closest pulsars with characteristic ages in the range of 100 kyr to 1 Myr. They both have spin-down powers of the order 3×10^{34} ergs s^{-1} at present. The winds of these pulsars had most probably powered pulsar wind nebulae (PWNe) that broke up less than about 100 kyr after the birth of the pulsars. Assuming that leptonic particles accelerated by the pulsars were confined in the PWNe and were released into the interstellar medium (ISM) on breakup of the PWNe, we show that, depending on the pulsar parameters, both pulsars make a nonnegligible contribution to the local cosmic ray (CR) positron spectrum, and they may be the main contributors above several GeV. The relatively small angular distance between Geminga and B0656+14 thus implies an anisotropy in the local CR positron flux at these energies. We calculate the contribution of these pulsars to the locally observed CR electron and positron spectra depending on the pulsar birth period and the magnitude of the local CR diffusion coefficient. We further give an estimate of the expected anisotropy in the local CR positron flux. Our calculations show that within the framework of our model, the local CR positron spectrum imposes constraints on pulsar parameters for Geminga and B0656+14, notably the pulsar period at birth, and also the local interstellar diffusion coefficient for CR leptons.

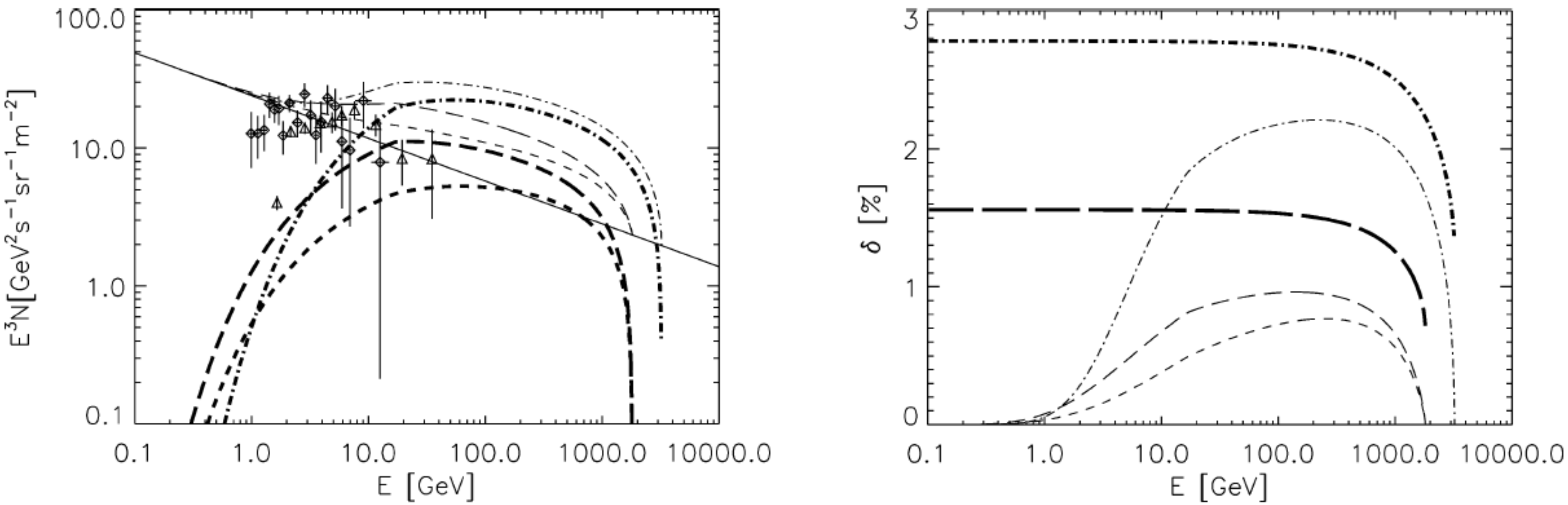

FIG. 2.—Same as Fig. 1 but for B0656+14.

290pc

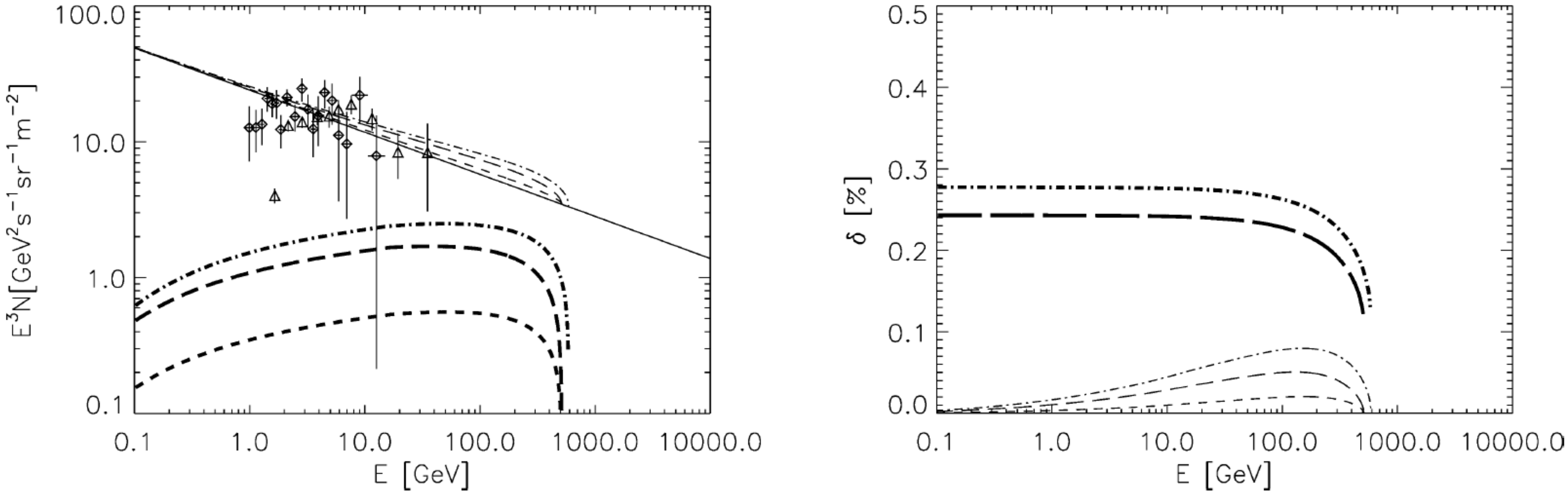

FIG. 1.—*Left*: Contribution of Geminga to the positron LIS for k_0 = 0.1 kpc^2 Myr^{-1} and P_0 = 40 ms, T = 20 kyr (*long-dashed line*), P_0 = 40 ms, T = 60 kyr (*dot-dashed line*), and P_0 = 60 ms, T = 20 kyr (*dashed line*) on top of an isotropic background (*solid line*). The thin lines mark the combined spectra (pulsar contribution plus background), whereas the thick lines give the contribution of the pulsar alone. Also shown are data from Boezio et al. (2000) (*diamonds*) and DuVernois et al. (2001) (*triangles*). *Right*: The expected local anisotropy in the case where only Geminga contributes to the LIS (*thick lines*), and in the case where Geminga contributes on top of an isotropic background positron flux (*thin lines*) as given by Barwick et al. (1998) (*solid line in left panel*). The line styles correspond to the cases as given for the left panel. The thick-dashed and long-dashed lines coincide.

157pc

Pulsars as the Sources of High Energy Cosmic Ray Positrons

Dan Hooper
Theoretical Astrophysics, Fermi National Accelerator Laboratory, Batavia, USA and Department of Astronomy and Astrophysics, The University of Chicago, USA

Pasquale Blasi
Theoretical Astrophysics, Fermi National Accelerator Laboratory, Batavia, USA and INAF-Osservatorio Astrofisico di Arcetri, Firenze, Italy

Pasquale Dario Serpico
Physics Department, Theory Division, CERN, CH-1211 Geneva 23, Switzerland and Theoretical Astrophysics, Fermi National Accelerator Laboratory, Batavia, USA

Recent preliminary results from the PAMELA satellite indicate the presence of a large flux of positrons (relative to electrons) in the cosmic ray spectrum between approximately 10 and 50 GeV. As annihilating dark matter particles in many models are predicted to contribute to the cosmic ray positron spectrum in this energy range, a great deal of interest has resulted from this observation. Here, we consider pulsars (rapidly spinning, magnetized neutron stars) as an alternative source of this signal. After calculating the contribution to the cosmic ray positron and electron spectra from pulsars, we find that the spectrum observed by PAMELA could plausibly originate from such sources. In particular, a significant contribution is expected from the sum of all mature pulsars throughout the Milky Way, as well as from the most nearby mature pulsars (such as Geminga and B0656+14). The signal from nearby pulsars is expected to generate a small but significant dipole anisotropy in the cosmic ray electron spectrum, potentially providing a method by which the Fermi gamma-ray space telescope would be capable of discriminating between the pulsar and dark matter origins of the observed high energy positrons.

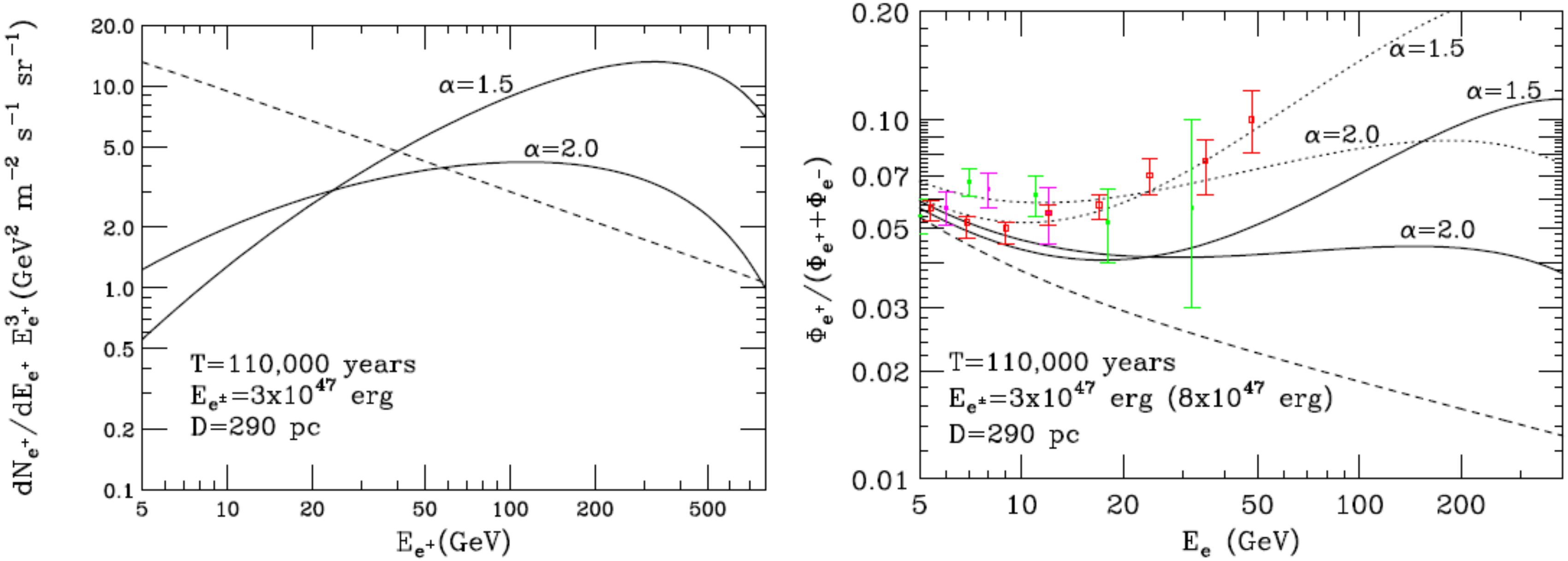

FIG. 3: As in Fig. 2, but from the nearby pulsar B0656+14. The solid lines correspond to an energy in pairs given by 3×10^{47} erg, while the dotted lines require an output of 8×10^{47} erg.

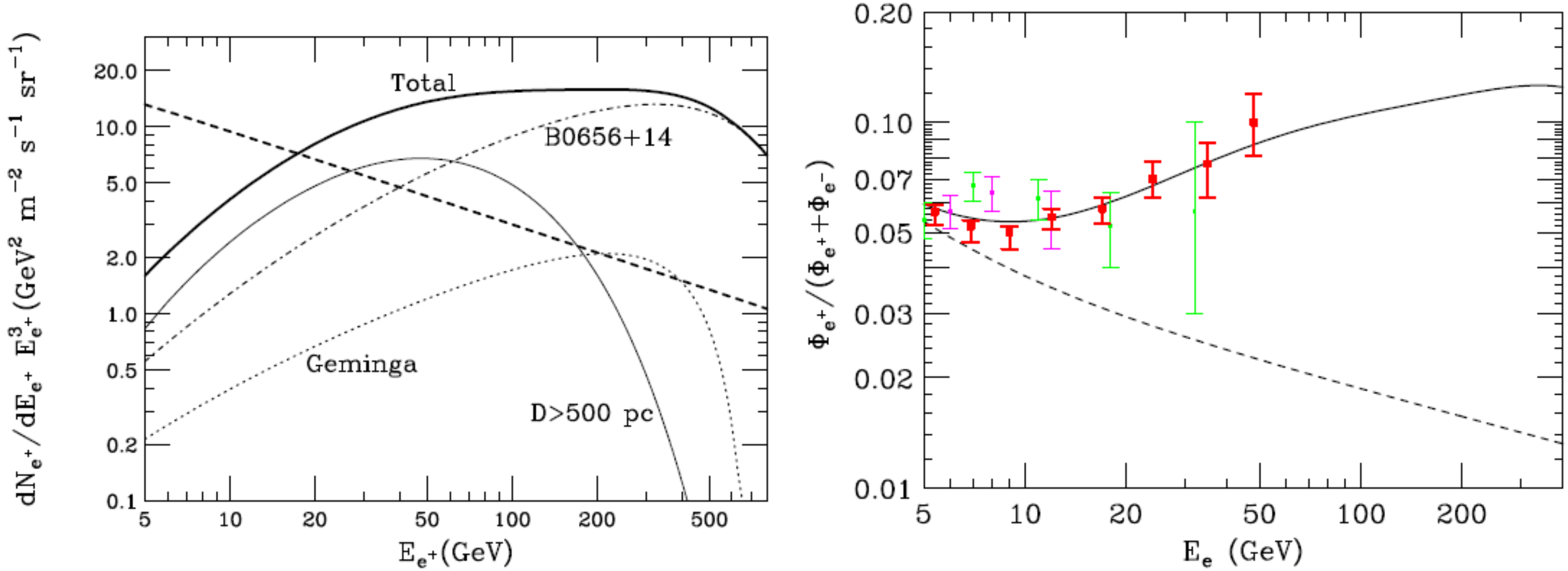

FIG. 4: The positron spectrum and positron fraction from the sum of contributions from B0656+14, Geminga, and all pulsars farther than 500 parsecs from the Solar System.

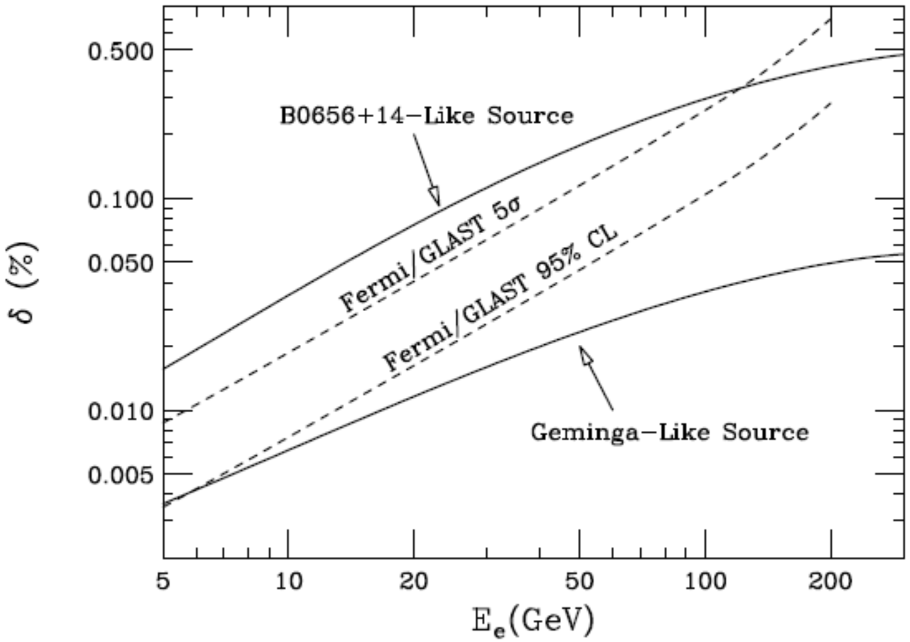

FIG. 5: The dipole anisotropy in the electron+positron spectrum from a source 110,000 years old at a distance of 290 pc (B0656+14-like) and from a source 370,000 years old at a distance of 157 pc (Geminga-like). In each case, we have normalized the energy output to match the PAMELA data and have used a spectral shape of $dN_e/dE_e \propto E_e^{-1.5}\exp(-E_e/600\,\mathrm{GeV})$. Also shown as dashed lines is the sensitivity of the Fermi gamma-ray space telescope to such an anisotropy (after five years of observation). The Fermi sensitivity shown is for the spectrum integrated above a given energy.

$$\delta = \frac{I_{\max} - I_{\min}}{I_{\max} + I_{\min}} = \frac{3K|\nabla(dN_e/dE_e)|}{c\,(dN_e/dE_e)},$$

In addition to studying the gamma-ray sky, the Fermi gamma-ray telescope will also be able to measure a flux of electrons (and positrons, though without charge discrimination) at a rate of approximately 3×10^7 electrons per year above 10 GeV [29]. This implies that Fermi should be able to detect (at the 2σ confidence level) a dipole anisotropy in the electron flux above 10 GeV if $\delta \gtrsim 0.05\%$ in one year or $\delta \gtrsim 0.03\%$ in 5 years.

TABLE II: Data for a few selected nearby pulsars and SNR's. $E_{\rm out}$ is the energy output in $e^{\pm}$ pairs in units of 10^{48} erg (for the ST model column we assumed $f_{e^{\pm}} = 3\%$). The energy output for the SNR Loop I and Cygnus Loop are not estimated within the ST model, but via estimates of the total SNR output. The $f_{e^{\pm}}$ column indicates the $e^{\pm}$ output fraction used to compute the fluxes shown in fig. 4 and 5 assuming the ST model.

Name	Distance [kpc]	Age [yr]	$\dot{E}$ [ergs/s]	$E_{\rm out}$ [ST]	$E_{\rm out}$ [CCY]	$E_{\rm out}$ [HR]	$E_{\rm out}$ [ZC]	$f_{e^{\pm}}$	g
Geminga [J0633+1746]	0.16	3.42×10^5	3.2×10^{34}	0.360	0.344	0.013	0.053	0.005	0.70
Monogem [B0656+14]	0.29	1.11×10^5	3.8×10^{34}	0.044	0.133	0.006	0.020	0.020	0.70
Vela [B0833-45]	0.29	1.13×10^4	6.9×10^{36}	0.084	0.456	0.006	0.372	0.0015	0.14
B0355+54	1.10	5.64×10^5	4.5×10^{34}	1.366	0.677	0.022	0.121	0.2	0.61
Loop I [SNR]	0.17	2×10^5		*0.3*				0.006	
Cygnus Loop [SNR]	0.44	2×10^4		*0.03*				0.01	

TABLE III: Possible combinations of multiple pulsars contributing to explain the PAMELA and the ATIC data. P/A refers to whether the pulsar dominantly contributes to the PAMELA or to the ATIC signal. $E_{\rm out}$ is the energy output in $e^{\pm}$ pairs in units of 10^{48} erg.

Name	P/A	Distance [kpc]	Age [yr]	$E_{\rm out}$ [ST]	$E_{\rm out}$ [CCY]	$E_{\rm out}$ [HR]	$E_{\rm out}$ [ZC]
J1918+1541	P	0.68	2.31×10^6	0.99	0.33	0.023	0.022
B0450+55	P	0.79	2.28×10^6	1.16	0.37	0.025	0.025
B0834+06	P	0.72	2.97×10^6	0.11	0.07	0.011	0.001
B1845-19	P	0.95	2.93×10^6	0.01	0.015	0.005	0.0002
B0919+06	A	1.20	4.97×10^5	0.158	0.178	0.010	0.016
B0355+54	A	1.10	5.64×10^5	1.366	0.677	0.022	0.121
B1055-52	A	1.53	5.35×10^5	0.82	0.49	0.017	0.075
J1849-0317	A	1.90	4.81×10^5	0.06	0.10	0.007	0.007
B1742-30	A	2.08	5.46×10^5	0.24	0.22	0.012	0.022

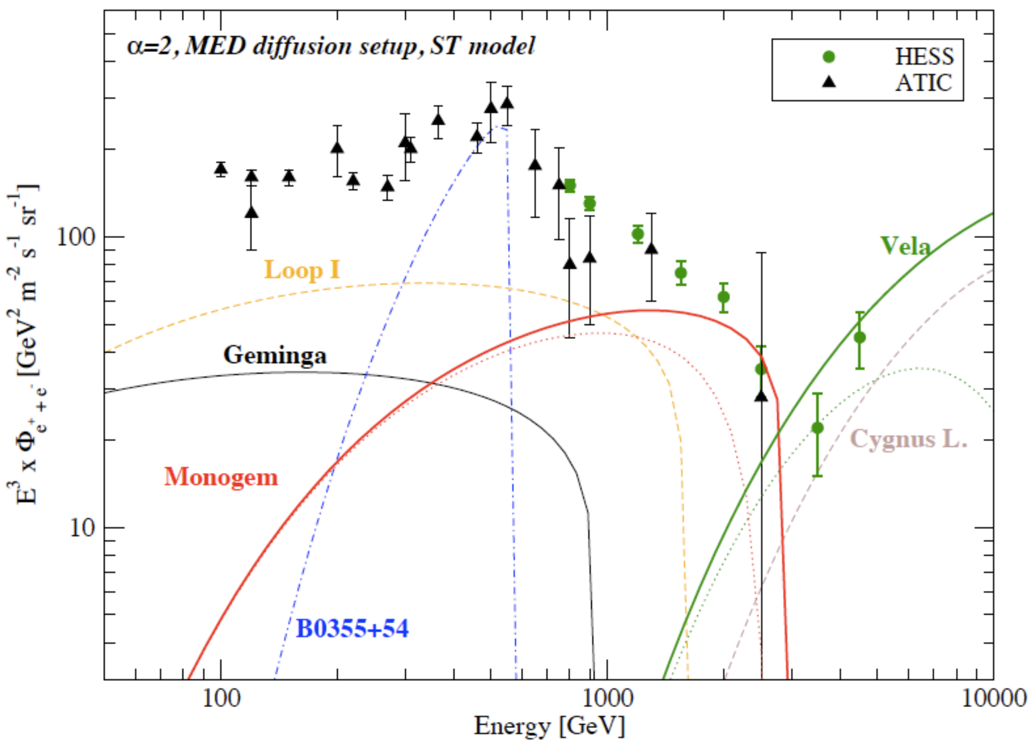
α=2, MED diffusion setup, ST model
HESS
ATIC
$E^3 \times \Phi_{e^+ + e^-}$ [GeV^2 m^{-2} s^{-1} sr^{-1}]
Loop I
Geminga
Monogem
B0355+54
Vela
Cygnus L.
Energy [GeV]
100
10
100
1000
10000

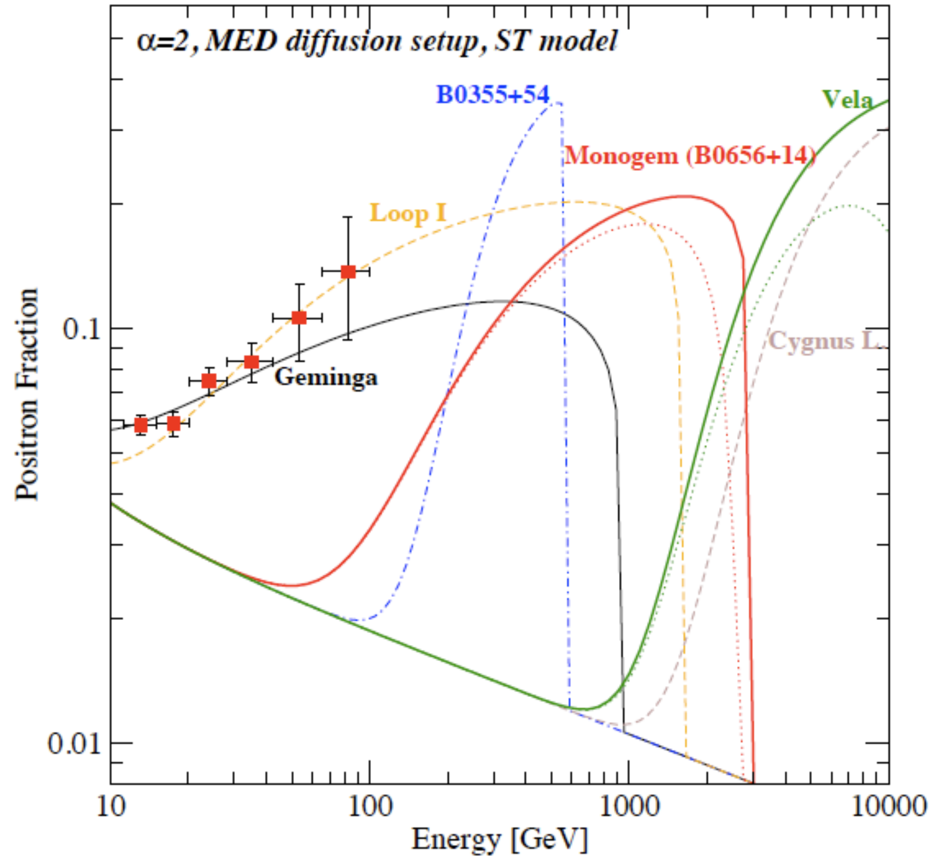
α=2, MED diffusion setup, ST model
B0355+54
Vela
Monogem (B0656+14)
Loop I
Geminga
Cygnus L.
Positron Fraction
0.1
0.01
10
100
1000
10000
Energy [GeV]

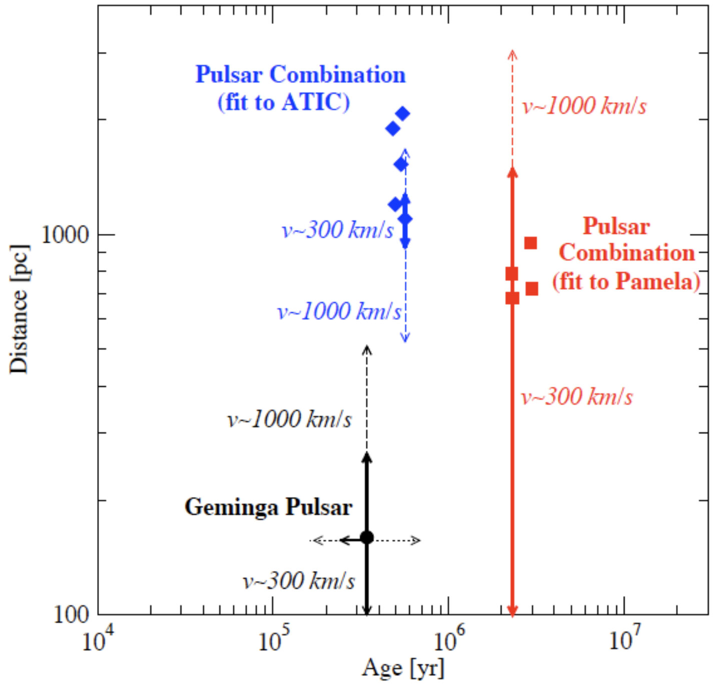
Pulsar Combination
(fit to ATIC)
v~300 km/s
v~1000 km/s
v~1000 km/s
Geminga Pulsar
v~300 km/s
v~1000 km/s
Pulsar
Combination
(fit to Pamela)
v~300 km/s
Distance [pc]
1000
100
10^4
10^5
10^6
10^7
Age [yr]

Composition

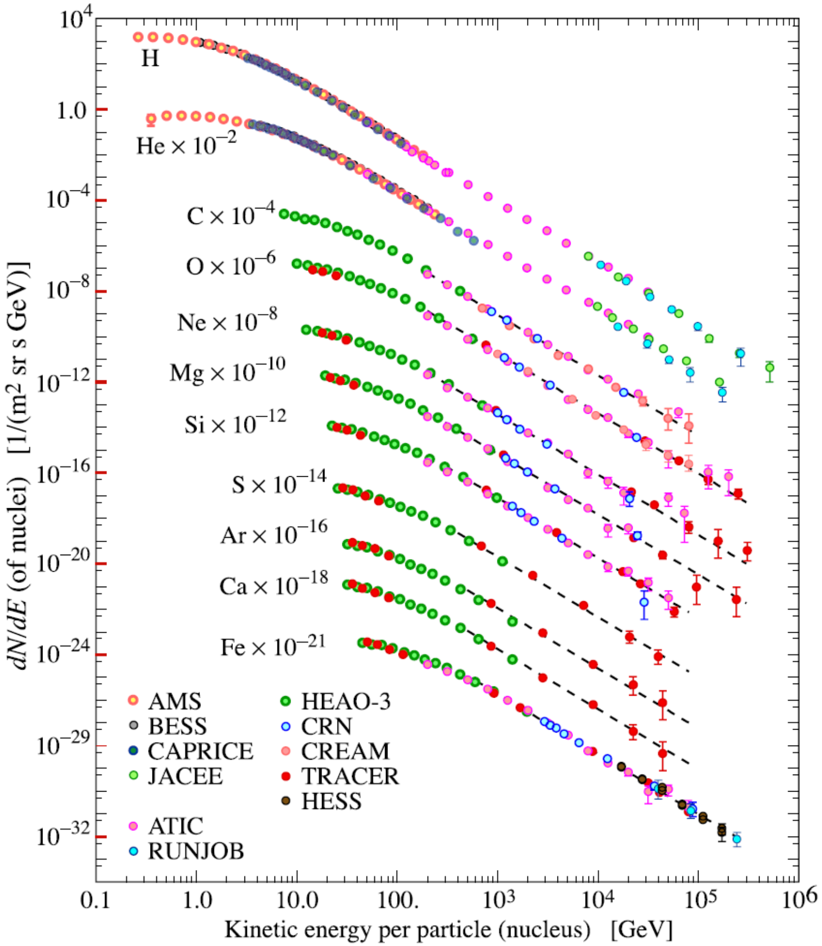

Figure 24.1: Major components of the primary cosmic radiation from Refs. [1–12]. The figure was created by P. Boyle and D. Muller.

PDG 08

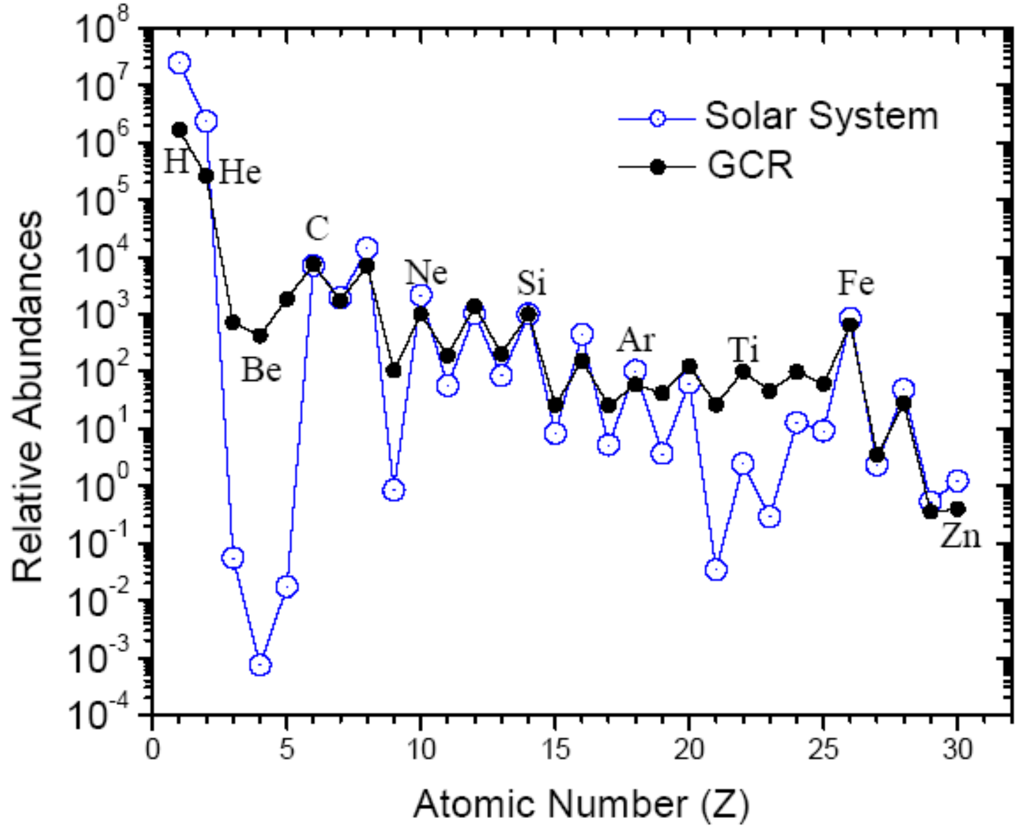

Advanced Composition Explorer (ACE)

Li, Be, B: spallation of C, O